GEOPHYSICAL AND GEOTECHNICAL INVESTIGATION OF THE EFFECT OF BLASTING AND OPEN CAST MINING ON WORKED-OUT UNDERGROUND MINES AND MODES OF FAILURE OF THESE WORKINGS

Andries Benjamin Fourie

A Dissertation Submitted to the Faculty of Engineering, University of the Witwatersrand, Johannesburg (in partial fulfilment of the requirements) for the degree of Master of Science.

JOHANNESBURG 1980

ABSTRACT

To make the method of coal-mining known as 'strip-mining' economically viable extremely large amounts of explosive need to be detonated in any one particular blast. This is to ensure enough rock is broken to keep the large earthmoving machinery, used in this type of mining, productive. This type of coal-mining operation was undertaken at Rietspruit Opencast Colliery in the Eastern Transvaal. Adjacent to this colliery is an existing underground coal-mine, and it was feared that the large amount of energy released by the surface blasting would be sufficient to damage the coal pillars. The investigation of the above problem formed the basis of this dissertation.

Moving-coil seismometers were installed underground in what was considered a representative pillar, and continuous records of ground particle motion due to blasting were obtained from these instruments. Further field instrumentation consisting of tape-recording decks and electronic packages to amplify and record the seismic signals was located on surface in an instrument hut built specifically for this purpose.

The object of obtaining the above records was to establish damage criteria, whereby charge weights could be estimated, for given distances from the blast to the underground workings, which would not cause appreciable damage underground. Propagation laws were established relating peak particle velocity, which is widely used as an indicator of possible damage, to the distance from the blast and either the square-root or cube-root of the maximum charge weight per delay. These results are presented graphically and could be used to determine allowable charge weights to ensure a certain particle velocity is not exceeded.

Accurate acceleration and displacement records were calculated from the original velocity records, and it was found that assumptions of simple harmonic motion for seismic records of blasting can result in under-estimation of particle acceleration. Relative displacements between various points in the pillar were determined and the instantaneous stresses generated by the blasting were calculated. These stresses were found to be a small percentage (1 ~ 2%) of the in-situ stress.

The use of Fourier analysis techniques in the interpretation of blast vibration data was undertaken. Power spectra were calculated to see whether there was a possibility of resonance occurring in the hanging-wall. The spectra indicate that the damping of the system is far too large for this to be a problem. The energy present in a seismic signal was successfully related to the total charge weight detonated, and finally, known source parameters (size of blast) were compared with the resulting spectral density and a tentative relationship developed.

Kuwe Adelheid ngibonga Kakhulu

ACKNOWLEDGMENTS

I wish to express my thanks to Dr Rod Green, of the Bernard Price Institute for Geophysical Research, for his assistance in the collection of data for this investigation, and for his guidance in the processing of this data. To Mr Frank Arnott and Mr Chris Neill, both of the Bernard Price Institute, for their assistance in learning the idiosyncracies of the *Wits computer system*. Special thanks to Mrs Fatima Variava for her assistance in the preparation of the text, particularly her patient typing. Finally, thanks is due to the Council for Scientific and Industrial Research, and Barlow-Rand without whose financial assistance this dissertation would not have been possible.

CONTENTS

		Page
CHAPTER 1		
1.	INTRODUCTION	1
CHAPTER 2		
2.	INSTRUMENTATION	10
2.1	Field Equipment	10
2.1.1	Seismometers	10
2.1.2	Electronic Package	10
2.1.3	Recording Deck	11
2.2	Replay Equipment	12
2.3	Digitization System	13
2.4	Setting-up and Servicing Procedure	14
2.5	Replay Procedures	15
2.5.1	Setting-up the Replay System	15
2.5.2	Replaying and Recording a Blast	15
CHAPTER 3		
3.	PEAK PARTICLE VELOCITIES, RECORDS AND PROPAGATION LAWS	17
3.1	Location of Seismometers	17
3.2	Calibration of Records	19
3.3	Reading a Record	20
3.4	Frequency Response of System	23
3.5	Particle Velocity Records	25
3.6	Propagation Laws	30
3.7	Verification of Particle Velocity as a Damage Criterion	33
CHAPTER 4		
4.	THE DIGITIZATION PROCESS - PROCEDURE, RESULTS AND ANALYSIS	36
4.1	The Digitizing Procedure	36
4.2	Plotting Procedure	38
4.3	Acceleration and Displacement Records	39
4.4	Comparison of Acceleration Records	41
4.5	Relative Displacements and Induced Stress Determinations	42
4.6	Comparison of Induced Stress with Original Stress Conditions	47
CHAPTER 5		
5.	FOURIER ANALYSIS TECHNIQUES IN THE INTERPRETATION OF BLAST VIBRATION DATA	49
5.1	Introduction	49
5.2	Fourier Series and Transforms	49
5.3	The Discrete Finite Transform	50
5.4	Windowing	52
5.5	Application of Fourier Techniques to Seismic Data Analysis	54
5.6	The Power Spectrum	54
5.7	Fourier and Spectral Analysis of Blasting Data	55
5.7.1	Investigation into possible Resonance using the Power Spectrum	55
5.7.2	Relation between Energy present in a signal and size of Blast	58
5.7.3	Calculation of source moment from Spectral Density	59
5.8	Conclusions	60

		Page
APPENDIX A:	Statistics related to blasting operations	62
APPENDIX B:	Graphical representation of blast vibration data	72
APPENDIX C:	Computer programs	74

REFERENCES

LIST OF FIGURES

Figure		Page
1.1	Connection between amplitude, frequency and damage	3
1.2	Layout of Rietspruit Opencast Mine	8
2.1	Electronic package in protective casing	after 10
2.2	Tape-deck used in the investigation	after 11
2.3	Laboratory replay system	after 12
3.1	Orientation of bord and pillar seismometers	17
3.2	Orientation of footwall seismometers	18
3.3	Record of internal calibration (Hi level)	after 19
3.4	Record of external calibration	20
3.5	Record of blast on 10/7/1979	21
3.6	Section of frequency response record	24
3.7	Frequency response curve	26
3.8	Sketch showing method of computing effective distance	after 29
4.1	Comparison of original analog signal with equivalent digitized signal	after 38
4.2	Examples of data files	after 38
4.3	Data file containing DC offset	40
4.4	Comparison of data files before and after removal of DC offset	after 40
4.5	Comparison of acceleration values obtained [illegible] differentiation and simple harmonic assu[illegible]	after 43

Page

Figure

5.1	Rectangular window and transform	53
5.2	Hanning window and transform	53
5.3	Power spectra for hanging-wall seismometer	after 56
5.4	Input and processed results for blast vibration data	after 57
5.5	Graph of total charge weight vs $r^2 v^2$	after 58
5.6	Graph of total charge weight vs low frequency plateau hypocentral distance	after 60
5.7	Amplitude Spectral Densities for Hanging Wall seismometer	after 61

CHAPTER 1

1. INTRODUCTION

At the request of Barlow-Rand the Bernard Price Institute of Geophysical Research at the University of the Witwatersrand agreed to undertake an investigation as to the effects of vibrations on an underground coal mine.

The site of investigation was Barlow-Rand's Rietspruit Open-cast coal mine. This mine was situated about 25 km from Ogies on the Ogies-Bethal road in the eastern Transvaal coalfields.

Adjacent to the open-cast workings was an existing underground bord and pillar coal mining operation which was the property of another mining group. Extremely large blasts (charge weights exceeding a total of 450 000 kg on occasion were necessary to ensure enough rock was produced per blast for efficient production. It was feared that the large amounts of energy released could damage, or in the extreme destroy, the underground coal pillars, as they were already in a relatively highly stressed state. The difficulties associated with this situation suggested that a research and control program be instituted to limit the possibility of damage.

In the past most of the attention focussed on the effects of blasting vibrations has been directed towards the damage caused to structures. The objectives of these tests may be divided into two distinct categories:

1) The establishment of reliable damage criteria, i.e. the relationship between the magnitude of the ground vibrations and the damage produced in a structure, and

2) To establish a propagation law for ground-borne surface vibrations that could be used to link the magnitude of ground vibrations with the mass of the explosive charge and the blast to measuring point distance, as well as any other variables which may be relevant, e.g. method of initiation, geology or directional effects.

One of the first investigations into this problem was summarised in a report in 1942 by the United States Bureau of Mines, Bulletin 442 (1), wherein particle acceleration was suggested as the best criterion for estimating damage. In 1949 Crandell (2) introduced the concept of the Energy Ratio. Making the basic assumption that vibration in the ground is simple harmonic in nature and starting with the equation that:

$$\text{Kinetic Energy} = WV^2/2g$$

He showed this equation can be reduced to give an equation in terms of acceleration, viz.

$$\text{K.E.} = \left(\frac{W}{2g4\pi^2}\right)\left(\frac{a^2}{n^2}\right)$$

where W is the weight of the system

g is the acceleration due to gravity

a is the acceleration in ft/sec/sec

n is the frequency of the vibration

The first fraction of the equation is a constant at any location depending on the mass set into vibration. The Kinetic Energy may therefore be considered to be proportional to $\frac{a}{n^2}$ which is referred to by Crandell as the Energy Ratio. He found that for buildings of sound construction and material, no damage is done if the Energy Ratio is kept below 3. A report published in 1958 by Langefors, Westerberg and Kihlström (3) was a result of measurements taken during a reconstruction project which required blasting in rock, close to existing buildings. A procedure of using large blasts and then repairing damage caused to adjacent structures was adopted. This enabled them to record actual damage and the associated level of vibration. Their classification used particle velocity instead of acceleration as the damage criterion. The limit below which they suggested no damage would occur was 71,1 mm/sec (2,8 in/sec). Their data is summarised in Figure 1.1. All subsequent investigations showed that

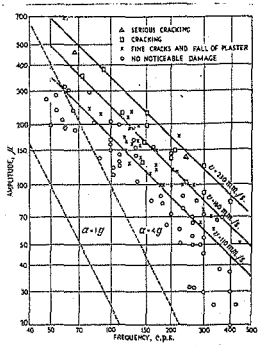

FIGURE 1.1 Connection between amplitude, frequency and damage.

particle velocity correlates best with the degree of damage. In 1960, (5) Edwards and Northwood concluded that damage was likely to occur if the particle velocity reached 102 - 107 mm/sec (4 to 5 in/sec). To facilitate the inclusion of a safety factor a safe vibration limit of 50 mm/sec (2 in/sec) was recommended. In South Africa tests done at the Bernard Price Institute by R. Green confirm the applicability of particle velocity as a damage criterion (6). Although an Energy Ratio of below 3 causes no damage to an average structure, to include a safety factor an Energy Ratio of 1 was designated as an upper limit in these tests. From simple harmonic considerations the Energy Ratio may be rewritten in terms of the metric velocity as:

$$E.Rm = V^2/23,5$$

where V = particle velocity in cm/sec.

Limiting the Energy Ratio to 1, this results in a velocity $V = 4,85$ cm/sec. Limiting the ground particle velocity to below 50 mm/sec would therefore seem an adequate, if somewhat conservative, means of preventing damage (to structures) from blasting vibrations.

Very little work had been done on the effect of blasting vibrations other than possible damage to residential structures. In his paper entitled, "Blasting effects and their control in open-pit mining", (7) L. Oriard concludes that for particle velocities of 50 - 100 mm/sec (2 - 4 in/sec) the occasional falling of loose stones on slopes may be expected. At 127 - 380 mm/sec (5 - 15 in/sec) the falling of partly loosened sections of rock underground and on above-ground slopes,

sections of rock that might otherwise remain in place may be expected. Above 635 mm/sec (25 in/sec) some damage to the relatively unsound rock types that are found in most open-pit mine slopes could occur. In 1977 the results of blast vibration monitoring programs from six hydro-electric sites were discussed by L. Keil and A. Burgess (8). From their results the authors concluded that the risk of causing excessive damage (formation of cracks or openings of discontinuities) to rock can be minimised if peak particle velocities are limited to 610 and 305 mm/sec (24 and 12 in/sec) at supported and unsupported faces respectively. The only noted work done on vibration levels in underground coal mines was that by Rupert and Clark in 1978 in the United States of America (4). Various combinations of three component moving coil geophones were located along a segment of the intake portion of the mine. They concluded that only minor damage of the form of localised thin spall and possible collapse of portions of previously fractured coal ribs resulted from those shots having associated peak particle velocities in excess of 50 mm/sec (2 in/sec).

Because of the scarcity of relevant results it was decided to set 50 mm/sec as an upper limit for the vibration levels generated in the underground workings. From the foregoing discussions this may have seemed a somewhat conservative limit, but it was considered justified in view of the limited knowledge available for this particular application.

Once a safe vibration criterion has been decided on the next problem is to determine which variables contribute significantly to the vibration level. Of primary interest is the relationship between the size of the explosive charge, shot-to-gage distance, and the magnitude of ground

vibration. A general propagation equation of the form

$$A = kW^{b}D^{n}$$

where A = peak amplitude
W = charge weight
D = distance from blast,

and k, b and n are constants for particular site conditions and blasting procedure became widely used. A rigorous dimensional analysis of this problem was done by Ambraseys and Hendron (9). This investigation concluded that "cube-root scaling" is theoretically the most correct propagation law (b = -1/3 and n = 1 for cube root scaling). However, most investigators have found that square-root scaling (b = $-\frac{1}{2}$ and n = 1) provides a better fit to experimentally found data. It is difficult to state whether square-root scaling or cube-root scaling is preferable. At any particular site it seems advisable to do some vibration measurements and then from the data, determine which of the two propagation laws is preferable. In the investigation done by Clark and Rupert (4) on underground workings they found that square-root scaling was slightly superior for expressing the roof, rib and bottom total peak velocity. Cube-root scaling was however found to be best for predicting the peak velocity for the vertical roof component.

In the case of the Rietspruit Opencast workings the layout is shown on Fig. 1.2. The region shown shaded in dark is the area the mine workings will occupy once they are complete, sometime in the late 1990's. Mining operations started in the region marked (A) on the plan and then proceeded in the direction indicated by the red arrows, approaching the underground workings of Tavistock

Colliery which is shown as shaded in blue. Photograph (A) shows the same layout, here looking from East to West. The raw coal stockpile and washing plant are slightly left of centre in the background. In the photograph mining operations proceeded from the foreground to the area in the background. In the centre of the photograph is a section of ground where the overburden had been loosened by an explosion, the loose rock then being removed by the drag line shown adjacent to the exposed bed. Photograph (B) shows a clearer view of the dragline working in the open pit, stripping overburden. As can be seen from the page of the blast statistics shown in Appendix A1, there is no direct relationship between the cost per bulk cubic metre and the amount of explosive used. Therefore increasing the weight of explosive does not necessarily mean a decrease in the cost per bulk cubic metre. The main economic consideration in using extremely large blasts in this mining operation was to ensure that the dragline remained idle for as little time as possible.

As mentioned before, it was considered that limiting the peak ground particle velocity to below 50 mm/sec would ensure that no damage would be caused to the underground workings. To monitor the level of ground motion six seismometers were installed in the underground workings on 25th January 1979. These seismometers were installed in what was considered to be a representative pillar, i.e. not adjacent to any ribs or other such restraints, and provided a continuous record of particle velocities at the various locations. A comprehensive description of the instrumentation used will be presented in Chapter 2. The above seismometers were all installed in either the pillar or the adjacent hanging wall. To attempt to obtain some idea of spalling rate around the pillar, 5 further seismometers were installed in the footwall around it, on March 2nd, 1979. A further seismometer was installed

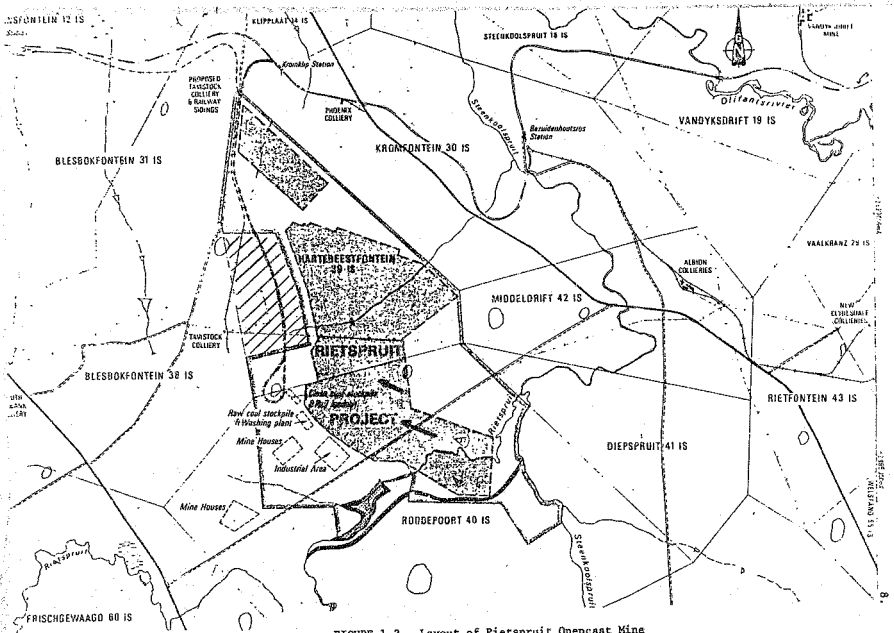

FIGURE 1.2 Layout of Pietspruit Opencast Mine

on the surface. The analogue records obtained from these seismometers were then replayed in the laboratory at the Bernard Price Institute and records sent back to the mine of peak particle velocities for all major blasts, which were considered as those for which particle velocities exceeded 1 mm/sec. An example of such a record is shown in Appendix A2. This data was then used for, among other things, verifying empirical propagation laws. A full discussion of the data analysis will follow in subsequent chapters.

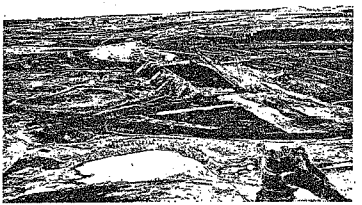

PHOTOGRAPH A: Showing Opencast Mining Operations

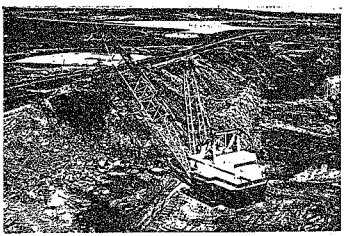

PHOTOGRAPH B: Drag-Line Bucket Excavator

CHAPTER 2.

2. INSTRUMENTATION

2.1 Field Equipment

This consisted of eleven underground seismometers connected, via a hydrophone cable, to two electronic packages and recording decks located on surface in an instrument hut provided specifically for this purpose. Two further seismometers were placed on the surface, inside the hut, and connected to the recording equipment.

2.1.1 Seismometers

All seismometers were of the moving coil or moving magnet type, which generate an electric signal and send it via an amplifier in the electronic package to the recording deck. The six seismometers located in the pillar and hanging wall were all 4,5 Hz natural period geophones and these were connected to channels 1 - 6 of the first electronic package. The five footwall and one surface seismometer had a cut-off frequency of 14,5 Hz and together with the other surface seismometer which was an EV17, with a cut-off frequency of 1 Hz, were connected to the second electronic package, on channels 1-7.

2.1.2 Electronic package

Two of these units were located in the instrument hut. The package, shown in figure 2-1, contained, from left to right; the Power Supply, Clock, Radio, Test Panel and the eight Data Channels. Details of the system have been described by Green (1972).

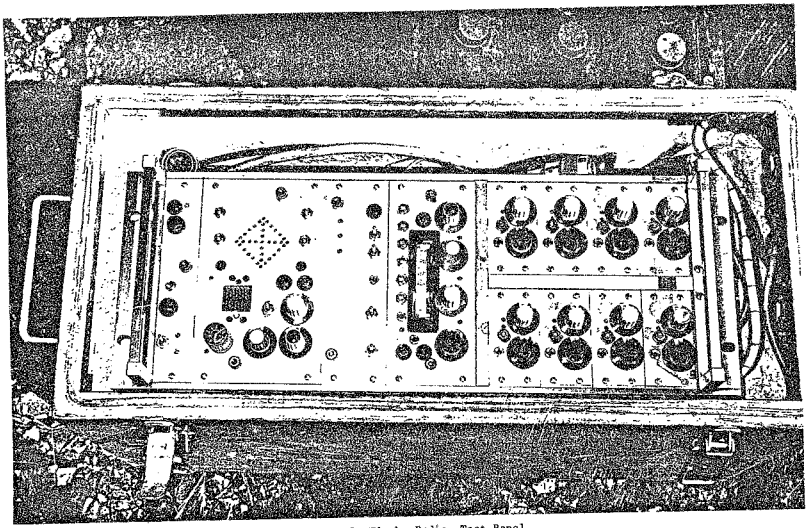

FIGURE 2.1 Electronic package showing Power Supply Clock, Radio, Test Panel and eight Data Channels

Time marks are recorded on the tape from a clock and radio. The radio facility was not used in this investigation since it is a completely independent and localized project. The clock primary signal is derived from a 1 MHz quartz crystal. The output of the clock in days, hours and minutes is translated into a Standard Vela C code.

In order to check the overall operation of the electronic package a complete test facility was provided to check the operation of both the input conditions as well as the recording current levels of the tape recording head. A switch on the test panel enables the operator to record an internal calibration signal at two levels, which is independent of the seismometer input signal. This calibration signal is recorded at a frequency of just less than 1 Hz on all input channels simultaneously. The high and low level signals are of constant amplitude with a separation of approximately 40 db. The electronic package was designed so that if a switch was left in the incorrect position a warning light came on. For example, a warning light came on if the internal calibrator was switched on, or if the bias was switched off.

Power was to have been supplied by a standard 240 v A.C. mains supply, but because of the isolated location of the hut this was never realized for this project. The primary power source for each package, including tape deck was derived from two 90 ampere hour, 6,3 volt lead acid batteries. This was convenient since most operational amplifiers use both positive and negative supplies. The batteries were connected to a power supply unit (DC-DC converter), which generated all the voltages required by the electronic package. The design and operation details have been described (Green, 1979).

2.1.3 Recording Deck

The tape recorders feature a locked-loop tape drive transporting tape

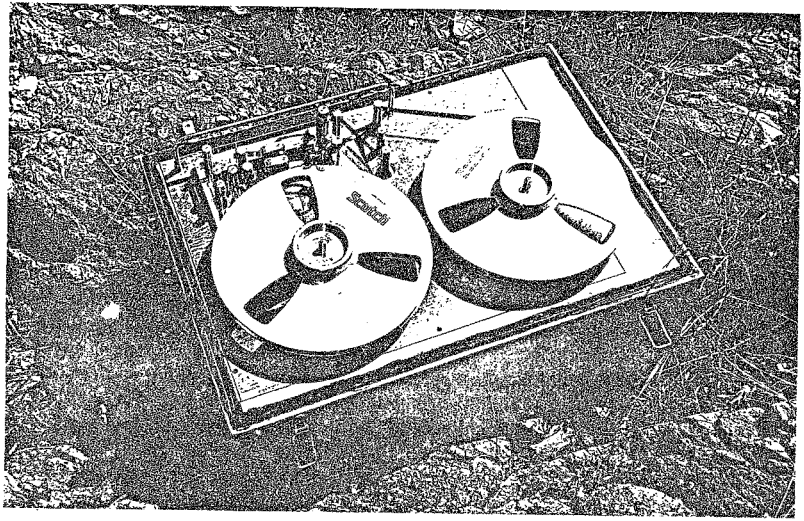

FIGURE 2.2 Tape recorder used in investigation

at recording speeds of either mm/sec or 12,5 mm/sec, the former being used for our investigation. This meant that one 35,5 cm (14 in) tape reel, accomodating 2800 metres (9200 ft) of tape, provided 12 days of continuous record. The take up reel was driven via a slipping clutch by the drive motor. Tape tension was controlled by a spring loaded brake acting on the feed reel. Connections from the electronic package to the recording head were as follows:

Tracks	1 to 4	: seismic channels
Track	5	: clock channel
Track	6	: radio channel
Tracks	7 to 10	: seismic channels.

All the units utilized plug-in construction to facilitate field servicing. The tape recorder, which is shown in Figure 2-2, was constructed on a hinged bed plate to enable easy maintenance of the system. Both units had clip latches on the lids which may be locked if required. Both the tape recorder and the electronics were housed in galvanized steel boxes which had waterproof seals and plugs. The silver colour of the boxes was useful in limiting temperature extremes and the boxes were lined internally with expanded polystyrene to restrict internal temperature fluctuations.

2.2 Replay equipment

The analog magnetic tapes from the portable seismographs were replayed on a tape replay system shown in Fig. 2.3 in the laboratory at the Bernard Price Institute. For normal replay or digitization of the data a replay speed of 63,6 mm/sec was utilized, which was twenty-five times higher than the recording speed. For searching the tape the replay speed was 380 mm/sec.

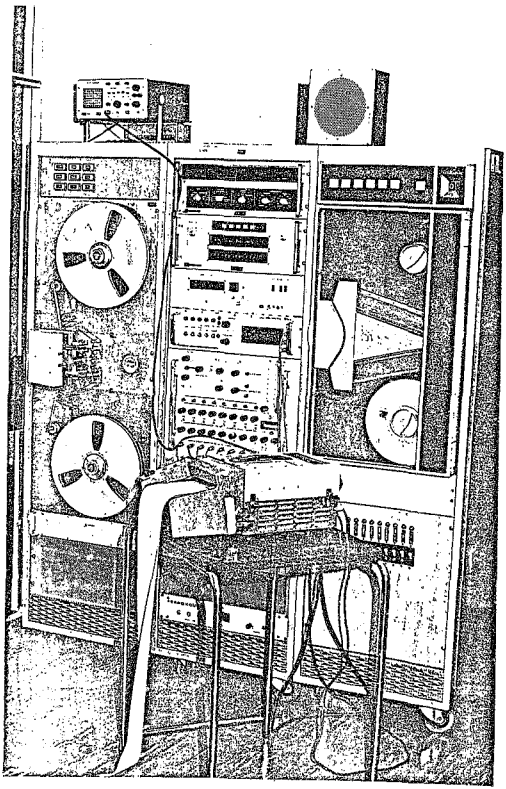

FIGURE 3.3 Replay equipment located in BFI Laboratory

The tape was searched manually at this speed as the seismic signals being monitored were in the audible range. These signals were monitored audibly on a loudspeaker as well as visually on an oscilloscope screen.

Output from the replay head was via a pre-amplifier followed by a main amplifier for each channel. The main amplifiers each incorporate gain adjust facilities and a low pass filter with nominal cut-off frequencies ranging from 0,25 Hz to 2500 kHz.

The final signal may be recorded on ultra-violet light sensitive paper using a multi-channel Oscillograph recorder. An analog to digital converter and digital tape drive enabled the digitization of one channel at a time. Additional equipment included a time-code translator which indicated the time on the clock channel on a visual display. This unit was also used to control start and stop times of the paper recorder and the digitization process.

2.3 Digitization System

The object of this circuitry was to digitize and convert an analog signal obtained from the replay equipment (2.2) into an IBM compatible nine track digital tape.

The digitization rate was a maximum of 320 conversions/sec or a minimum of 3 sec on the recorded time scale. This ensured that there was a minimal loss of high frequency resolution of the analog data in this study. Digitization was controlled by the clock, and for this reason each sample was known in true recorded time and direct correlation between digitized traces was a simple matter. The digitized data was written in Standard 9 track

360 IBM 800 bits per inch format with two bytes of data for each sample and 1024 samples per block.

2.4 Setting up and servicing procedures

Once the seismometers had been installed underground each one was connected to a main amplifier in the electronic package. All units in the electronic package were checked for correct operation by means of the test panel. The clock was set up to the correct time and placed in the RUN mode at the appropriate moment.

For the first 3 - 4 months of the investigation, maintenance of the system required weekly, and sometimes bi-weekly visits to the site. The maintenance procedure consisted of checking battery voltages as well as all internal supply voltages. The amplifiers were checked for zero d.c. output and adjusted where necessary. The coding of the clock was checked against actual time and the necessary corrections made. Tape cleaners had to be replaced often because of the severe conditions under which the system operated. The tape heads were also routinely cleaned with a magnetic tape head cleaner.

Very few really serious problems occurred. On one occasion one of the tapes became tangled with a guide roller, damaging several metres of tape. Once a worn spring had been replaced the tape deck functioned normally again. The most common problem was that the clocks were frequently found to be incorrect. They were therefore accurately set approximately an hour before each major blast. The d.c. offset on some of the amplifiers also had to be periodically zeroed. Problems caused by a non-zero offset will be discussed in Chapter 4. By far the largest problems were associated with the batteries or battery connections.

2.5 Replay procedures

When replaying the analog tapes obtained from the field the operator could listen to any one of 10 channels on the tape.

In the PLAYBACK mode the tape could be replayed at a speed of either 64 mm/sec or 380 mm/sec, while the replay speed for the FORWARD and REVERSE modes was 380 mm/sec.

2.5.1 Setting up the replay system

Eight or nine output channels (7 or 8 seismic channels and one channel for the clock) from the replay system were connected to the Oscillograph ultra-violet recorder. A T-piece adaptor allowed the output of one seismic channel as well as the clock channel to be displayed on an oscilloscope screen.

1 Hz gain and filter settings were set to their required positions, and one seismic channel was selected for monitoring on the loudspeaker. When searching for a blast on the tape it was found useful to monitor the channel to which the surface EV17 seismometer was connected, as its output was a great deal higher than any of the other seismometers used. The tape was replayed at 380 mm/sec during this searching procedure.

2.5.2 Replaying and recording a blast

Once a blast was located on the loudspeaker it was replayed at 64 mm/sec and a paper copy of the blast recorded on the ultra-violet recorder.

The first paper copy was made at a recorder speed of approximately 25 mm/sec. This copy was used to determine the time of a blast as well as providing a basis for final gain settings. The second paper record was made at a speed of about 625 mm/sec. This record was used for determining peak particle

velocities and corresponding frequencies for the various seismometers.

3. PEAK PARTICLE VELOCITIES, RECORDS AND PROPAGATION LAWS

3.1 Location of seismometers

As mentioned in Chapter 1 a total of eleven seismometers were installed underground and one on surface. The footwall seismometers were located at a depth of approximately 60 m, in a seam known as 2 SEAM. This coal underlay approximately 56 m of overburden which consisted primarily of sandstone and shale. A log of a borehole which was sunk close to the pillar under investigation is included in Appendix A3.

Figure 3.1 below shows the orientation of the six seismometers which were installed in January 1979 in the bord and pillar. These seismometers are referred to as Array 1.

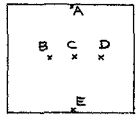

Elevation of Pillar B2

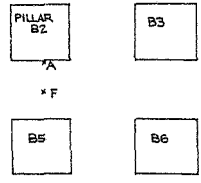

Plan View

FIGURE 3.1 Orientation of bord and pillar seismometers

The orientation of these seismometers was:

A was the vertical seismometer in the top of the pillar

B was horizontal radial (radial to approach of blasting operations) in pillar centre

C was vertical seismometer in centre of pillar

D was horizontal tangential seismometer, in pillar centre

E was vertical seismometer in bottom of pillar

F was vertical seismometer in bord hanging wall (approximately midway between two pillars)

Array 2 consisted of the seismometers 1 - 5 located in the footwall as shown in Figure 3.2 Seismometer 6 was located on surface.

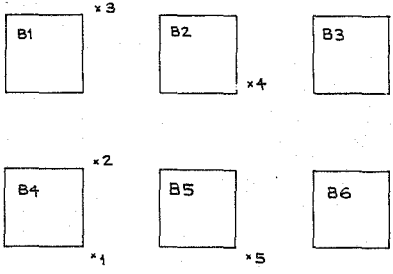

FIGURE 3.2 Orientation of footwall seismometers

Initially it was thought that blasting operations would commence at approximately 4 km from the underground working and then proceed gradually

towards them. This would have made it possible to obtain a sequential record of the increase in vibration levels underground. However, due to changes in the planned production, blasts close to the pillar ($\pm$ 300 m) became necessary a lot earlier than originally intended. The results presented later in this chapter are therefore independent of time.

? Calibration of records

In order to make the paper record of a blast obtained from the analog signal meaningful, it was necessary to calibrate the equipment. This was done by feeding a signal of known amplitude and frequency into the electronic package and recording equipment, and then obtaining a copy of the output which was used as a reference for quantifying the records.

The internal calibrator was usually used for this purpose. However, as is seen from Figure 3.3, the output thus obtained was not satisfactory. The signal was overdriven and consequently the sine-wave was distorted. In addition the calibrator frequency was on the end of the bandpass and the accuracy was thus limited.

For this reason it was decided to use an external calibrator. Every time the site was visited, the signal from either an 11 Hz or a 17 Hz calibrator was used as an input for the recording equipment. The output from the calibrator was measured with a voltmeter, and noted. This calibration signal was then also replayed in the laboratory and a paper record made of it, as shown in Figure 3.4

This is a copy of a signal from the 11 Hz calibrator. The trace shown in the middle of the record is the visual record of the clock. The one second mark is shown on the Figure. On either side of the clock signal is the calibration signal from the seven seismic channels of tape deck 2. The measurements of interest is the peak-to-peak amplitude, indicated as (A) on the record for channel which is proportional to the input voltage. The gain settings on the replay equipment must be noted for comparison with the seismic records gain settings.

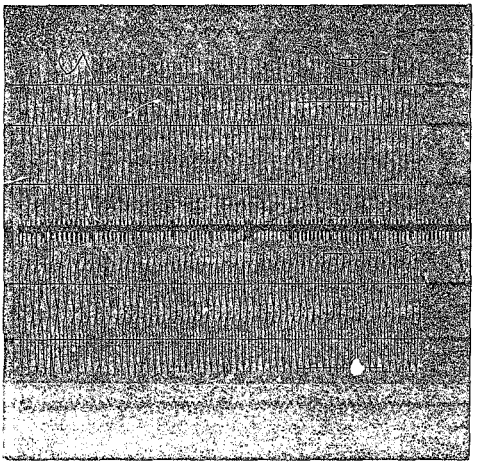

FIGURE 3.3 Record of internal calibration (Hi level)

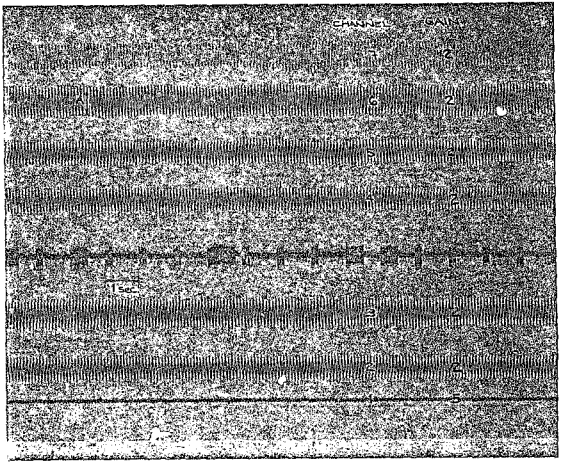

FIGURE 3.4 Record of external calibration

3.3 Reading a record

Once a paper copy of a seismic event had been made, the next step was to obtain values of peak particle velocities and corresponding frequencies for each channel from this record. The method of determining these values will be explained with reference to an example of an actual blast record.

Shown below in Figure 3.5 is the record for the blast which occurred on July 10, 1979, as recorded on *seismometer* Array number 2.

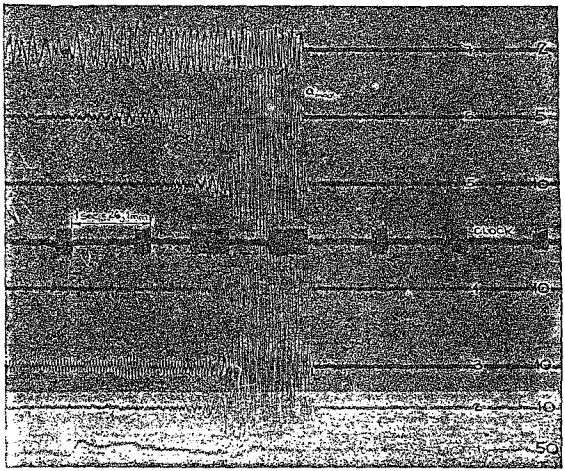

* FIGURE 3.5 Record of blast on 10/7/1979

The *seismic channels* are numbered 1-7 in black and the replay equipment gain settings are shown in red. To enable channels 2-5 to be accurately read the gain settings would be reduced to 5 to prevent *the overlap* occurring which is evident on the Figure. Channel 7 was connected to the EV17 seismometer, and as can be seen from the Figure the signal was markedly *overdriven*. Even though the gain setting for channel 7 was only 2, the trace still had large *amplitudes*. The EV17 channel was used

* Note: Time *scale is from* right to left.

for detecting blasts because of its larger output signals. It is also interesting to note the velocity amplitudes for channel 6 are approximately the same size as those of channels 2-5 even though the gain setting is half the value. This was found to be the case for the majority of the blasts, i.e. the vibration levels on surface are substantially larger than those underground in the footwall.

Channel 6 will be used as a reference channel for calculating the peak velocity. A pencil line is drawn through the centre of the signal. This line must be the zero velocity line as shown. The largest deviation either side of this line was then measured in mm, in this case indicated by Amax. Some investigators suggest measuring the amplitude of a particular wave either side of the zero velocity line, summing these 2 values and then dividing by two. The former method was used throughout the investigation because of the non-uniform nature of the signals. The corresponding frequency of the wave with amplitude Amax was found by firstly measuring the half-wavelength of this wave in mm, which was denoted as T/2 (T/2 = 0,75 mm for channel 6). The distance represented by one second is then measured in mm from the record, and denoted as F (F = 26,1 mm for channel 6). The frequency of the wave is then given by $\nu = F/T$. For channel 6, ν therefore equals $\frac{26,1}{2 \times 0,75} = 17$ Hz.

The peak particle velocity was then calculated for channel 6, with a peak amplitude Amax, of 14,8 mm. Referring to Figure 3.4, the calibration record, it will be seen that the peak-to-peak amplitude for channel 6 is 8,9 mm with the gain set at 2. The output of the calibrator, measured in the field with a voltmeter, had an R.M.S. value of 42 mV. This corresponds to a peak-to-peak value of 119 mV. Therefore, 1 mm deflection represents 119/8,9 = 13,0 mV. The blast record gives a deflection of 14,8 x 13,0 = 196,8 mV, which must be multiplied by the ratio of the calibration record gain to the blast record gain, in this case 2/5. The peak

particle velocity is therefore equivalent to 197 x 2/5 = 79 mV.

Different seismometers were used for arrays 1 and 2.

The Sensitivity of the seismometers used in array 1 was arranged to be 100 mV/cm/sec. The sensitivity of the array 2 seismometers had to be determined. This was done by securing two seismometers of either type to the same surface by means of plaster of paris, providing an input to these seismometers by dropping a heavy weight close to the supporting surface, and comparing their relative outputs. These outputs were recorded in the same manner as described before. Sixteen of the above tests were performed, which gave a mean sensitivity of 158 mV/cm/sec.

3.4 Frequency response of system

The peak particle velocity is then given by the following calculation: V = 79 mV ÷ 158 mV/cm/sec = 0,5 cm/sec i.e. 5 mm/sec. This would then be the final peak particle velocity for channel 6 if the frequency response of the recording equipment were flat. By this is meant that the amplitude of the recorded signal is independent of its frequency content. This is almost impossible to achieve, and frequency response curves had to be determined for the recording equipment. Two types of tape were used in the investigation, Quantum CX and 3M 871, and two different curves had to be determined.

A WAVETEK model 1145 signal generator was used as a source in place of a seismometer. The signal was fed directly into the recording equipment which was set at a gain setting of 1. A pre-amplifier was not used. This input signal was monitored on an oscilloscope and a digital voltmeter. Recordings were made of constant amplitude signals at varying frequencies. The input signal frequency was varied from 0,5 Hz to 50 Hz. By using the same type of 'doubling-up' plug as was used for the calibration input, the input signal was recorded on all channels simultaneously. These recordings were then replayed in the lab. and records made of them. A section of one

of these records is shown in Figure 3.6. This is a record of 5, 2,5 and 1 Hz input signals. The amplitude and corresponding frequency were then noted for each channel for four complete tests. The scatter of results between different channels was found to be no greater than that between different tests on the same channel. For this reason only one curve was drawn for either tape to cover all channels. The input frequency and relative frequency were then plotted using the PHYSPLOT facility on the University computer, to obtain frequency response curves.

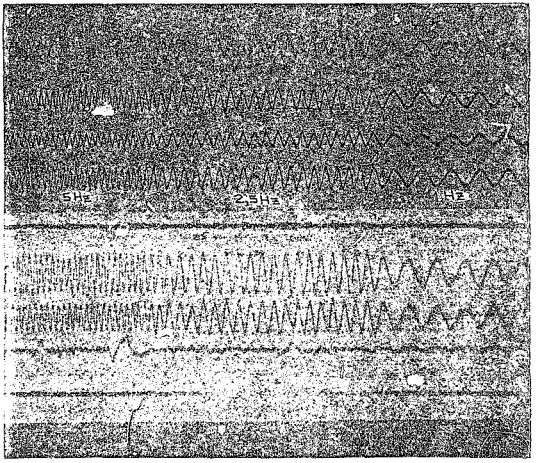

FIGURE 3.6 Section of frequency response records

This plot is shown in Figure 3.7. An exaggerated scale was used for the vertical axis for improved accuracy, (a much flatter curve is usually indicated in frequency response curves).

The value of peak particle velocity must now be corrected for the effect of this frequency anomaly. This is done by multiplying the value of velocity obtained in the previous section by the ratio of the relative amplitudes of the calibration frequency to the blast frequency, i.e. A/B on Figure 3.7. For channel 6, A = 0,24 and B = 0,22 and the velocity must be increased to compensate for the lower response at 17 Hz. The final value of peak particle velocity is then given by

$$5 \times {}^{0,24}/_{0,22} = 5,5 \text{ mm/sec}$$

3.5 Particle velocity records

All the peak particle velocities which were recorded for significant blasts are shown in Tables 1 and 2. The data is tabulated according to the date of blast, peak particle velocity (Vmax) and frequency (F) for each seismometer, distance from blast to pillar (D), charge weight per delay (W), and the 2 scaling parameters $D/W^{1/3}$ and $D/W^{1/2}$.

Various results are missing from these tables. It was decided that from April 1 to approximately the end of July, no major blasting would occur close to the instrumented pillar. Consequently tape deck 1 was removed from site and returned to the laboratory where it was overhauled. This explains the gap in the results for array 1 from 28/3 to 10/8. During this period array 2 did produce some results, but the velocities were low and in some cases only registered significantly on the surface seismometer. Once tape deck 1 was re-installed, difficulty was experienced with seismometers A, C and E. The faults were all eventually traced and normal

FIGURE 3.7 FREQUENCY RESPONSE OF TAPES 3M 871 AND QUANTUM CX

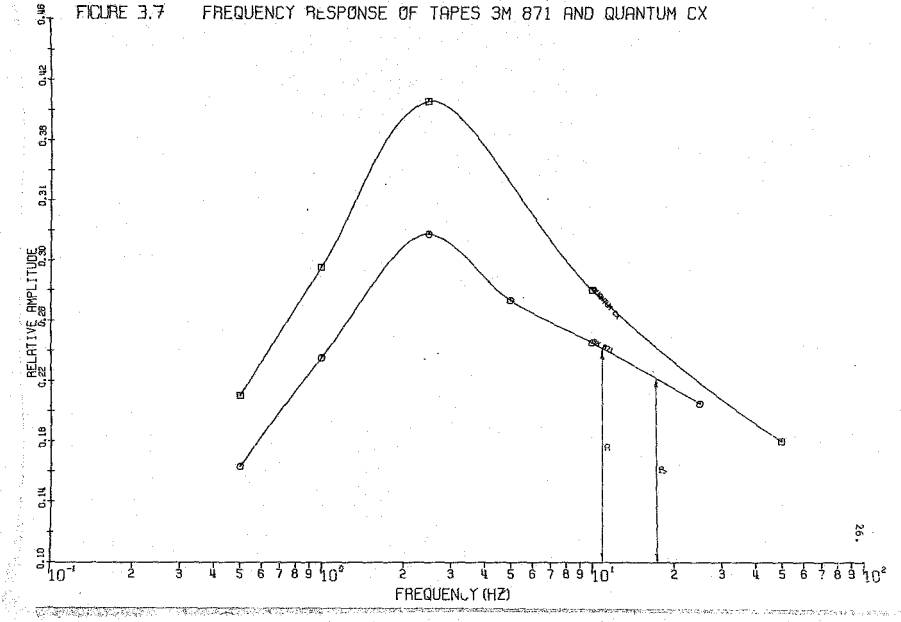

TABLE 1.

PEAK PARTICLE VELOCITY RECORDS

ARRAY 1.

DATE	SEIS. A.		SEIS. B.		SEIS. C.		SEIS. D.		SEIS. E.		SEIS. F.		DISTANCE (m)	WEIGHT (Kg)	$D/W^{1/3}$	$D/W^{1/2}$
	V max (mm/s)	F (Hz)	V max	F	V max	F	V max	F	V max	F	V max	F				
31/1	2,4	7	2,8	15	2,7	8	3,1	13	2,4	19	3,1	7	373	500	47,0	16,7
2/3	4,8	10	5,3	23	6,8	21	-	-	2,3	10	7,0	12	310	2495	22,9	6,2
14/3	4,9	22	7,5	16	6,4	18	7,9	16	4,4	16	9,0	18	250	2900	17,5	4,6
20/3	1,7	16	1,2	13	1,1	16	1,2	13	1,5	16	-	-	1500	9000	72,1	15,8
28/3	1,8	8	2,3	5	2,1	12	2,4	7	1,5	17	1,8	8	1300	10500	59,4	12,7
10/8	-	-	-	-	-	-	-	-	-	-	6,3	25	500	7800	25,2	5,6
13/8	-	-	1,4	12	-	-	3,0	17	-	-	4,1	15	750	3500	49,4	12,6
15/8	-	-	9,1	14	-	-	12,28	15	-	-	11,2	18	270	1850	22,0	6,2
16/8	-	-	14,05	15	-	-	15,3	28	-	-	22,3	18	190	2260	14,5	4,0
17/8	-	-	6,6	14	-	-	14,6	18	-	-	16,4	24	125	2050	9,8	2,7
16/10	2,3	9	4,4	12	3,9	17	7,4	15	7,3	30	8,2	20	155	500	19,5	6,9

TABLE 2.

PEAK PARTICLE VELOCITY RESULTS — ARRAY 2

DATE	SEIS. 1		SEIS. 2		SEIS. 3		SEIS. 4		SEIS. 5		SEIS. 6		DISTANCE (m)	WEIGHT (Kg)	$D/W^{1/3}$	$D/W^{1/2}$
	V max (mm/s)	F (Hz)	V max	F	V max	F	V max	F	V max	F	V max	F				
28/3	-	-	1,5	15	-	-	2,0	37	1,8	18	3,2	7	1300	10500	59,4	12,7
10/4	-	-	1,4	23	-	-	2,9	45	2,7	13	6,0	13	1200	12000	52,9	11,0
23/4	-	-	1,8	22	-	-	2,8	44	1,6	17	4,0	12	1000	12850	42,7	8,8
10/5	-	-	0,1	23	-	-	1,1	41	0,7	15	0,7	17	1500	2253	114,4	31,6
11/5	-	-	0,2	19	0,6	50	0,9	37	0,7	30	0,9	19	2000	10230	92,1	19,8
28/5	-	-	0,3	21	1,6	32	2,02	43	0,8	16	2,0	13	2000	8000	100,0	22,4
14/6	-	-	-	-	-	-	-	-	-	-	0,2	13	2300	13268	92,7	20,0
22/6	-	-	-	-	-	-	-	-	-	-	0,3	12	2000	7615	101,7	22,9
25/6	-	-	-	-	-	-	-	-	-	-	0,4	25	1500	11700	66,1	13,9
10/7	-	-	2,7	20	3,3	26	5,8	31	6,2	22	5,2	17	700	13 490	29,4	6,0
24/7	-	-	-	-	2,9	21	4,1	27	5,2	20	3,6	10	500	7600	25,4	5,7
10/8	-	-	-	-	3,4	12	4,2	25	5,2	23	3,7	12	500	7800	25,2	5,6
13/8	-	-	-	-	1,8	20	3,8	38	2,8	27	3,4	20	750	3500	49,4	12,6
15/8	-	-	-	-	3,5	23	4,6	32	6,2	30	4,8	18	270	1850	22,0	6,2
16/8	-	-	-	-	3,6	31	5,5	52	7,3	54,4	6,1	31	190	2260	14,5	4,0
16/10	-	-	-	-	3,3	11	-	-	5,4	21	5,5	15	155	500	19,5	6,9

service was resumed on 10/10. In array 2 seismometer 1 provided no results whatsoever and from 24/7 onwards seismometer 2 ceased to function. On examination it was found that this instrument was covered with coal, which had spalled from the adjacent pillar, and had become dislocated from its original position. Other gaps which appear in the data are due to equipment malfunctions or operator errors which were usually easily traced and rectified (e.g. tapes being loaded onto recorder incorrectly). As can be seen from the tables there is a fair scatter amongst the data. Possible reasons for the discrepancies are:

a) Random addition and subtraction effects between wave trains generated from successive delays. This point is important in respect to the complex delay patterns that were used. In addition, the Gaussian distribution of the delay times played a role as all delays are normal. The calculations assume that the peak particle velocity is due only to the detonation of the maximum charge per delay.

b) Scattering and reflection from joints, free faces and other geological features which cause random addition and subtraction within the wave train. Since most of the geology is horizontal and the transmission paths are not vastly different this effect is probably small.

c) Differing transmission characteristics of the rock.

d) Variation in explosive energy transmitted to the rock by the blast, due to, e.g. charge density, packing and stemming.

e) Errors in computing the effective distance between the monitor and the shot. Shown in Figure 3.8 is the method of computing this distance, e.g. from the monitor to the nearest hole in the blast. This is sufficiently accurate at some distance from the blast, but for distances less than about 200 m the effective distance is probably greater than this value.

f) Instrument and reading accuracy. For example, the eyeglass used to read the records had an accuracy of 0.05 mm. This latter reason probably contributed the least to errors introduced to the records.

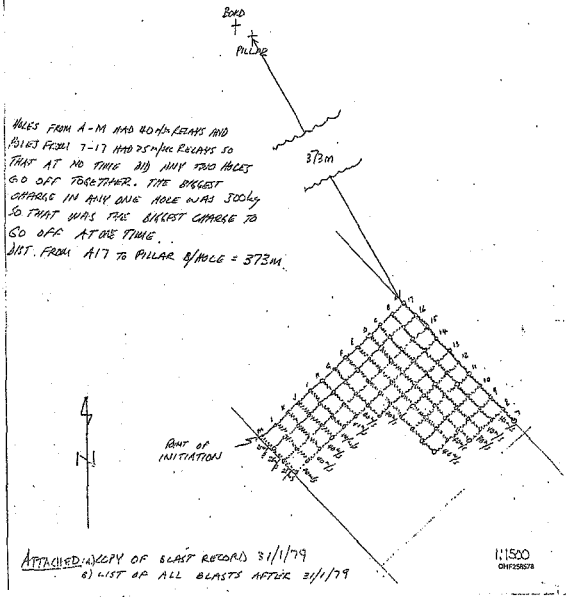

FIGURE 3.8 Sketch showing method of computing effective distance

From the above discussion it is evident that a rigorous error analysis of the data is not possible. The data has been left untouched, and confidence intervals are calculated in Appendix C1.

3.6 Propagation laws; comparison and verification

The object of obtaining the particle velocity records was so that, by extrapolation, the combinations of monitor-to-blast distance (D) and charge weight (W) for which the maximum velocity limit of 50 mm/sec would be exceeded, can be predicted.

It is for this reason that propagation laws have been developed. As mentioned in chapter 1 there is some disagreement as to whether cube-root scaling ($D/W^{1/3}$) or square-root scaling ($D/W^{1/2}$) should be used. A program to fit a least-squares straight line to a set of x and y co-ordinates was developed. This program was also used to calculate the square of the error between the predicted least squares velocity value and the actual measured value, e_i and the variance for each set of data, $^1/_n \Sigma e_i$. This program is included in Appendix C1. Particle velocity (V) vs $D/W^{1/3}$ and V vs $D/W^{1/2}$ values were used as input for this program. The results of this analysis are shown in Table 3. The choice between square-root and cube-root scaling was based on the minimum variance, which is a good indicator of how well the data fits a straight line. The data from the seismometers of array 1 fits cube-root scaling a lot better than square-root scaling, except for the vertical seismometer in the middle of the pillar, for which the difference in variance of the propagation laws is ±33%. The footwall seismometers (array 2) tend to follow a square-root scaling law. However, the difference in variance for these seismometers is a great deal less than for array 1. For seismometer 4 the difference is only 1,6%. and for seismometer 3 it is 4,3%. It is impossible for these seismometers to state whether cube-root or square-root scaling is preferable. This data is shown graphically in Graphs 1-3. Graph 1 is square-root scaling for seismometers 2,4 and 5. Once again the PHYSPLOT facility on the

RESULTS OF REGRESSION CALCULATIONS TABLE 3

SEISMOMETER	CUBE ROOT VARIANCE	SQUARE ROOT VARIANCE	SLOPE	Y-INTERCEPT	CUBE ROOT (C) OR SQUARE ROOT (S) SCALING CHOSEN
B	0,026	0,032	-1,06	2,14	C
C	0,012	0,018	-1,04	2,10	C
D	0,013	0,024	-1,22	2,51	C
E	0,018	0,034	-0,86	1,75	C
F	0,013	0,022	-1,23	2,56	C
2	0,023	0,020	-1,98	2,13	S
3	0,012	0,011	-0,80	1,12	S
4	0,012	0,013	-0,80 -0,81	1,77 (C) 1,28 (S)	BOTH
5	0,021	0,015	-1,30	1,72	S
6 without values of 28/9	0,087	0,089	-1,27	2,45	C
6 with values of 28/9	0,074	0,073	-1,31	1,69	S

University computer has been used. As well as plotting the data to log-log co-ordinates the program fits a least-squares straight line to this data. The variance calculated by this program is the same as that mentioned in the program of Appendix C1. An example of a section of output from the PHYSPLOT program is shown in Appendix C2.

Graph 2 is a plot of cube-root scaling for seismometers 3,4, C and E, and graph 3 cube-root scaling for seismometers B, D and F.

From the graphs it can be seen that for the underground seismometers, seismometer 2 would be the most restrictive, e.g. for Vmax = 50 mm/sec, $D/W^{1/2} = 1,55$. This means at a distance of 100 m the allowable charge weight is 4162 kg. However, since we are concerned with protecting the integrity of the bord and pillar the restriction should be based on the most conservative of the array 1 seismometers. This is the hangingwall seismometer, F. For V = 50 mm/sec, $D/W^{1/3} = 4,85$, and so if D = 100 m, the allowable charge weight = 8765 kg/delay. The fact that the hanging wall should provide the most restriction is logical since this region is in tension and therefore susceptible to disturbing forces. It is therefore suggested that graph 3, line F, is used for determining the maximum allowable blasting parameters D and/or W. Discussion of the results obtained from the surface seismometer have been left until last because of a strange anomaly that occurred. Sixteen results, covering the period 28/3 to 16/10, were obtained from this seismometer. Using the statistics program in Appendix C1 it was found that cube-root scaling fitted the data best. On 28/9 recordings were made along and adjacent to an earth dam, located in the open-pit workings, of a blast. Seismometers used were the same as those used for array 2, and were all located on the surface. The initial object of this test was to ensure velocity levels along the dam wall were below

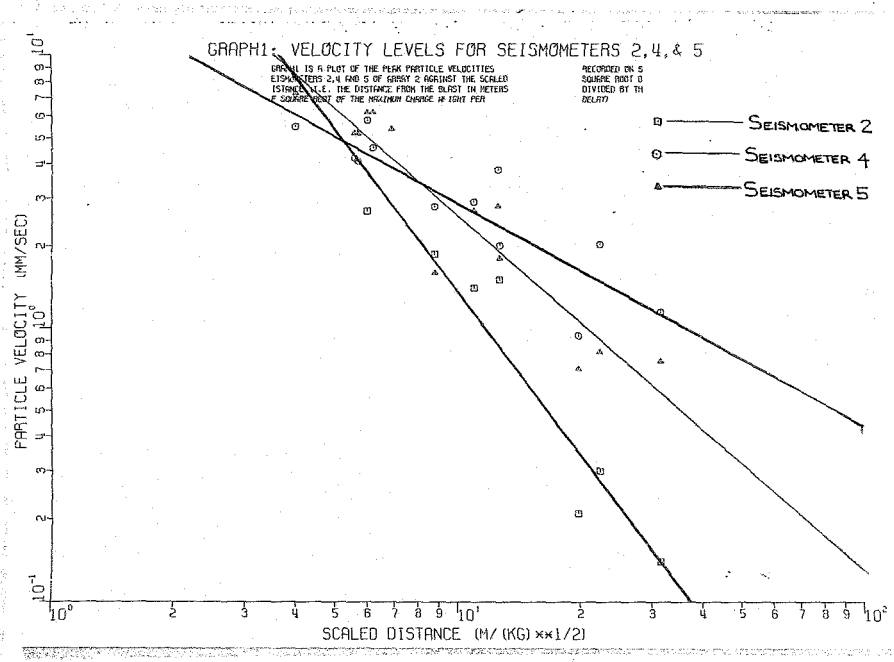
GRAPH1: VELOCITY LEVELS FOR SEISMOMETERS 2,4,& 5
GRAPH IS A PLOT OF THE PEAK PARTICLE VELOCITIES
EISMOMETERS 2,4 AND 5 OF GRAPH 2 AGAINST THE SCALED
ISTANCE, I.E. THE DISTANCE FROM THE BLAST IN METERS
E SQUARE ROOT OF THE MAXIMUM CHARGE WEIGHT PER
RECORDED ON S
SQUARE ROOT D
DIVIDED BY TH
DELAY)
SEISMOMETER 2
SEISMOMETER 4
SEISMOMETER 5
PARTICLE VELOCITY (MM/SEC)
SCALED DISTANCE (M/(KG)××1/2)

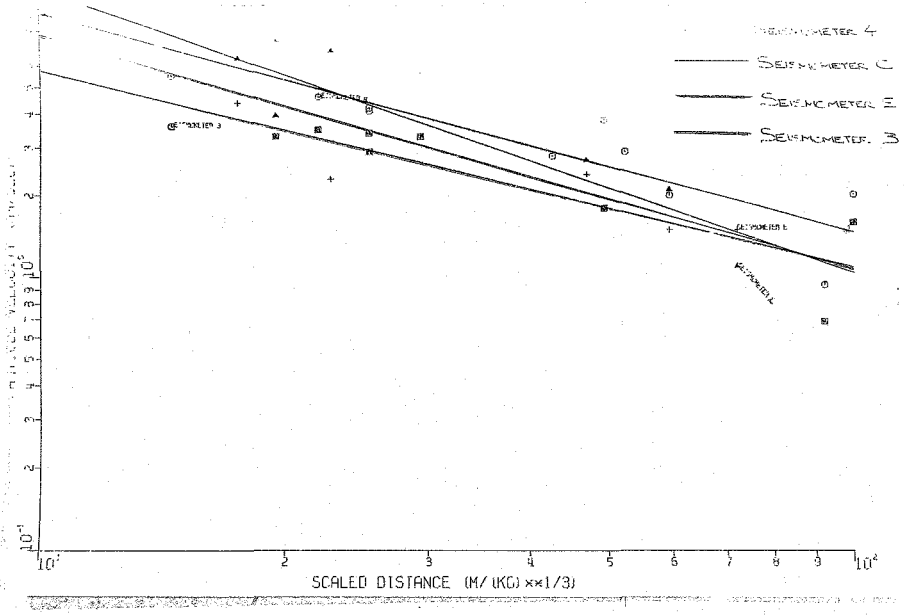
SEISMOMETER 4
SEISMOMETER C
SEISMOMETER E
SEISMOMETER B
SEISMOMETER 3
SEISMOMETER 4
SEISMOMETER E
SEISMOMETER C
10^{-1}
2
3
4
5
6
7
8
9
10^{0}
2
3
4
5
6
7
8
9
10^{1}
SCALED DISTANCE (M/(KG)××1/3)

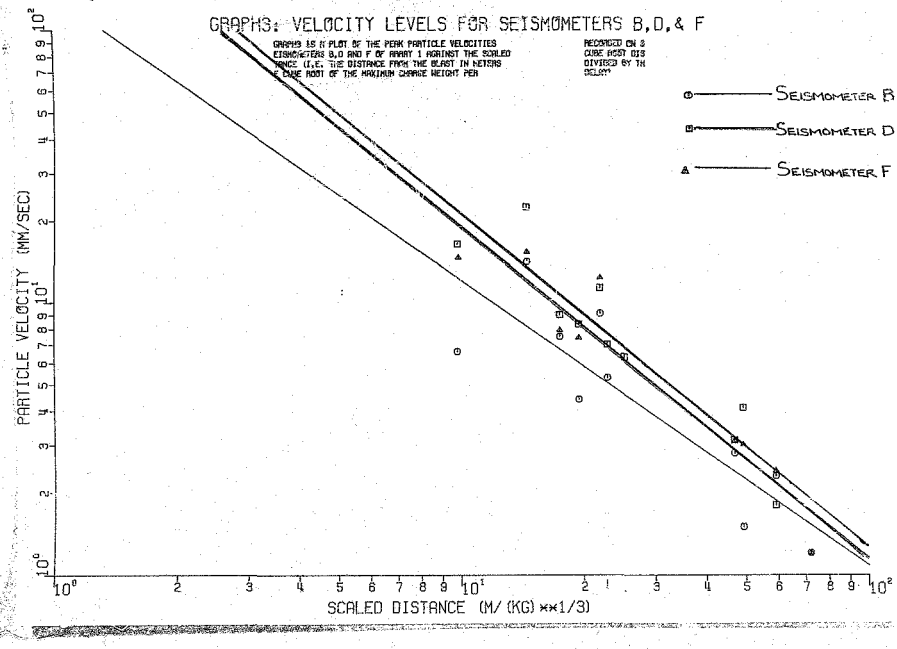
GRAPHS: VELOCITY LEVELS FOR SEISMOMETERS B,D,& F
GRAPHS IS A PLOT OF THE PEAK PARTICLE VELOCITIES
SEISMOMETERS B,D AND F OF AWAY 1 AGAINST THE SCALED
DANCE (I.E. THE DISTANCE FROM THE BLAST IN METERS
E CUBE ROOT OF THE MAXIMUM CHARGE WEIGHT PER
RECORDED ON A
CURE MOST HIS
DIVIDED BY TH
DELAY?
SEISMOMETER B
SEISMOMETER D
SEISMOMETER F
PARTICLE VELOCITY (MM/SEC)
SCALED DISTANCE (M/(KG)**1/3)

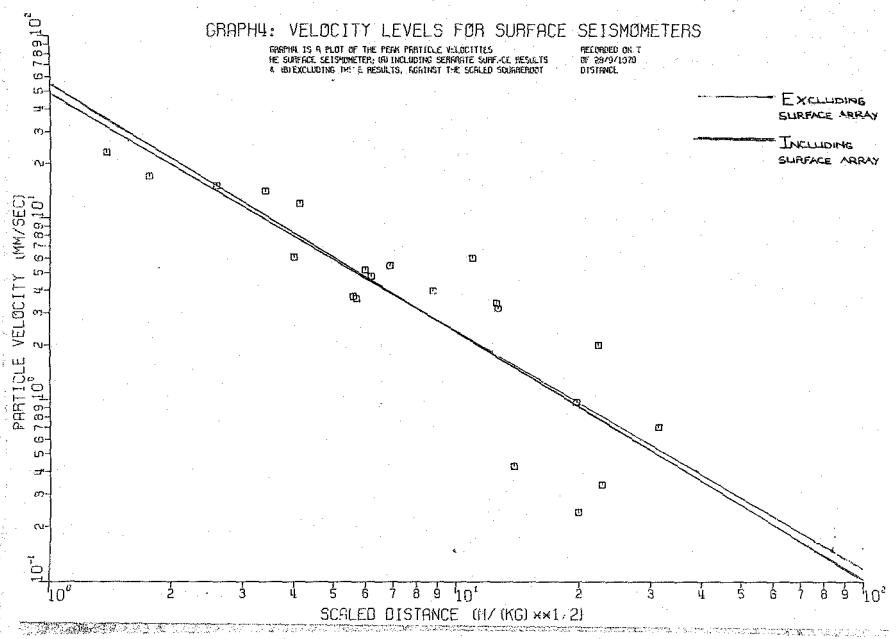
GRAPH4: VELOCITY LEVELS FOR SURFACE SEISMOMETERS
GRAPH4 IS A PLOT OF THE PEAK PARTICLE VELOCITIES RECORDED ON T
HE SURFACE SEISMOMETERS (A) INCLUDING SEPARATE SURFACE RESULTS OF 29/9/1970
& (B) EXCLUDING THESE RESULTS, AGAINST THE SCALED SQUAREROOT DISTANCE
EXCLUDING SURFACE ARRAY
INCLUDING SURFACE ARRAY
PARTICLE VELOCITY (MM/SEC)
SCALED DISTANCE (M/(KG)**1/2)

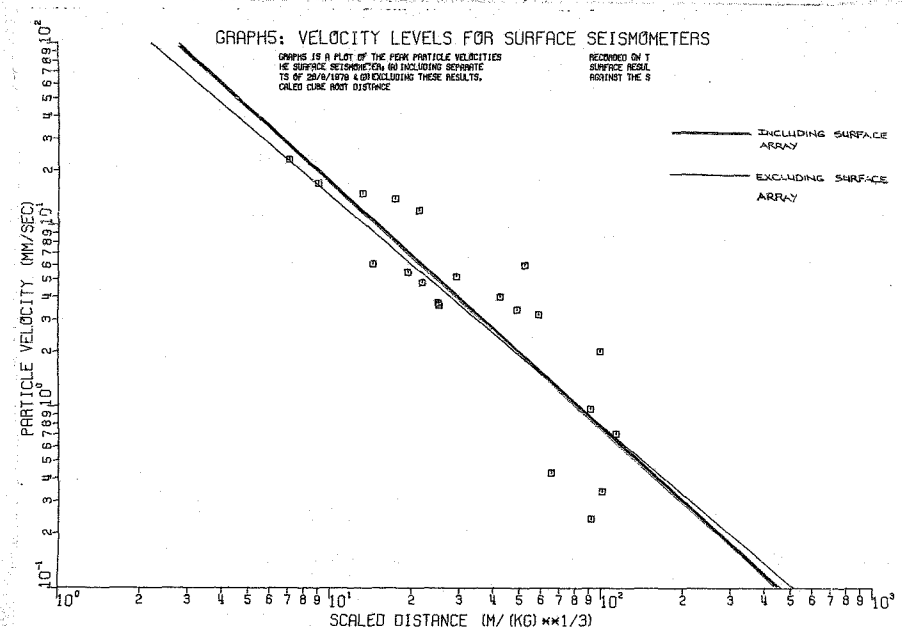
GRAPHS: VELOCITY LEVELS FOR SURFACE SEISMOMETERS
GRAPHS IS A PLOT OF THE PEAK PARTICLE VELOCITIES
HE SURFACE SEISMOMETER, (A) INCLUDING SEPARATE
TS OF 28/8/1978 & (B) EXCLUDING THESE RESULTS.
CALED CUBE ROOT DISTANCE
RECORDED ON T
SURFACE RESUL
AGAINST THE S
INCLUDING SURFACE ARRAY
EXCLUDING SURFACE ARRAY
PARTICLE VELOCITY (MM/SEC)
SCALED DISTANCE (M/(KG)**1/3)

50 mm/sec. This was found to be so, with the largest velocity being measured at 23,0 mm/sec.

It was found that when the five velocities (see Appendix B3) obtained on 28/9 were combined with the 16 results of seismometer 6 the resulting straight line had a lower variance, for cube-root and square-root scaling, than that of the original 16 points. This fact was especially pleasing since totally different recording equipment (BPI designed direct write recorder) was used for the blast of 28/9 and the surface array was located approximately 1 km from seismometer F. An interesting observation is that using the combined data (21 points) square-root scaling now provides the best straight line fit. It is because of this anomaly that 2 graphs, graphs 4 and 5, have been plotted for seismometer 6. Two lines are plotted on either graph, one excluding the results of the surface array of 28/9, and one including this array. For the surface seismometer (6), it is therefore difficult to state conclusively whether cube-root or square-root scaling is preferable. It is suggested that the one giving the most conservative results is always the best one to use, and the maximum value + 10% could possibly be used.

A possible positive result of the above discussion is that now the line for seismometer 6, using the combined data, can be used to limit the peak particle velocity to 50 mm/sec (or whatever limit is decided on) for surface structures, e.g. further earth dams.

3.7 Verification of velocity as a damage criterion

The use of peak particle velocity as a criterion of damage has been thoroughly investigated for surface structures (see Chapter 1 and Reference list). However, the applicability of the velocity criterion to underground systems has received very little attention. A conservative

limit on the allowable velocity level was therefore stipulated.

To determine if the pillars were infact sustaining damage a purely visual system of monitoring was instigated. The pillars were whitewashed so that if any material spalled off the pillars a distinctive black patch would be noticeable. These spalled areas were then marked with different colour paint to denote the time of the observation. Periodic visits were made underground to ascertain the extent of spalling. Initially the amount of damage appeared rather low and it is reasonable to suggest that the spalling which occurred would have occurred naturally, given time, being mainly highly fractured material in the corners of the pillars. The use of the velocity level suggested therefore seems justified in view of the low damage sustained. The question that then arises is what is a safe but not too restrictive allowable velocity level? If the 50 mm/sec velocity level is to be exceeded it would be advisable to install an accurate monitoring system, e.g. strain gauges, to enable the amount of damage to be quantified.

Using the above procedure one is automatically assuming that failure would eventually occur by a gradual spalling of the material from the pillars and hanging-wall. Although this seems a logical assumption one should not disregard the possibility of another mechanism of failure occurring. An attempt has been made in Chapter 5 to determine whether any chance of the natural frequency of the underground workings and thus resonance, being reached existed. This is a potentially dangerous situation where already highly stressed sections occur, e.g. in the hanging-wall. A suggestion for future research is to model the behaviour of a coal pillar under conditions of blast loading and try to predict this type of failure mechanism more accurately.

On the 23rd February 1979 a series of photographs of the whitewashed section of the underground working was taken. In January 1980 this procedure was repeated, an attempt being made to reproduce the same area covered by the original photographs. This was reasonably successful, as can be seen from the series of photographs from C - H. In these photographs the first photograph of the pair represents the condition of the pillar as at February 1979, and the second as at January 1980. The first pair of photographs show that very little damage infact occurred, the only spalling being the two dark patches on pillar B6E. The second pair show the bord area where the instruments were located. Photograph F shows how a large spall of coal in the hanging wall narrowly missed dislodging the instrument located in the hanging-wall. The spalling on the background pillars occurred mainly on the corners of the pillars. The third pair also show how the only spalling occurred in the corner regions of the pillars. An interesting aspect of this third pair is that in the earlier photograph water can be seen in the left foreground. This water originated from the hole drilled from the surface to the underground workings for the instrument cable. Since the bottom of the hole was located beneath the water table it served to drain the area. When the later photographs were taken this water appeared to have dried up. How the changing amount of water present in the rock surrounding the underground workings affected the transmission characteristics of the rock is hard to estimate, but its probable that the water made the transmission more efficient. This same situation is generated by the presence of the open pit as this will tend to dewater the surrounding area as well.

Photograph C

Photograph D

Photograph E

Photograph F

Photographs of underground workings showing damage before and after blasting operations

Photograph C

Photograph D

Photograph E

Photograph F

Photographs of underground workings showing damage before and after blasting operations

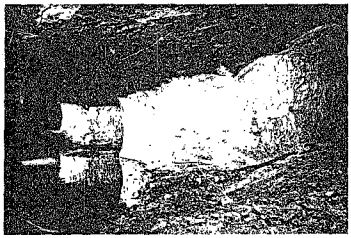

Photograph G

Photograph H

CHAPTER 4

4. THE DIGITIZATION PROCESS - PROCEDURE, RESULTS AND ANALYSIS

4.1 The digitizing procedure

Digitization of the particle velocity versus time records was necessary to facilitate further analysis of these records. The analog-to-digital conversions were performed in the laboratory at the BPI. Fundamental equipment characteristics are mentioned in Chapter 2. A comprehensive description of the equipment can be found in Reference 10.

A sampling rate of 208 and 368 samples/second was used for the above conversions. The sampling rate must be fast enough so that information is not lost in converting the signal into a digital form. A general rule regarding sampling is summarised in the sampling theorem which states, "no information is lost by regular sampling providing that the sampling frequency is greater than twice the highest frequency component in the waveform being sampled". For example, a sampling rate of 4 msec (250 samples per second) will allow perfect recording of a 75 Hz signal but 175 Hz and 250 Hz signals will appear as (i.e. will alias as) 75 Hz and a DC level respectively. Digitized records were only made of the seismic records of array 1, since relative displacements in the piller were to be determined. Frequencies detected by these seismometers rarely exceeded 30 Hz, and the sampling rate which was used should therefore be completely adequate.

One channel at a time was digitized, the digitized record being transferred onto a magnetic tape. During the digitising process a paper record was made of various digitizing parameters. These included the event being digitized, pulse rate, clock record and beginning and end point of digitization process. This record was made at an extremely high paper speed (75 cm/sec) to enable accurate resolution in later analyses.

At the end of each digitized record a digital tape mark was generated, and this defined the end of a file. During the digitizing process this tape mark number as well as the number of samples in the preceding file and the channel being digitized was noted. The significance of these values will be explained later in this chapter.

Whenever an error was encountered during the digitizing process a "parity error" light on the replay consol indicated on. Other types of errors which could occur were, for example, when the digitizer was initiated too late and part of the analog signal was not digitized, (this was recognized from the analog record). The occurrence of a parity error was not serious, unless it occurred on the first file, because subsequent erroneous files can simply be skipped out during later data processing. However if an error is detected on the first file, this file must be re-digitized until no error is present. This is because the main frame computer tape drives could not interpret a tape with an error in the first file. This problem caused a considerable amount of trouble and it sometimes became necessary to manually erase the objectionable first file, using the digitizing facilities.

Once the required number of seismic events have been digitized, the magnetic tape was transferred to the computing centre. This tape is known as a "NO LABEL" (NL) tape and was assigned the name RIETO1. A second tape was initialized as a "STANDARD LABEL" (SL) tape to enable it to be more easily processed by the IBM 370. The initialization program is shown in Appendix C3. This second tape was labelled RIETSL. The data from the NL tape was then transferred to the SL tape. A program for doing this is included in Appendix C4. It is during this transfer process that difficulties were encountered if the first file of the NL tape contained an error. This was the data that was used for further processing.

4.2 Plotting procedure

To ensure that the digitized form of the analog signal accurately represented the original data it was necessary to obtain a visual form of the digitized data which could then be compared with the paper record of the same data.

A program was therefore developed, a copy of which appears in Appendix C.5, to firstly read, and then plot data stored on the SL tape. The data was plotted to a length of 25 cm irrespective of the number of samples in the file being plotted and the maximum value of amplitude in the signal was plotted to 3 cm, the rest of the signal being scaled down accordingly. These plots could therefore not be used for calculating amplitudes or frequencies. Their main function was simply to ensure that the digital data was an adequate representation of the analog signal. This is illustrated in Figure 4.1. The original analog signal is shown on the paper record, which was made during the digitizing process. Figure 4.1b shows the plot from the digitized data. A visual comparison shows that very little data was lost in the digitizing, the only possible loss being of high frequency content.

The importance of noting the number of samples generated when digitizing an event will be explained with reference to an example. The digitization of channel 2 data, recorded on 16/8 generated 9216 samples. Figure 4.2 (a) shows a plot of the entire file of 9216 samples. It would clearly be impossible to tell if this record is an accurate representation of the original data, in this form. However, knowing that 25 cm represents 9216 samples, as shown, it can be seen that 5,6 cm of data is unnecessary and therefore $(5,6/25) \times 9216 \approx 2064$ samples can be neglected. (The method of doing this is covered in Appendix C.5). Figure 4.2(b) shows a second plot of the digital data. This time 2048 samples were skipped and only 1024 plotted. The result is distinctly clearer and can easily be compared with the original signal.

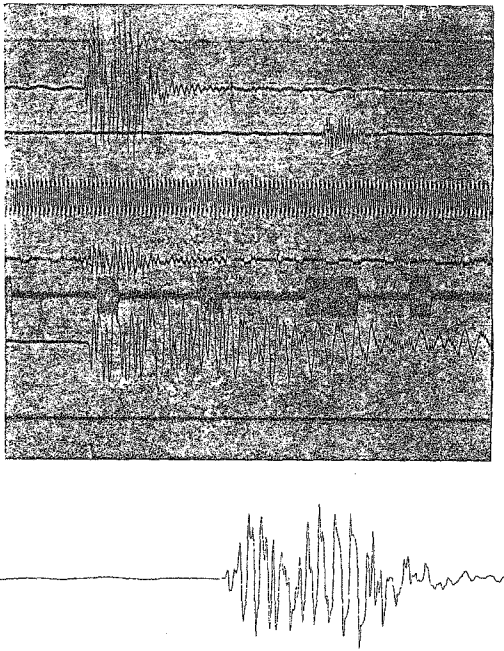

FIGURE 4.1 Comparison of original analog signal with equivalent digitized signal

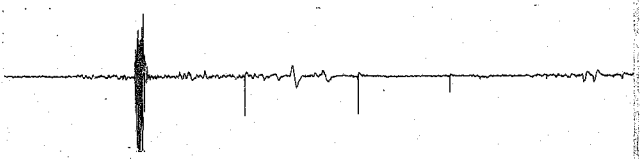

FIGURE 4.2 (a) Data file with all 9216 samples plotted

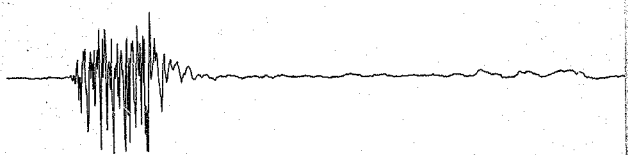

FIGURE 4.2 (b) Same data file with only 1024 points plotted

4.3 Acceleration and displacement records

Conventionally, particle accelerations and displacements have been determined from particle velocity versus time records simply by assuming that the seismic signal is simple harmonic in nature. From the examples shown so far this is clearly not a valid assumption. Having digitized records of particle velocities therefore was a perfect opportunity to determine accurate accelerations and displacements.

Acceleration records were calculated first, using a computer program. This program used the same method of reading data off a tape as the plotting program (C5). Once the data had been read, the acceleration was calculated using a numerical, central difference formula:

i.e. $*\ a_i = \dfrac{V_{i+1} - V_{i-1}}{2\Delta t}$ $\quad i = 1, \ldots\ldots n.$ n = number of

samples in velocity record. This data then had to be stored somewhere. A third tape was now used, also a standard label tape, called COALED. The acceleration records were written onto this tape using the above relationship and the program listed in Appendix C.6. A problem that occurred here was that only one particle velocity record could be differentiated at a time. This was because the FORTRAN tape drive facility on the IBM 360 could not accommodate reading a data file from a tape, processing this data, and then returning to the tape to read another data file all in one computer job. Therefore all computer programs used subsequently had to be run once for every file processed, i.e. a number of files could not be processed simultaneously in one job. If a way could be found to circumvent this problem in the future, the data processing could be greatly speeded up.

Numerical integration was used to calculate displacement-time data from the particle velocity-time records. This data was also stored on COALED. When this data was plotted, however, it was found that a linear trend had been introduced into the data. This meant that the data did not

* a_i - preferential formula $a_i = (v_i - v_{i-1})/\Delta t$

plot horizontally, i.e. before and after the blast record, when displacements should be equal and zero, the displacement values differed significantly. This was caused by a DC offset that had been introduced to some of the particle velocity records by the replay equipment. This means that the zero-velocity datum is offset from its correct position by a finite amount, as illustrated below in Figure 4.3.

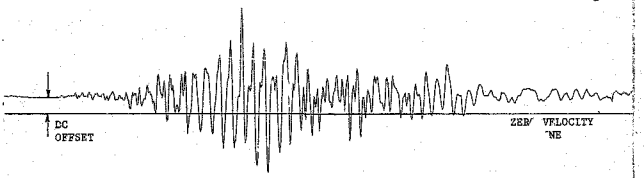

FIGURE 4.3 Data file containing DC offset

A loop was inserted into all programs used, which firstly calculated this DC offset and then removed it from the original data before further processing. The effect is shown in Figure 4.4 The first 4 traces are displacement files with the DC offset present. It would clearly be impossible to accurately determine relative displacements between the points represented by these traces. The last 4 traces are the same files with the DC removed, and it can be seen how the displacement now returns to zero once the blasting effect has subsided.

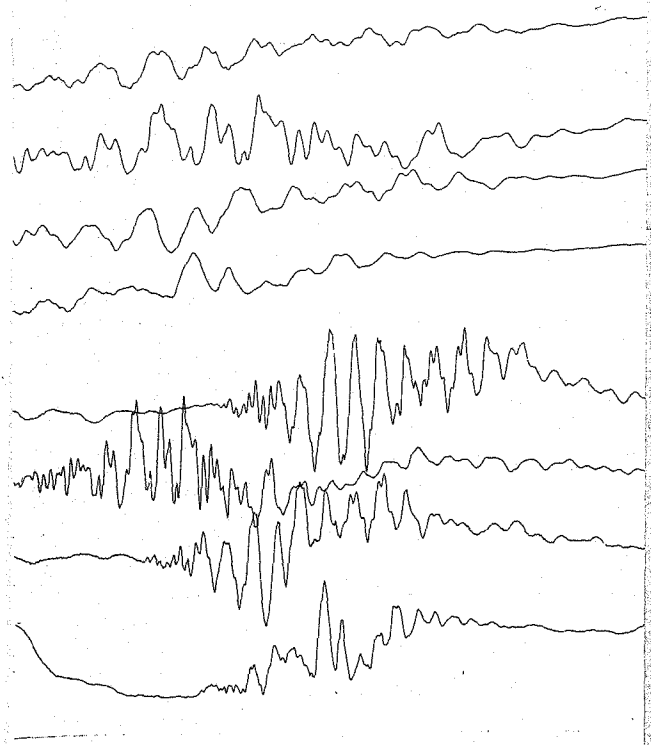

FIGURE 4.4 Comparison of 4 displacement files with a DC offset present and with the offset removed

The reason this error was generated by the displacement computation was that a cumulative integration calculation was used. Unfortunately, this problem did not manifest itself in the acceleration files, and although the shape of the traces were correct, the numerical values were not, and these records had to be recalculated. An example of an acceleration record and the corresponding velocity records is included in Appendix B.2. To determine if data was being lost by the numerical integration and differentiation, the record obtained from the differentiation of a velocity file and then integration of this record was compared with the original velocity record. The comparison was purely visual and as can be seen from Appendix B.3 the resolution is good, with the most predominant effect being to filter high frequencies. No data appears to be lost.

The acceleration and displacement records obtained in the above manner then had to be quantified. This was done with reference to the original paper records of peak particle velocity. The method of doing this is explained in Appendix B.1.

4.4 Comparison of acceleration records obtained from (i) direct differentiation and (ii) simple harmonic assumptions.

As has been mentioned before, it has been conventional in the past to obtain acceleration values from velocity records by assuming the seismic waves behave in a simple harmonic manner. The acceleration is then given by: $a = 2\pi fV$, where V = velocity and f = corresponding frequency of a particular wave. Since accelerations are used as a design criteria (e.g. earthquakes) in a large number of civil engineering codes of practice it was considered useful to determine how accurate the above method of calculating accelerations is. These values were therefore compared with the values found by numerical differentiation. This latter technique should give accurate values of acceleration since the time interval used is extremely small (±4,8 ms), which means the frequency content of the signal

is well defined. The results of this comparison are summarised in Table 4.

Figure 4.5 is a visual comparison of this data. The accelerations from simple harmonic motion calculations are plotted against accelerations obtained by direct differentiation. The line with a slope of 1,0 shows the relationship between these two accelerations if they have a 1:1 ratio. The majority of the points tend to fall below this line. This means the calculation based on the assumption of simple harmonic motion underestimates the value of the acceleration. This is a potentially dangerous situation, and the value of the ratio a_1/a_2 shown in Table 4 can be considered as being a factor of safety.

The accelerations found by the two methods shown appeared to have no direct correlation (i.e. sometimes their ratio is above one and sometimes below one). However, when the time at which the maximum acceleration and maximum velocity occurred were compared, an interesting feature became apparent. When the two peaks coincided with respect to time the value given by simple harmonic motion calculations gave an extremely accurate estimate of the actual acceleration. These points are circled in red on the graph and marked with an asterisk in Table 4. It can therefore be concluded that the assumptions of simple harmonic motion give an accurate estimate of acceleration when the peak acceleration and velocity coincide, and otherwise tend to underestimate the actual acceleration.

4.5 Relative displacements; and stress determinations

Using the displacement records obtained in the previous section it was possible, for the four vertically inclined seismometers, to obtain records of the relative displacements, between the points represented by these seismometers, with respect to time.

TABLE 4

Comparison of acceleration values obtained from direct differentiation with those obtained from assumptions of simple harmonic motion

DATE	SEISMOMETER	VELOCITY (mm/s)	FREQUENCY (Hz)	$a_1 = 2\pi fV$ (mm/s^2)	$a_2 = \Delta V/\Delta t$ (mm/s^2)	a_1/a_2
14/3	B	7,5	15,7	739,8	938	0,79
14/3	C	6,4	18,3	735,8	639,8	1,15
14/3	D	7,9	15,7	779,3	749,3	1,04 *
14/3	E	4,4	15,8	436,8	432,5	1,01 *
14/3	F	9,0	18,3	1034,8	1112,7	0,93 *
20/3	A	1,7	16,0	170,9	231,4	0,79
20/3	B	1,2	13,3	100,3	177,9	0,56
20/3	C	1,1	16,0	110,6	116,4	0,95 *
20/3	D	1,2	13,3	100,3	147,6	0,68
28/3	B	2,3	5,0	72,3	51,3	1,41 *
[illegible]	C	2,1	11,8	155,7	232,4	0,67
[illegible]	D	2,4	7,4	111,6	157,2	0,71
[illegible]	E	1,5	16,8	158,3	262,0	0,60
[illegible]	F	1,8	7,8	636,4	935,8	0,68 *

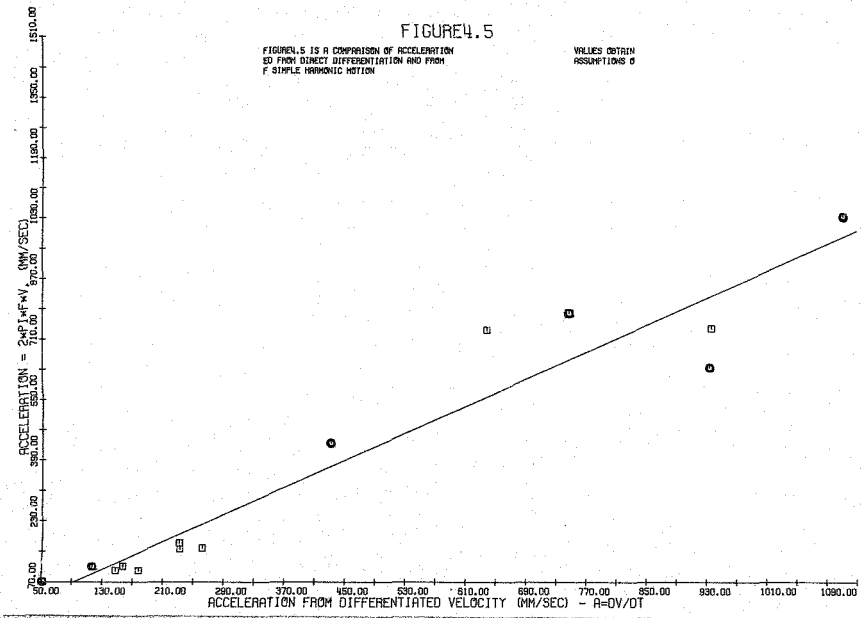
FIGURE4.5
FIGURE4.5 IS A COMPARISON OF ACCELERATION
ED FROM DIRECT DIFFERENTIATION AND FROM
F SIMPLE HARMONIC MOTION
VALUES OBTAIN
ASSUMPTIONS O
ACCELERATION = 2*PI*F*V (MM/SEC)
ACCELERATION FROM DIFFERENTIATED VELOCITY (MM/SEC) - A=DV/DT
50.00
130.00
210.00
290.00
370.00
450.00
530.00
610.00
690.00
770.00
850.00
930.00
1010.00
1090.00
70.00
230.00
390.00
550.00
710.00
870.00
1030.00
1190.00
1350.00
1510.00

To obtain these records the two displacement records to be used in the calculation were shifted with respect to one another, until a time origin common to both records was located, and the subtraction between the two records was then carried out. This data was stored on a magnetic tape in the same way as before. The program used in the above calculations is shown in Appendix C.7.

Relative displacements were calculated for four blasts. The maximum relative displacement was found for each set of two data points by scanning the relative data file. To determine what the instantaneous maximum stress level was during a blast a simple elastic equation of the form

$\sigma = E\varepsilon$ was used, where σ is the stress (N/mm^2)

E is Young's Modulus (N/mm^2)

and ε is the strain given by $\Delta L/L$,

where ΔL= increase in distance between two points

L= original distance between above two points

A representative value for $E = 4 \times 10^3$ MPa (40 kbar) was used. To determine the maximum stress ΔL was approximated by the maximum relative displacement between two points. The assumption of elastic conditions seems valid since the displacements occur over such a short period of time (the order of one tenth of a second). These results are presented in Table 5. The stresses do not appear to be directly related to the blasting parameters other than being approximately inversely proportional to the scaled distance. This is probably due to the inherent non-uniformity of the records. What is noticeable is the consistently low values for seismometers C and E. A possible reason for this could be that the two points are vibrating in phase, which is a potentially dangerous situation. This possibility was

investigated by writing a program to calculate the normalised cross-correlation between two sets of displacement data. The normalised cross-correlation is given by

$$\phi_{xy}(L)_{norm} = \frac{\phi_{xy}(L)}{\{\phi_{xx}(0)\phi_{yy}(0)\}^{\frac{1}{2}}}$$

where $\phi_{xy}(L) = \sum_{i=1}^{n} x_{i+L} y_i$ where L is the offset between the two data sets with respect to time (in our case L = 0).

$$\phi_{xx}(0) = \sum_{i=1}^{n} x_i^2 \quad \text{and} \quad \phi_{yy}(0) = \sum_{i=1}^{n} y_i^2$$

Normalised correlation values must lie between ±1. A value of +1 indicates perfect copy and a value of -1 indicates perfect copy if one of the traces is inverted. In this application therefore, a value of +1 would indicate that the two points are vibrating in perfect harmony.

To check the accuracy of the relative displacement determinations two digitized records were made of the same event. Numerical integration was carried out to get displacement records, and the normalised correlation was carried out after setting these two records to a common time origin as described before. A correlation of +0,969 was achieved which was considered sufficiently accurate. The correlation program, which is shown in Appendix C.8, was then applied to the pairs of displacement records. These values have been included in Table 5, for comparison purposes.

It does appear that a reasonably high degree of correlation occurs between the points represented by seismometers C and E. These values however, are not large enough to suggest resonance being a distinct possibility. From the results presented in Table 5, it would therefore appear that the relative response of points (in a vertical plane) in the underground workings is random and fairly independent of the blasting parameters.

TABLE 5

MAXIMUM RELATIVE DISPLACEMENTS AND CORRESPONDING INSTANTANEOUS STRESSES

DATE	SEISMOMETERS	MAXIMUM RELATIVE DISPLACEMENTS (mm)	MAXIMUM STRESS (MPa)	NORMALISED CROSS CORRELATION
14/3	A and C	0,89	0,03	-0,034
14/3	A and E	0,50	0,007	-0,097
14/3	A and F	1,98	-	0,058
14/3	C and E	0,17	0,004	0,532
20/3	A and C	0,44	0,015	0,319
20/3	A and E	0,83	0,011	0,569
20/3	C and E	0,11	0,002	0,553
28/3	A and C	0,84	0,028	-0,725
28/3	A and E	0,65	0,009	-0,683
28/3	A and F	0,70	-	-0,069
28/3	C and E	0,19	0,004	0,497
16/10	A and C	0,96	0,032	0,492
16/10	A and E	0,88	0,012	0,314
16/10	A and F	1,27	-	0,457
16/10	C and E	0,29	0,006	0,949

Comparison of induced stresses with original stress condition

The induced instantaneous stresses shown in Table 5 were relatively low considering that velocity levels approaching half the recommended maximum level were being achieved. To see what the percentage increase in stress level was a simple calcualtion based on the formula suggested by Salamon and Oravecz (12) was used. This formula is based on the assumption that the whole weight of the overburden above the workings is carried by the pillars. i.e. the average pillar load

$$P_a = \frac{WHA}{A_p} \quad (kPa)$$

where W is the weight of the overburden in kN/m^3

A is the total area of the workings (m^2)

A_p is the total area of pillars (m^2)

H is the depth of the workings below ground level (m)

The density of the material was determined using six samples of sandstone from the drilled cores. An average density of 2315,4 kg/m^3 was found, with a standard deviation of 127,6 kg/m^3. The weight of the overburden is therefore $2315,4 \times 9,81 \times 10^{-3}$

$= 22,71\ kN/m^2$

From measurements taken of the instrumented pillar:

Bord width = 6 m

Pillar width = 6 m

Therefore A = 144 m^2

and A_p = 36 m^2

$$P_a = \frac{22,71 \times 144 \times 56 \times 10^{-3}}{36} = 5,088 \text{ MP}_a$$

which although an approximation, indicates the original stress level to be more than one hundred times higher than the instantaneous induced stresses.

CHAPTER 5

5. FOURIER ANALYSIS TECHNIQUES IN THE INTERPRETATION OF BLAST VIBRATION DATA

5.1 Introduction

During World War II radar was widely used for the detection of aircraft. Problems occurred however, since noise frequency interfered with the interpretation of radar signals. Considerable effort was therefore directed at the detection of signals in the presence of noise. In the early 1950's a research group at the Massachusetts Institute of Technology studied the application of the new science to the field of seismic exploration. The simultaneous rapid development in digital computer technology revolutionarised seismic exploration.

Seismic data is the variation with time of the output of geophones, which record ground movements in the form of either displacement, velocity or acceleration. When dealing with this data we are dealing with the"time domain". It is useful to consider seismic signals as the superposition of a number of sinusoidal waves differing in frequency, amplitude and phase. We are now dealing with signals in the "frequency domain", that is, frequency is now the independent variable. This transformation of data from the time to the frequency domain is facilitated by the Fourier Transform.

5.2 Fourier series and transforms

The French mathematician Jean Baptiste Fourier discovered that periodic time functions can be broken down into an infinite sum of properly weighted sine and cosine functions of the proper frequencies. The mathematical equivalent of this discovery is

$$x(t) = a_0 + \sum_{n=1}^{\infty} a_n \text{Cos}\ (\frac{2\pi nt}{T}) + b_n \text{Sin}\ (\frac{2\pi nt}{T})$$

where T is the period of x(t), i.e. $x(t) = x(t+T)$

Although the Fourier Series is a very useful method of determining the frequency content of a time-varying signal it always requires a periodic time function. This is overcome by allowing the period of the waveform to approach infinity. The resulting function is known as the Fourier Transform. The Fourier Transform pair is defined as:

$$S_x(f) = \int_{-\infty}^{\infty} x(t) e^{-i2\pi ft}\, dt \quad \text{(forward transform)}$$

$$x(t) = \int_{-\infty}^{\infty} S_x(f) e^{i2\pi ft}\, dt \quad \text{(inver[illegible]rm)}$$

$S_x(f)$ is known as the Fourier Transform of x(t) and contains the amplitude and phase information at every frequency present in x(t)

5.3 The discrete finite transform

In order to implement the Fourier transform digitally the continuous analog signal must first be converted into a series of discrete data samples.

The Fourier transform is now calculated as follows:

$$S_x''(f) = \Delta t \sum_{n=-\infty}^{n=+\infty} x(n\Delta t) e^{-i2\pi fn\Delta t} \quad \ldots\ldots\ 5.1$$

where $x(n\Delta t)$ are the measured values of the input function.

The Fourier transform as calculated by the above equation no longer contains entirely accurate magnitude and phase information at all of the frequencies contained in $S_x(f)$. $S_x''(f)$ instead accurately describes the spectrum of x(t) up to some maximum frequency F_{max}, given by

$$F_{max} = \frac{1}{2\Delta t} \quad \text{where } \Delta t = \text{sample spacing.}$$

If the input data is sampled from a zero time reference to time T seconds, then

$$T/\Delta t = N$$

where N is the number of samples, and T is the "time window". This is equivalent to truncating the above equation, meaning we no longer have an infinite number of time points. It is not possible therefore to calculate magnitude and phase values at an infinite number of frequencies between zero Hz and F_{max}. The truncated version of equation 5.1 does not give a continuous spectrum. The discrete finite transform (D.F.T.) is then given by

$$S_x^1(m\Delta f) = \Delta t \sum_{n=0}^{n-1} x(n\Delta t)e^{-i2\pi m\Delta f n\Delta t} \quad \ldots\ldots\ldots 5.2$$

Since only periodic functions have such a 'discrete' frequency spectra, equation 5.2 requires that the input function be periodic with T, i.e. the function observed between zero and T seconds repeats itself with period T for all time. Since a seismic signal does not repeat itself this assumption of periodicity is violated, causing distortion of the transform and the reconstruction of x(t) via the inverse transform.

This effect can be reduced by:

(i) Subtracting any d.c. offset or linear trend from the data.

(ii) Tapering the data at the edges, prior to transforming.
This is called "windowing".

5.4 Windowing

Using the discrete finite transform implies that only a window T units long of the original signal x(t) is being considered, i.e. if the function to be transformed is $f^1(t)$ then

$$f^1(t) = W(t).f(t)$$

where W is the shape of the window function.

Making use of the convolution theorem

$$F^1(\omega) = W(\omega) * F(\omega) \quad (\omega \text{ representing frequency})$$

which is the convolution of the true transform with the transform of the window function.

The most desirable features of a window function are:

(i) A narrow bandwidth, for high frequency resolution, and

(ii) a nearly flat band for good amplitude accuracy.

The simplest window is the "boxcar" function, defined as

$$\Pi(t) = 0 \qquad |t| > \tfrac{1}{2}$$
$$= 1 \qquad |t| < \tfrac{1}{2}$$

The transform of this function is $\frac{\sin \omega}{\omega}$, which possesses a narrow, but strongly sloping central lobe, with high and slowly decreasing side lobes as shown below

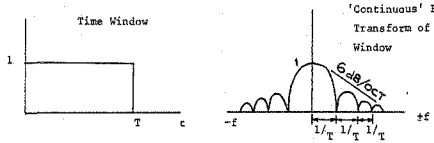

FIGURE 5.1 Rectangular Window and Transform

The strongly sloping central lobe gives poor amplitude accuracy, while the high side lobes cause "ringing" and mask nearby frequencies.

A better window is one which tapers the edges of the function to 0 and T e.g. the Hanning window.

$$W(t) = 1(\tfrac{1}{2} - \tfrac{1}{2}\cos(2\pi t/T))1$$

This then has a wider, less strongly sloping central lobe and small side lobes. This gives better amplitude accuracy and better separation of nearby frequencies. A disadvantage is that the wider centre lobe means that the position of any spectral line is less well defined, as is shown below

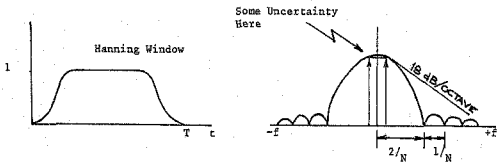

FIGURE 5.2 Hanning Window and Transform

5.5 Application of Fourier techniques to seismic data analysis

Apart from the application of Fourier analysis to conventional seismic data processing various other applications have been instigated, e.g. in 1975 Spottiswoode and McGarr (13) used data from an underground geophone array at E.R.P.M. mine in Boksburg to calculate magnitude and energy content of rockbursts in the vicinity of the above mine, using spectral analysis techniques. Although this investigation was aimed primarily at determining source parameters for the seismic events, whereas our source parameters (blast size, shot distance, etc) are well defined, the analysis techniques are very similar.

The application of spectral analysis techniques to the potential damage capacity of blast induced vibrations is a much neglected field. The object of this chapter is to investigate the usefulness of spectral analysis techniques in analysing blast vibration data. It is by no means a conclusive study, but some very interesting possibilities for further study present themselves.

5.6 The Power spectrum

The power spectrum of a signal is defined as:

$$P(\omega) = F(\omega)\ \overline{F}(\omega)$$

where $P(\omega)$ is the power spectrum

$F(\omega)$ is the Fourier Transform of the time domain $x(t)$

$\overline{F}(\omega)$ is the complex conjugate of $F(\omega)$

The power spectrum by itself gives an immediate indication of the relative importance of various frequencies in a signal. However, it is not a full characterisation of the signal as all the original phase information is lost.

The power spectrum has found many applications in engineering, from

detecting a periodic signal buried in noise to diagosing malfunctions in electrical and mechanical systems (called "Signature Analysis"). The object of this study was to use the power spectrum as a tool for determining whether there was a possibility of resonance occurring in the underground workings.

5.7 Fourier and spectral analysis of blasting data

In order to analyse the velocity-time data using the spectral analysis techniques just discussed a program was developed to calculate, among other things, the Fourier Transform of the original signal, displacement-time relationships, energy, power spectrum and spectral density of the original signal. This program is included in Appendix C9 together with a discussion of the input requirements and capabilities of the program. No further discussion of the program will be included in this chapter, and only the results obtained using the program and accompanying discussion will be included. The input for the program was limited to data obtained from the hanging-wall seismometer. This was due to two reasons:

(i) This seismometer provided more data than any of the other seismometers (nine events).

(ii) Peak-particle velocities were a maximum in the hanging-wall and since this zone is usually in tension and is less restrained than the pillars, the possibility of resonance occurring seemed more likely.

5.7.1 Investigation into possible resonance using Power Spectrum

As mentioned before, the Power Spectrum of a signal gives a very good indication of the relative importance of different frequencies present in the signal. A capacity for calculating the Power Spectrum of the Fourier

Transformed data was therefore included. To test the effectiveness of this calculation, a digitized 14 Hz calibration signal was used as input for the program. The resulting Power Spectrum is shown in Figure 5.3 (a). As can be seen, only one peak occurs, that at 14 Hz. The peak should theoretically be a spike at 14 Hz. The reason for the shape in Figure 5.3 (a) can be seen from the original raw data input, shown in Figure 5.4. It is clearly impossible to get a completely undistorted signal and therefore the amplitude of the power spectrum either side of 14 Hz is a finite value. This is also due to time digitizing errors i.e. not all the frequencies have exactly the same number of samples in them. The amplitude of the power spectrum at 14 Hz is 1140 units while the amplitude of the input signal (48 mv) correspond to 4,8 mm/sec.

The power spectrum of the nine blast induced seismic signals can now be compared with Figure 5.3 (a). These are shown in Figure 5.3 (b) - (k). There is a general trend for higher frequencies to be present in those signals recorded for blasts which occurred close to the monitoring equipment e.g. Figures 5.3 (d), (e) and (h) which correspond to distances of 125 m, 190m and 155 m respectively. Compare this with Figure 5.3 (j) for which there is no significant signal above 30 Hz. This spectrum corresponds to a distance of 1500 m. The reason for this is because the higher frequencies are attenuated more rapidly whereas low frequencies (<20 Hz) are transmitted for large distances as the energy loss is proportional to frequency and in addition these frequencies possess most of the energy.

There appears to be no direct correlation between the amplitude of the Power Spectrum and either distance from blast (d), charge weight/delay (w), velocity (v) or $D/\sqrt{W}$. This was established by plotting the various combinations on both ordinary and log-log graph paper. It was therefore concluded that the power spectrum is not dependent on any of the blasting parameters previously discussed. A blasting parameter which could affect the power spectrum amplitude is the delay interval which occurs between

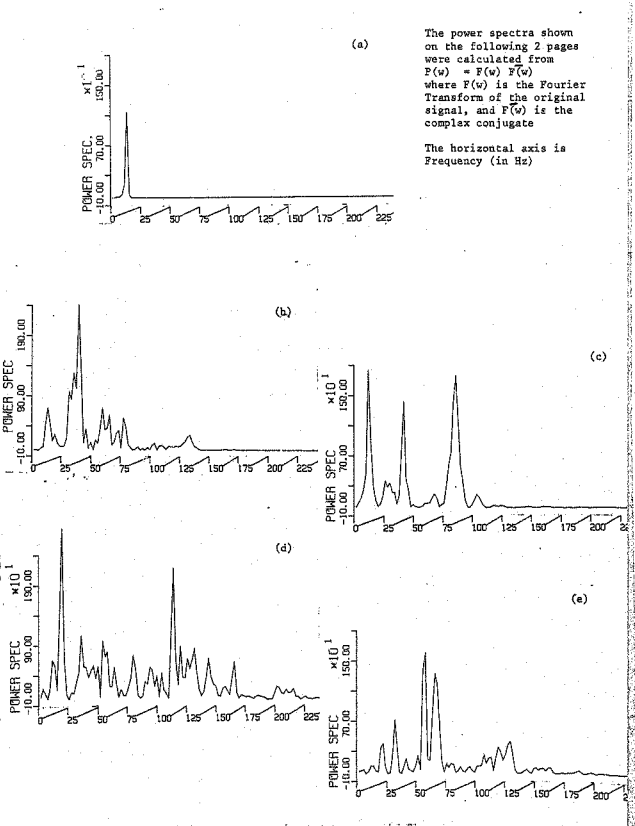

The power spectra shown on the following 2 pages were calculated from $P(w) = F(w)\,\overline{F(w)}$ where $F(w)$ is the Fourier Transform of the original signal, and $\overline{F(w)}$ is the complex conjugate

The horizontal axis is Frequency (in Hz)

FIGURE 5.3 Power Spectra for hanging-wall seismometer

(f)
POWER SPEC.
×10 1
150.00
70.00
-10.00
0
25
50
75
100
125
150
175
200
(g)
POWER SPEC.
×10 1
70.00
30.00
-10.00
(h)
POWER SPEC.
×10 1
70.00
30.00
-10.00
(j)
POWER SPEC.
310.00
150.00
-10.00
(k)
POWER SPEC.
×10 1
150.00
70.00
-10.00

(f)
POWER SPEC
×10 1
150.00
70.00
-10.00
0
25
50
75
100
125
150
175
200
(g)
POWER SPEC
×10 1
70.00
30.00
-10.00
(h)
POWER SPEC
×10 1
70.00
30.00
-10.00
(j)
POWER SPEC.
310.00
150.00
-10.00
(k)
POWER SPEC.
×10 1
150.00
70.00
-10.00

the detonation of the various holes constituting a blast. Insufficient data concerning this factor was available to make a significant comparison. An interesting feature is the single large amplitude spike in Figure 5.3 (k). This could have been predicted by looking at the raw data for this signal shown in Figure 5.4. There appears to be a very regular frequency present in this signal which manifests itself as the large spike.

This brings us to the question of whether there is a danger of resonance occurring in the hanging-wall. The largest amplitude is barely twice as large as the calibration signal, which only corresponded to a peak particle velocity of 4,8 mm/sec. This, coupled with the fact that no extraordinary large displacements were recorded, leads to the conclusion that the hanging-wall system is too restrained and damped for resonance at these frequencies to be a danger.

The maximum values of power spectrum are tabulated below in Table 6.

TABLE 6

Figure 5.3	Power Spectrum	Kg/relay	Distance (m)	Velocity mm/sec
(a)	1140			4,8
(b)	241	500	373	3,1
(c)	1830	2495	310	7,0
(d)	2847	2050	125	16,4
(e)	1610	2260	190	22,4
(f)	1868	1850	270	11,3
(g)	897	10500	1300	1,8
(h)	633	500	155	8,3
(j)	447	9000	1500	9,0
(k)	1852	2900	250	-

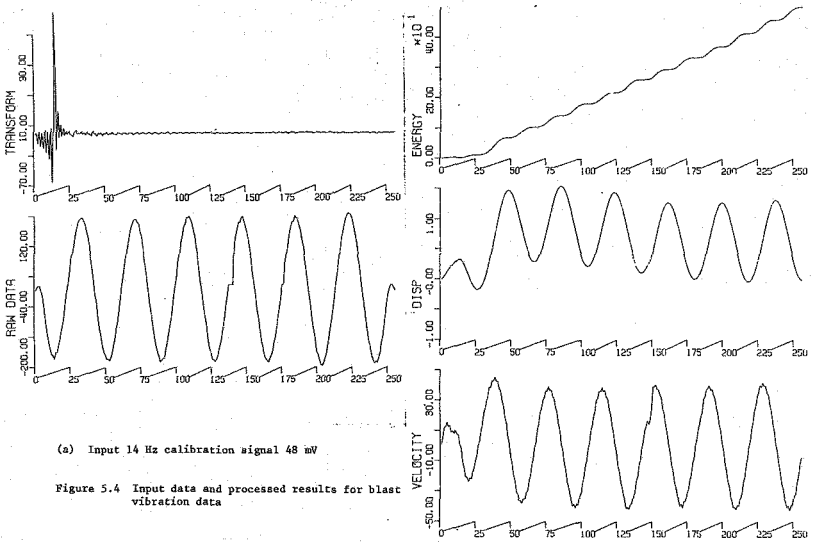

(a) Input 14 Hz calibration signal 48 mV

Figure 5.4 Input data and processed results for blast vibration data

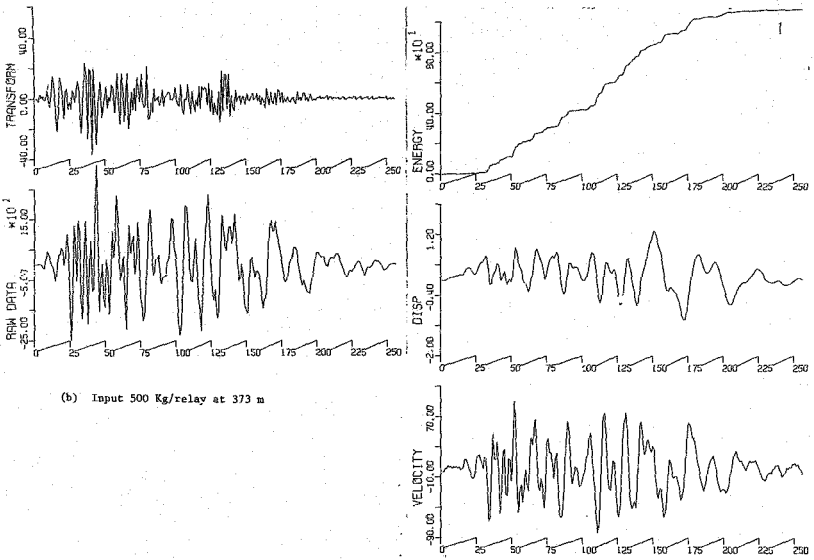

(b) Input 500 Kg/relay at 373 m

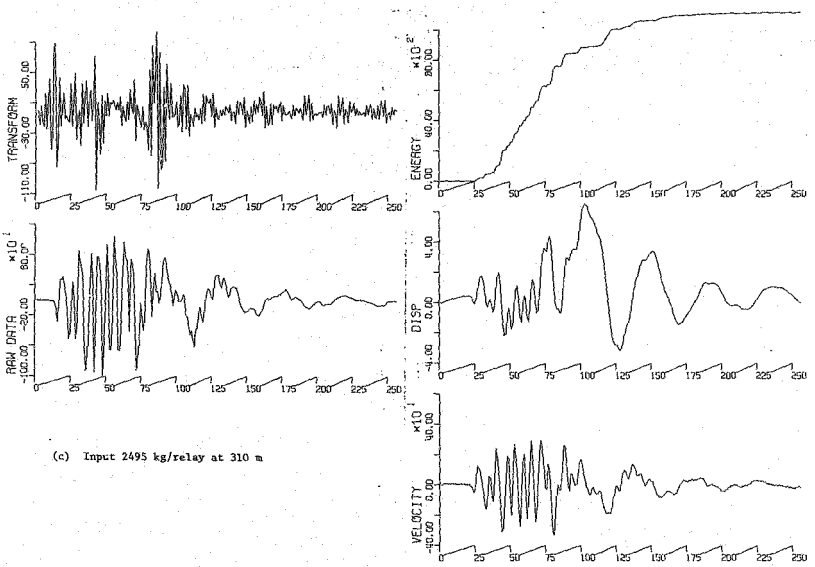

(c) Input 2495 kg/relay at 310 m

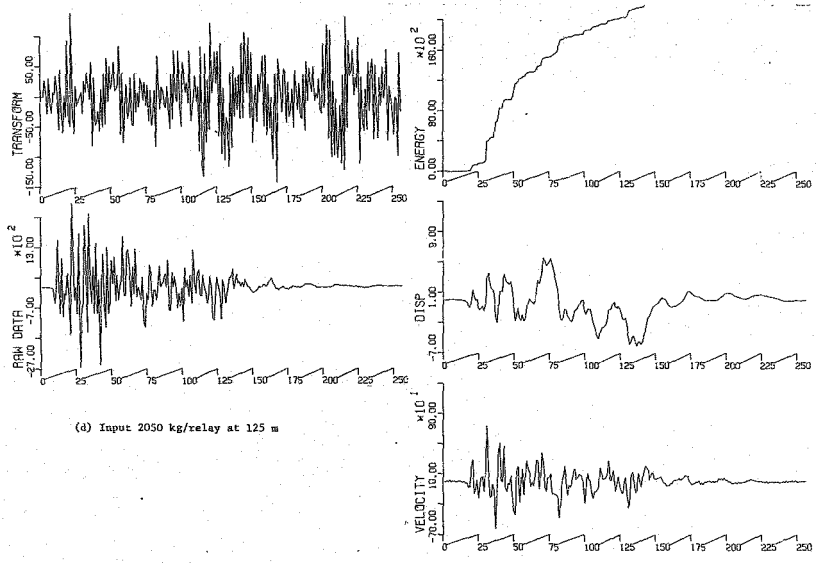

(d) Input 2050 kg/relay at 125 m

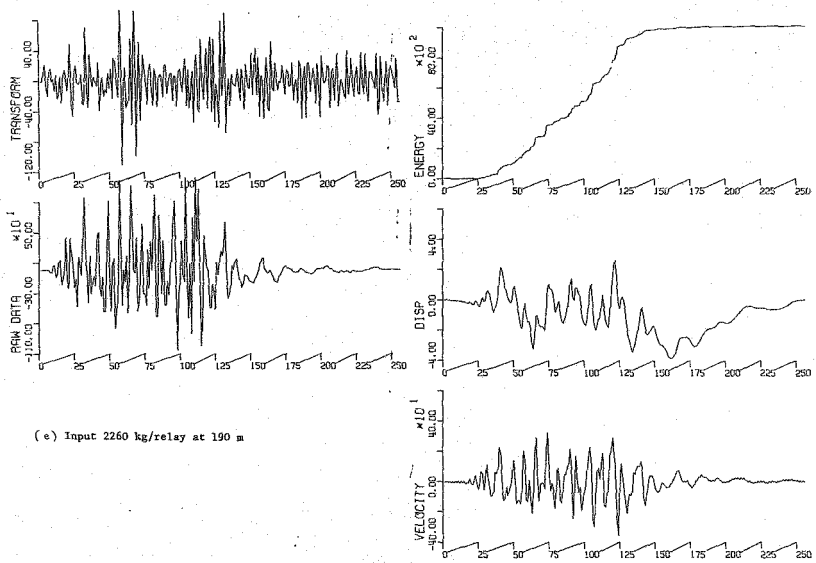

(e) Input 2260 kg/relay at 190 m

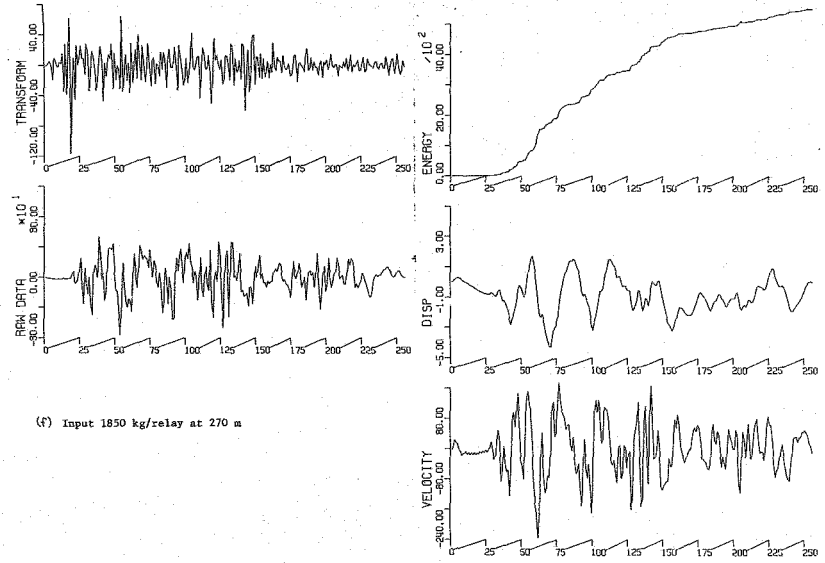

(f) Input 1850 kg/relay at 270 m

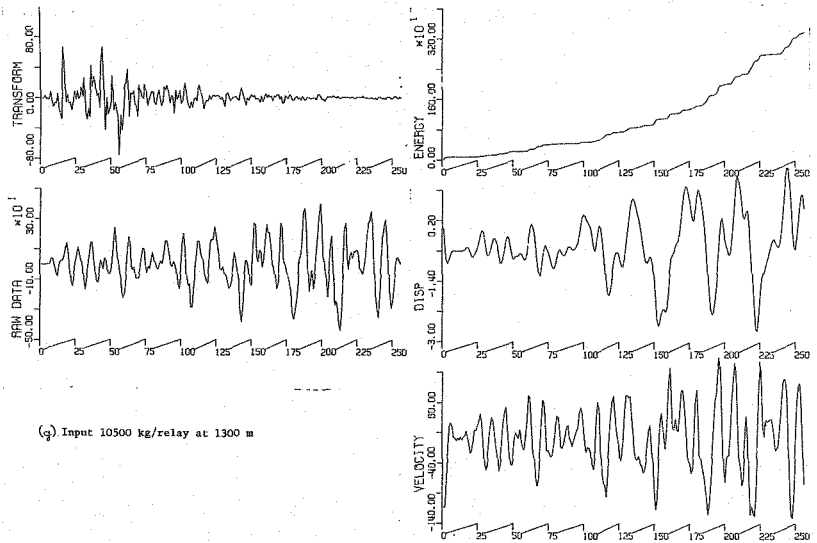

(g) Input 10500 kg/relay at 1300 m

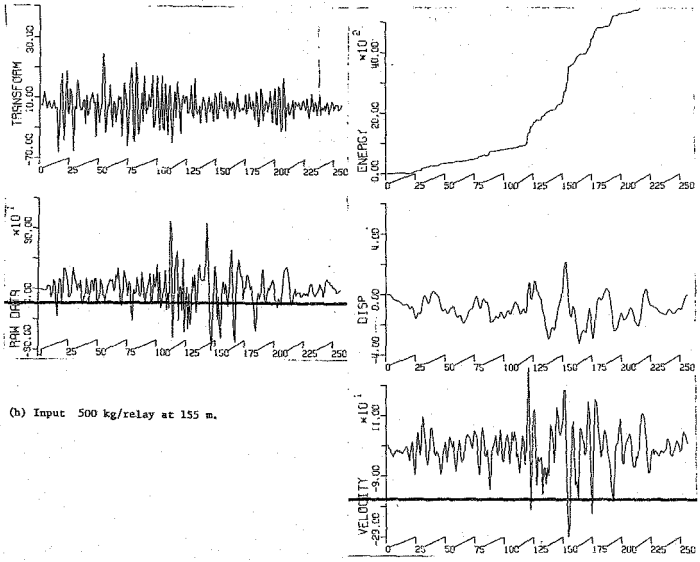

(b) Input 500 kg/relay at 155 m.

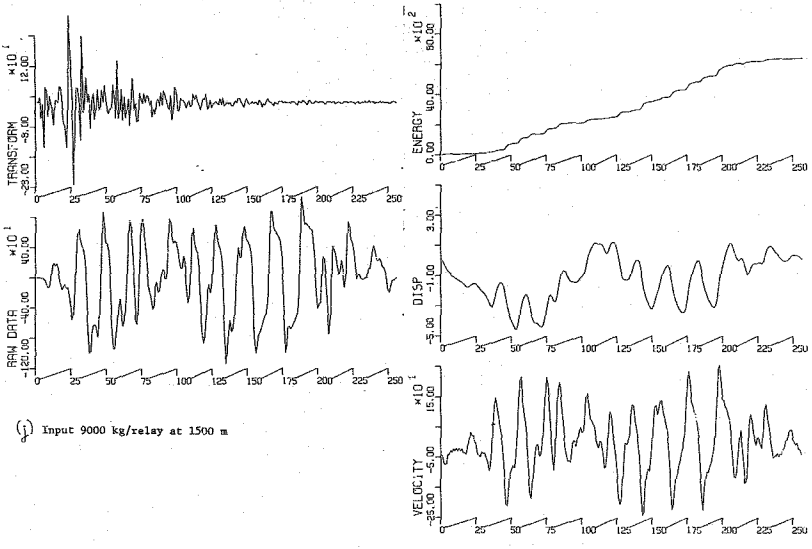

(j) Input 9000 kg/relay at 1500 m

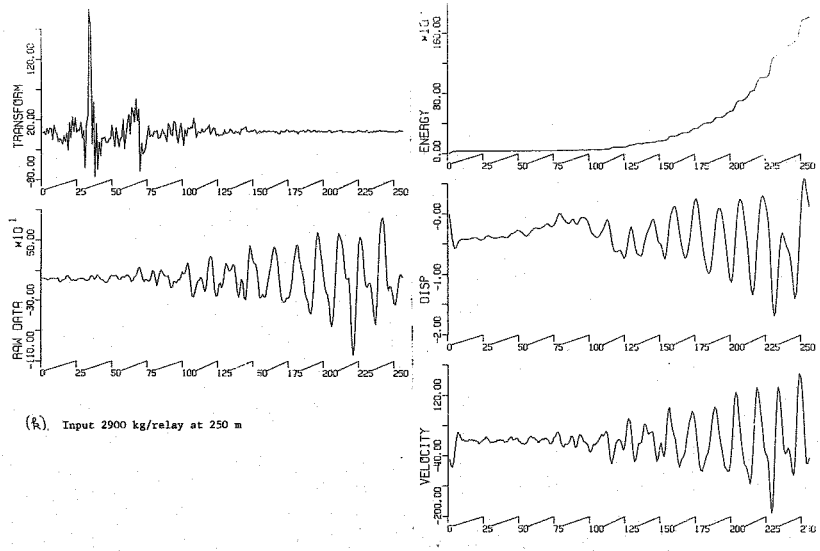

(k). Input 2900 kg/relay at 250 m

FIGURE 5.5 GRAPH OF TOTAL ENERGY PRESENT IN A SIGNAL

THIS GRAPH PLOTS THE ENERGY IN A SEISMIC SIGNAL, OBTAINED FROM THE SQUARE OF THE SUM OF THE GROUND PARTICLE VELOCITIES MULTIPLIED BY THE HYPOCENTRAL DISTANCE SQUARED, AGAINST THE TOTAL CHARGE WEIGHT OF A MINING BLAST

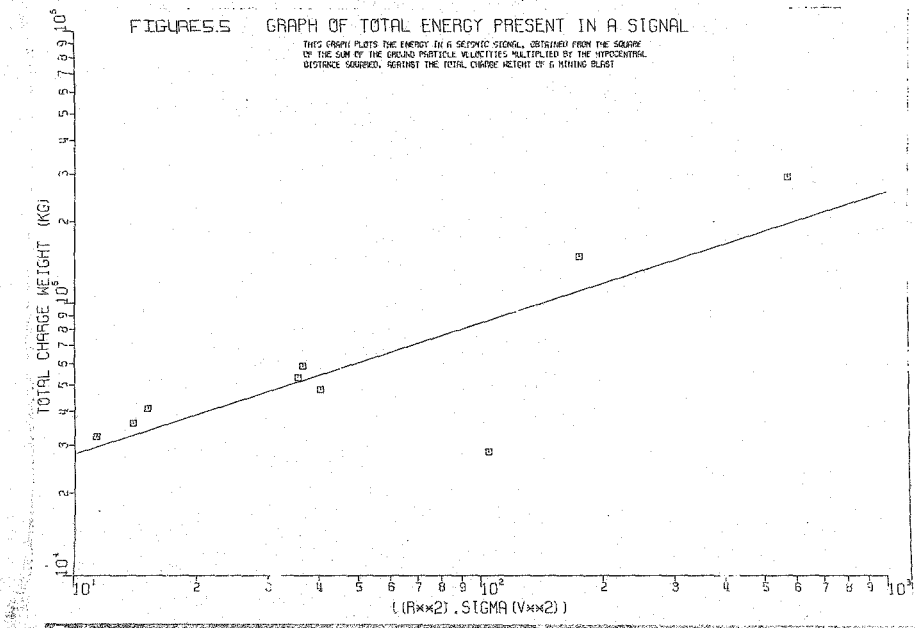

5.7.2 Relation between energy present in a signal and size of blast

In 1972 Perret (17) showed that for equidirectional radiation and for r>>c/w (where r is the hypocentral distance, c is seismic wave velocity and w is angular frequency), the seismic energy radiated by the source in the form of P or S waves is

$$E_c = 4\pi\rho c r^2 \int v_c^2 dt$$

The average seismic wave velocity for sandstone is about 2,5 - 4,0 km/sec (18) and the average frequency for seismometer F was ±20 Hz, therefore

$$w = 125,66 \text{ Hz}$$

$$c/w = 2500/125,66$$

$$= 19,89 \text{ m (or } 31,8 \text{ m if 4 km/sec is used)}$$

and since the minimum value of r is 125 m the above formula may perhaps not be strictly applicable. The energy content of the signal is determined in the program from a summation of the square of the velocity.

Using the value obtained in this manner a relationship between Σv^2 and size of blast was sought. It was found that the total weight per blast, and not the maximum charge weight per delay, provided the best relationship when plotted against $r^2\Sigma v^2$. This relationship is shown in Figure 5.5. A straight line was fitted to the data using log-log coordinates and although there is some scatter, and one outlier (the blast of 2/3), the direct proportionality relationship between energy and $r^2\Sigma v^2$ is verified. A possible reason for the scatter of results is that it was not always possible to ensure the time window chosen included all the velocity-time data. Some data may therefore have been lost.

The above relationship could be useful in determining the size of

an unknown blast by measuring the velocity-time history. The unknown distance could be obtained from standard earthquake location programs. It is unfortunate that much of the data is closely grouped. This is because of the mine practice of having very similar sized blasts.

The establishment of the above proportional relationship is especially pleasing since both seismic velocity and density are assumed to be constant by writing charge weight as $r^2 v^2$. There is in fact a variation of these properties (Shale, sandstone and coal all having different properties). A worthwhile study may be to establish whether this is the case for other rock/soil system as well.

5.7.3 Calculation of source moment from spectral density

The low frequency "plateau" of the spectral density is proportional to the seismic moment. The exact relationship is given by: (16)

$$\Omega(o) = \frac{M_o \beta^2 R_p(\theta,\phi)}{4\pi r G \alpha}$$

where $\Omega(o)$ is the low frequency limit

M_o is the seismic moment

$R_p(\theta,\phi)$ is the geometric radiation pattern

r is the source-monitoring point distance

α, β are the P and S-wave velocities respectively

From the above equation, $M_o \propto \Omega(o).r$ and since r is known for each blast and $\Omega(o)$ can be found from the displacement spectrum, relative values of M_o can be calculated for each blast. Absolute values were not calculated because the radiation pattern is a totally unknown quantity, especially considering the number of free faces encountered by the seismic signal. To see if this relationship holds for blasting vibrations the

product $\Omega(o)$ was calculated in program C9 and is stored in array SPECT. For further details see comment statements in Appendix C9.

The values calculated as above are shown in Figure 5.6 and the spectral densities are included in Figure 5.7. Once again when the parameters (total charge weight and $\Omega(o).r$) were plotted on log-log coordinates a very good correlation was found to exist. Figure 5.6 shows this data plotted on log-log axis with a straight line fitted to the points. A correlation as good as that obtained is very surprising because the geometric radiation pattern away from the source is assumed to be constant, which is unlikely because of the layering of the overburden and the numerous free faces present in the underground workings.

However, the direct relationship is obvious and this once again enables unknown blast sizes to be established to some degree of accuracy simply by measuring ground movements. Amplitude spectra observed shows that the product $\Omega(o).r$ is proportional to the rockburst size, or the energy released by the rockburst. This study indicates that this value could perhaps be quantified and related to the amount of energy released by mining excavations.

5.8 Conclusions

Theuse of spectral analysis techniques in analysing blast vibration data provides some useful information. If the danger exists that vibrations due to blasting may have the same frequency as the natural frequencies (fundamental and overtones) of an underground system, this will become evident by the constant monitoring of the Power Spectrum induced by such blasting. It is suggested that this fact may find even more significant application in determining the overall stability of already built above-ground slender structures, e.g. microwave towers and high-rise buildings.

The relationship between the total charge weight of a blast and both the products $r^2 Iv^2$ and $\Omega(o).r$ were reasonably successfully proved.

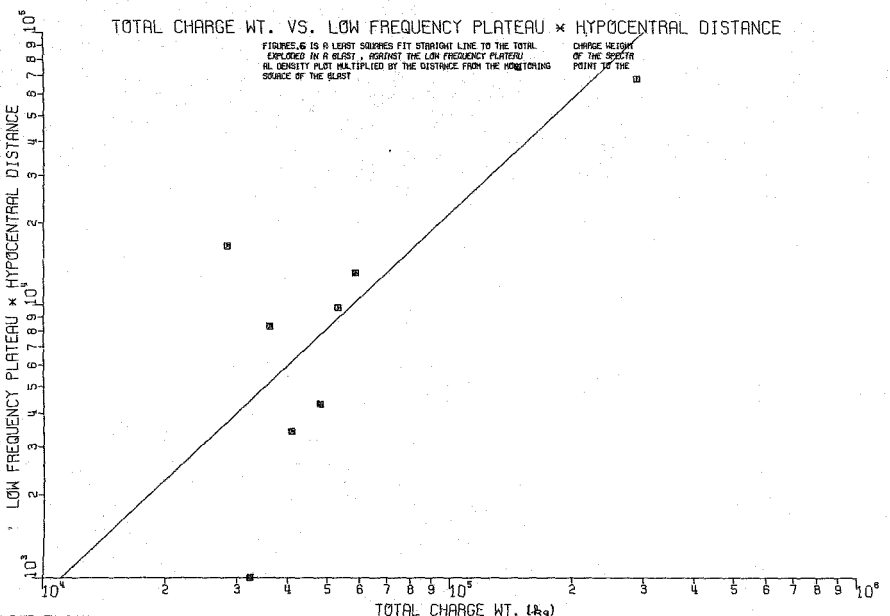
TOTAL CHARGE WT. VS. LØW FREQUENCY PLATEAU × HYPOCENTRAL DISTANCE
FIGURE 6 IS A LEAST SQUARES FIT STRAIGHT LINE TO THE TOTAL CHARGE WEIGHT
EXPLODED IN A BLAST , AGAINST THE LØW FREQUENCY PLATEAU OF THE SPECTRA
AL DENSITY PLOT MULTIPLIED BY THE DISTANCE FROM THE MONITORING POINT TO THE
SOURCE OF THE BLAST
LØW FREQUENCY PLATEAU × HYPOCENTRAL DISTANCE
TOTAL CHARGE WT. (lbs)

Figure 5.7 Amplitude Spectral Densities for Hanging Wall Seismometer
(a) Input - 14 Hz calibracion signal, 49 mV

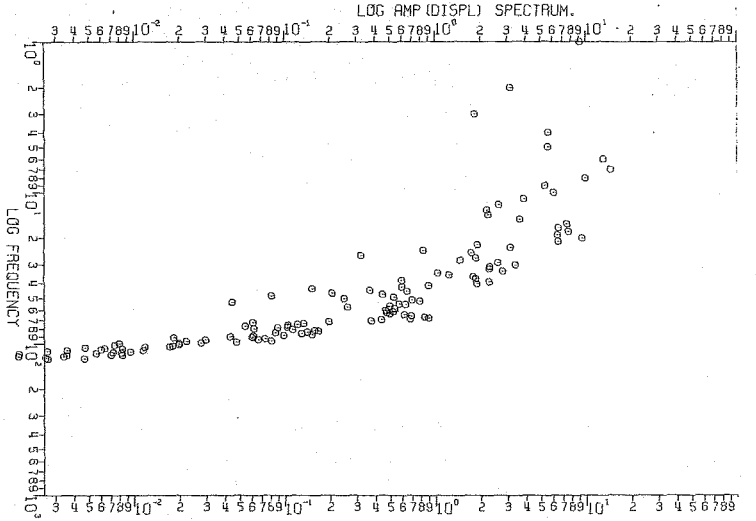

(b) Input 500 Kg/relay at 373 m

(d) Input 2050 Kg/relay at 125 m

(e) Input 2260 Kg/relay at 190 m

(f) Input 1850 Kg/relay at 270 m

(g) Input 10500 Kg/relay at 1300 m

(h) Input 500 kg/relay at 155 m

(j) Input 900 Kg/relay at 1500 m

(k) Input 2900 Kg/relay at 250 m

APPENDIX A : Statistics related to Blasting Operations

APPENDIX A1 Example of blast statistic supplied by mine

TIME	DATE	TYPE	NUMBER OF HOLES	BURDEN	SPACING	AVE DEPTH	BCM OR TONS	KG EXPLOSIVES	% AL	CORDTEX ROLL	CORDTEX TYPE	PENTOLITES NO	PENTOLITES TYPE	DELAY NO	DELAY TYPE	P.F. TARGET	P.F. ACTUAL	AVE. COLLAR ELEVATION	DIST FROM TAVISTOCK	DIST FROM DAM WALL	TIME OF BLAST	kg/RELAY	TOTAL COST	COST BCM OR T	REMARKS
[illegible]	1-7-77	COAL	200	4	6	7	53760t	7943	6	14	[illegible]	200	130	–	–	0,14	0,15	+1519	2200		1635	7943	[illegible]	R 0,[illegible]	
[illegible]	[illegible]-5-77	[illegible]	620	3	3	1,5	133721t	3000	[illegible]	16	[illegible]	–	–	–	–	0,2	0,27	+1509	3500		1600	3000	2547	0,19	
[illegible]	[illegible]	COAL	365	4	6	6	F40%t	16743	6	21	[illegible]	172	150	–	–	0,14	0,17	+1518	2100		1600	16743	7251	0,0[illegible]	
[illegible]	[illegible]	[illegible]	264	3	3	1	[illegible]	825	DYN.	7	[illegible]	–	–	–	–	0,2	0,25	+1520	1900		1215	825	547	0,26	
[illegible]	[illegible]	COAL	177	4	6	6	[illegible]	7647	6/4	12	[illegible]	394	150	–	–	0,14	0,17	+1517	1900		1505	7647	[illegible]	0,07	
[illegible]	[illegible]	COAL	137	4	6	6	[illegible]	5546	9	[illegible]	[illegible]	579	150	–	–	0,14	0,15	+1519	1900		1645	5546	2256	0,07	
[illegible]	[illegible]	[illegible]	[illegible]	5,6	11,2	12-42	125000	450 677	11	154	[illegible]	911	400		40	0,7	0,7	+1573	500		1500	7800	[illegible]	0,27	
[illegible]	[illegible]	COAL	174	4	6	6	[illegible]	6132	4	14	[illegible]	358	150	–	–	0,14	0,14	+1536	1500		1530	6132	[illegible]	0,56	
[illegible]	[illegible]	[illegible]	243	3	3	1	[illegible]	1075	DYN	12	[illegible]	[illegible]	–	[illegible]	–	0,2	0,49	+1512	3600		1115	1075	1217	0,[illegible]	
[illegible]	[illegible]	[illegible]	44	5,6	11,2	12	[illegible]	22 000	11	5	[illegible]	[illegible]	[illegible]		40	0,7	0,66	+1571	750		1515	3500	[illegible]	0,27	
[illegible]	[illegible]	COAL	150	4	6	5	[illegible]	4455	4	10	[illegible]	[illegible]	150	–	–	0,14	15	+1534	1400		1600	4455	2046	0,07	
[illegible]	[illegible]	[illegible]	260	8	8	21	[illegible]	[illegible]	6	30	[illegible]	[illegible]	400		[illegible]	0,7	0,5	+1532	3600		1415	5650	[illegible]	0,19	
[illegible]	[illegible]	[illegible]	474	3	3	1,5	[illegible]	[illegible]	6/4	17	[illegible]	915	150	–	–	0,3	0,78	+1507	3700		1415	8328	[illegible]	0,37	
[illegible]	[illegible]	[illegible]	164	8	8	15	100000	48034	9	28	[illegible]	200	400		40	0,5	0,45	+1573	270		1520	1850	1906	0,19	
[illegible]	[illegible]	COAL	320	4	6	5	[illegible]	10561	4	21	[illegible]	[illegible]	[illegible]	–	–	0,14	0,17	[illegible]	1400		[illegible]	10561	[illegible]	0,075	
[illegible]	[illegible]	[illegible]	104	8	8	19	[illegible]	56745	9	[illegible]		[illegible]	400	[illegible]	[illegible]	0,5	0,47	+1581	190		1505	2260	[illegible]	0,19	
[illegible]	[illegible]	[illegible]	201	4	6	6	46300t	6075	4	15	[illegible]	[illegible]	150	–	–	0,14	0,13	+1532	1300		1715	6075	[illegible]	0,06	
[illegible]	[illegible]	[illegible]	104	8	8	19	[illegible]	53185	9	36	[illegible]	[illegible]	400			0,5	0,42	+1583	125		1500	2050	[illegible]	0,20	
[illegible]	[illegible]	COAL	241	4	6	6	35526t	8100	6	8	2	–	–	–	–	0,14	0,15	+1508	4400		1630	8100	7772	0,07	
[illegible]	[illegible]	COAL	66	4	6	6	[illegible]	[illegible]	6	3	[illegible]	[illegible]	150	–		0,14	0,19	+1509	4200		1215	[illegible]	1366	0,09	
[illegible]	[illegible]	COAL	[illegible]	4	6	6	[illegible]	5180	6	5	[illegible]	[illegible]	[illegible]	–	–	0,14	0,17	[illegible]	1900		1600	5180	[illegible]	0,08	
[illegible]	[illegible]	[illegible]	67	8	8	[illegible]	[illegible]	[illegible]	9	10	[illegible]	[illegible]	400			0,5	0,60	+1572	450		1500	[illegible]	15855	0,16	
[illegible]	[illegible]	[illegible]	167	3	3	–	[illegible]	1050	DYN	5	[illegible]	–	–	–	–	0,2	0,22	+1505	3900		[illegible]	1050	1140	0,24	
[illegible]	[illegible]	[illegible]	73	8	8	21	[illegible]	57277	9	11	[illegible]	1	[illegible]			0,5	0,38	+1582	125		1500	510	10852	0,15	
[illegible]	[illegible]	COAL	261	4	6	7	70157t	9850	[illegible]	10	[illegible]	25	150	–	–	0,14	[illegible]	+1536	1500		[illegible]	9850	[illegible]	0,065	
[illegible]	[illegible]	COAL	164	4	6	5	31492t	4282	4	7	[illegible]	[illegible]	150	–	–	0,14	0,18	+1536	1600		1215	4282	[illegible]	0,07	
[illegible]	[illegible]	[illegible]	78	9	8	26	[illegible]	64765	9	10	[illegible]	[illegible]	400			0,5	0,55	+1585	150		1500	830	[illegible]	0,19	
[illegible]	[illegible]	[illegible]	166	3	3	3	2024	1050	DYN	[illegible]	[illegible]	–	–	–	–	0,2	0,55	+1505	590		1700	1050	971	0,22	
[illegible]	[illegible]	COAL	147	4	6	5	[illegible]	3627	4	4,5	[illegible]	[illegible]	150	–	–	0,14	0,13	+1534	1700		1300	3638	1742	0,06	
[illegible]	[illegible]	COAL	164	4	6	6	37786t	4417	4	6	[illegible]	16	150	–	–	0,14	0,12	+1530	1100		1330	4417	2155	0,06	
[illegible]	[illegible]	[illegible]	352	3	3	1	5069t	1100	[illegible]	6	[illegible]	–	–	–	–	0,14	[illegible]	+1504	3900		1100	1100	1251	0,25	
[illegible]	[illegible]	[illegible]	493	8	9	22	780912	83 203 / 466 02[illegible]	9/11	50	[illegible]	5	400			0,7	0,7	+1529	4200		1045	MAX. 5600	217593	0,28	
[illegible]	[illegible]	COAL	80	3	3	2	2304t	250	DYN	2	[illegible]	–	–	–	–	0,14	0,14	+1504	4000		1300	250			

APPENDIX A2 Example of blast vibration record

Rietspruit open-cast coalmine Blasting vibration levels

Shown below are the maximum velocities and corresponding frequencies for the blast of 16/10/1979 for geophones of array 1 and array 2.

ARRAY 1		
GEOPHONE	MAXIMUM VELOCITY (mm/sec)	FREQUENCY (Hz)
A	1,65	19,8
B	4,35	11,9
C	3,95	16,9
D	7,42	14,8
E	7,35	29,6
F	8,29	19,8

ARRAY 2		
GEOPHONE	MAXIMUM VELOCITY (mm/sec)	FREQUENCY (Hz)
C	3,3	11,4
D	1,5	34,1
E	3,4	21
F	5,6	15,2

The distance from the blast to the instrumented pillar was 155 m and the maximum weight of explosives per relay was 500 kg.

APPENDIX A3 Log of borehole sunk adjacent to instrumented pillar

BOREHOLE No. EXT 8 INCLINATION VERTICAL PROPERTY RIETFONTEIN (TRANSVAAL COAL)

REPORT No. REPORT FOR WEEK ENDING

CHANGE IN STRATA m	cm	Geol. Section	GEOLOGICAL DESCRIPTION OF CORE	APPT DIP
			Top overburden	
12	47		Sandstone, medium grained, brown, weathered.	
14	83		Sandstone, medium grained, abundant shaly lam, brown, ferruginised, weathered.	
15	20		Alternating sandstone fine grained, grey with dark dotted grey lam and thin beds; grading to:	
18	00		Shale, dark grey, moderately silty/sandy lam	
22	09		Sandstone, very fine grained, light grey, mottled (muddy matrix)	
23	10		Sandstone, silty, dark grey to pale dark grey lam; grading to:	

SCALE 1:100

RMP 248A

EXT B ..... INCLINATION ..... PROPERTY .....

..... REPORT FOR WEEK ENDING .....

CHANGE IN STRATA m	cm	Geol. Section	GEOLOGICAL DESCRIPTION OF CORE	APPT DIP
	0	18		
			Shale, dark grey + abundant silty lam.	
25	88		Shale, blackish	
43	67		Coal 4L SEAM, slightly weathered	
27	09		Shale, dark grey occasional silty lam.	
29	99			
			Coal 4L SEAM.	
2	82		Siltstone, micaceous, slightly carbonaceous;	
3	04		Sandstone, very fine gr, buff grey, quartzose;	
7	20		Siltstone, silty grey, with grain study lam.	
2	71		Sandstone, very fine grained, light grey, well sort'd, weakly mott'd	
71	20			
			Sandstone, arosic, light grey to white, medium grained with occasional coarse grained, fair grained and gritty intervals. Laminated in places.	

RME

Date: .....

EXT 8 INCLINATION ______ PROPERTY ______

No. ______ REPORT FOR WEEK ENDING ______

CHANGE IN STRATA m	cm	Geol. Section	GEOLOGICAL DESCRIPTION OF CORE	APPT DIP
52	58			
			Shale, blackish, occasional sandy bed.	
53 / 55	[illegible]		sandstone, fine grained, grey, pyrite lenses, irregular shale lenses	
			Coal 2 SEAM.	
60	[illegible]			
			Coal, non coring - mined out.	
[illegible] / 64	[illegible] / 96		Mudstone, gritty, carbonaceous matrix.	
		F F	Felsite slightly weathered	
64	[illegible]		End of hole.	

RMP

Date: ......

PAGE No.

FORM 3. 68.

K 8 INCLINATION VERTICAL PROPERTY CIETSREUIT (TAVISTOCK COLL)

REPORT FOR WEEK ENDING

Depth M	Depth CM	Geol. Section	Sample No.	Sample Width CM	True Width CM	GEOLOGICAL DISCRIPTION OF CORE	Sampling Results
25	68					Shale, thalite	
25	87					Coal mainly bright ~60%	
26	03					Coal stony	
26	10					Coal dull	
			EXT B	135	135		
			44/A			Coal mainly bright ~60%	
26	58					Coal dull, coaly shale in parts	
26	79						
26	88					Coal mainly dull, ~10% bright	
27	03					Coal dull, <5% bright coal	
						Shale, dark grey, occasional silty lams.	
27	33						
						Coal dull, occasional shaly beds	
27	77						
27	97					Coal dull with ~10% bright coal	
			EXT B	125	125		
			44/B			Coal dull bedrom to dull, occasional pyrite lams and vertical intervals and occasional bright coal lams + stringers.	
			EXT B				
			44/A	122	122		
27	82					Siltstone, micaceous slightly carbonaceous	

FORM 3. 69.

INCLINATION ..... PROPERTY .....

REPORT FOR WEEK ENDING .....

Depth M	Depth CM	Geol. Section	Sample No.	Sample Width CM	True Width CM	GEOLOGICAL DISCRIPTION OF COAL	Sampling Results
53	71					Sandstone fine grained, pyrite traces, shaly base	
						Coal dull to coal shaly	
53	83						
						Coal dull to dull bottom	
			EXT @ 2/D	139	139	occasional pyrite lenses	
55	93						
						Coal shaly	
56	14						
						Coal dull to dull bottoms	
56	70					Coal, shaly to dull, pyritic	
56	95						
			EXT @ 2/E	130	130		
						Coal dull to dull bottom	
						occasional calcite veinlets + pyrite bands	
			EXT @ 2/B	100	100		
59	32		EXT @	100	100	Limestone, carbonaceous	
59	77						

PAGE No.

FORM 3.

... EXT. 8 ..... INCLINATION ..... PROPERTY .....

...ORT No. ..... REPORT FOR WEEK ENDING .....

2488

Depth M	Depth CM	Geol. Section	Sample No.	Sample Width CM	True Width CM	GEOLOGICAL DISCRIPTION OF CORE	Sampling Results
						Coal drill.	
60.	00.					60,0m end of core	

APPENDIX A4 Record of surface velocities adjacent to earth dam - 28/9/1979

Rietspruit open-cast coalmine Blasting vibration levels - 28/9/1979

To determine the effect of blasting on the earth dam located in the pit workings six geophones were installed at increasing distances from the blast. Shown below are the velocity levels and distances from the blast for these geophones:

Maximum velocity (mm/sec)	Distance (m)	Orientation	$D/\sqrt{W}$	$D/\sqrt[1/3]{W}$
23	190	Vertical	1.38	7.12
17	243	Vertical	1.76	9.11
15	355	Vertical	2.58	13.3
14	469	Vertical	3.40	17.58
12	570	Vertical	4.14	21.36
6	570	Horizontal		

These peak values occurred at 2,8 sec after blast initiation.

APPENDIX B : Graphical Representation of Blast Vibration Data

APPENDIX B.1

Method of quantifying the acceleration and displacement records

The acceleration at any sample i was determined from the formula

$$a_i = \frac{V_{i+1} - V_{i-1}}{2\,t}$$ where t is the sample spacing and V is velocity

A program was written to scan a file of data and write out the maximum absolute digital value found in this file and the sample number of which it occurred. This value then represented the peak value (e.g. particle velocity) in that particular file of data. Since the actual values of the peak particle velocities were also known, from the original records, it was then possible to calculate how many units of digital data represented 1 mm/sec. This scanning program was then used on the acceleration files and the maximum value, and sample number at which it occurred, i, were noted. The digital values of velocities at samples i+1 and i-1 were then determined and converted into values in mm/sec. δt is known from the sampling rate (in seconds). The actual value of the maximum acceleration can then be obtained from the formula at the top of this page.

APPENDIX B2 Example of velocity and corresponding acceleration record

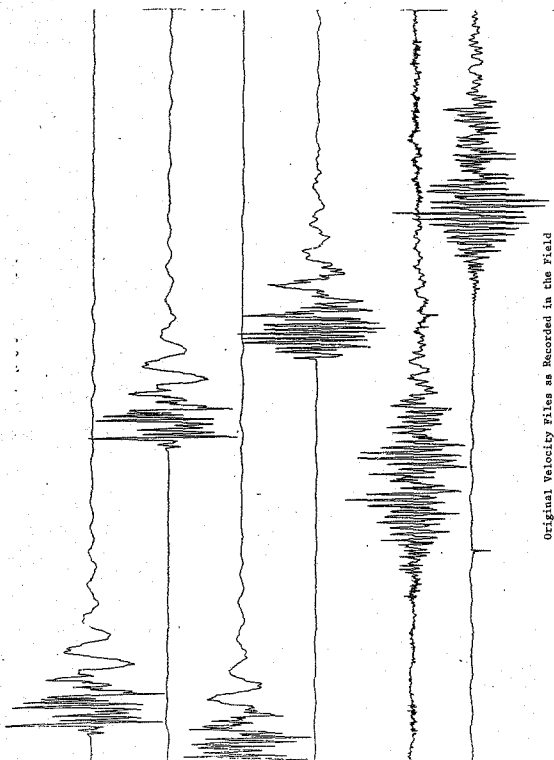

Original Velocity Files as Recorded in the Field

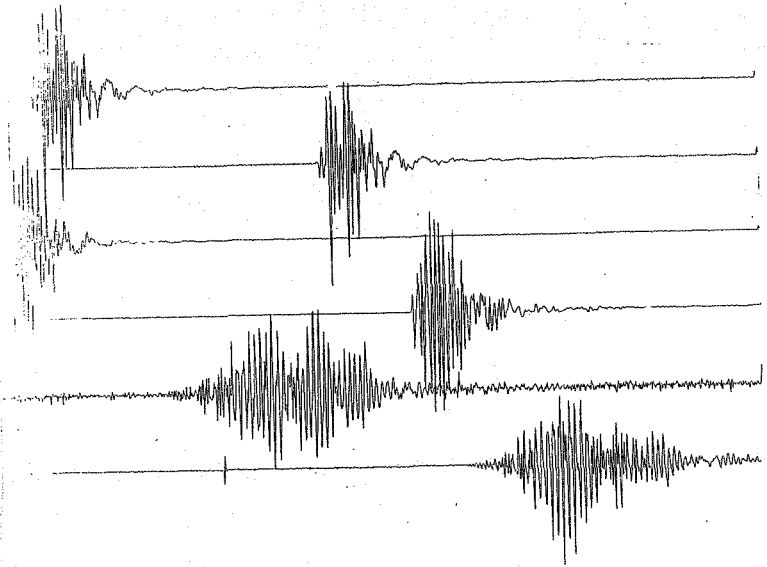

Corresponding acceleration files obtained from Numerical Differentiation

APPENDIX B3 Comparison of data file subjected to differentiation, and then integration, with original file

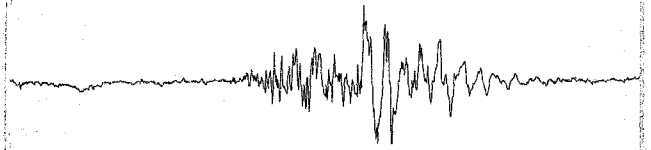

Original velocity file as recorded in field

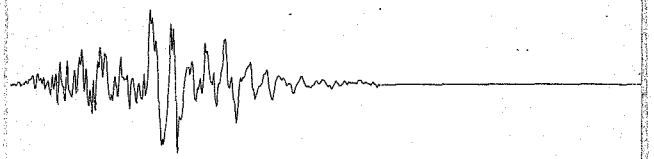

Velocity file after differentiation and reverse integration

Note: Attenuation of high frequency peaks, with no other significant data loss

APPENDIX C : Computer Programs Used in Data Analysis

APPENDIX C.1

Calculation of confidence intervals

The main object of calculating the particle velocity records shown in Chapter 3 was so that safe limits could be estimated for monitor-to-blast distance or charge weight per delay. This is done by extrapolating the Chapter 3 graphs back to 50 mm/sec velocity limit and then determining the corresponding allowable scaled distance. Some inaccuracy is inevitable when dealing with a problem incorporating as many unknowns as the propagation of seismic waves through the earth's surface layers, and it is the aim of this Appendix to determine the confidence limits with which the above graphs can be used to predict future velocity levels. A 95% confidence level was chosen. This means that the probability of the data predicted by the empirical scaling law falling within the calculated confidence interval is 0,95.

A 100(1 -α)% confidence interval for

$A + Bx_o$ is given by:

$$(\hat{A} + \hat{B}x_o) \pm t_{n-2;1-\alpha/2} \sqrt{\{\frac{1}{n} + \frac{(x_o - \bar{x})^2}{S(X^2)}\} s^2_{ey}}$$

where A and B are the actual values of the y-intercept and slope of the empirical propagation law respectively.

$\hat{A}$ and $\hat{B}$ are the values predicted by the linear regression calculations.

x_o is any value for which the corresponding y value is required.

t is a statistical random variable, [illegible] student - t distribution.

n is total number of points.

$\bar{x}$ is mean of x-values.

$S(X^2) = \Sigma x_i^2 - 1/n(\Sigma x_i)^2$

$$S_{ey}^2 = \{ \Sigma y_i^2 - {}^1/n\ (\Sigma y_I)^2 - \hat{B}\ (\Sigma x_i y_i - {}^1/n(\Sigma x_i)(\Sigma y_i))\}/n-2$$

The program that was used to calculate the variances shown in Chapter 3, table 3 was extended to calculate the term shown under the square root sign. The input data for this program was the same data as that used to plot graphs 1 - 5. The y-values are particle velocity and the x-values are scaled distance (either cube-root or square-root scaling). The samllest value of scaled distance that was recorded for any particular set of data was used as the value for XO in this program. This is shown in Table 3 which was drawn up from the results of the above analysis.

The confidence limits calculated in this manner are shown below:

SEISMOMETER	CONFIDENCE LIMIT ± (mm/sec)
A	-
B	1,6
C	1,4
D	1,4
E	1,5
F	1,4
1	-
2	1,8
3	1,3
4	1,4
5	1,3
6 including data of 28/9	1,8
6 excluding data of 28/9	2,0

APPENDIX C1 Program for calculation of least squares straight line

FRI 25/1/80 (80-025)

```
L.0001          DIMENSION X(21),Y(21),FIT(21),ERR(21)
L.0002          READ(5,3)(X(I),I=1,9)
L.0003          READ(5,3)(Y(I),I=1,9)
L.0004          WRITE(6,9)(X(I),I=1,9)
L.0005          WRITE(6,9)(Y(I),I=1,9)
L.0006  9       FORMAT(12F6.2)
L.0007  3       FORMAT(12F6.2)
L.0008          N=9
L.0009          DO 6 I=1,N
L.0010          X(I)=ALOG10(ABS(X(I)))
L.0011          Y(I)=ALOG10(ABS(Y(I)))
L.0012  6       CONTINUE
L.0013          XM=0.0
L.0014          YM=0.0
L.0015          Z=0.0
L.0016          ZZ=0.0
L.0017          C=0.0
L.0018          DO 1 I=1,N
L.0019          C=X(I)*Y(I)+C
L.0020          XM=XM+X(I)
L.0021          YM=YM+Y(I)
L.0022          Z=Z+X(I)**2
L.0023          ZZ=ZZ+Y(I)**2
L.0024  1       CONTINUE
L.0025          D=C-((XM*YM)/N)
L.0026          E=Z-(XM**2)/N
L.0027          B=D/E
L.0028          F=XM/N
L.0029          G=YM/N
L.0030          A=G-B*F
L.0031          SUM=0.0
L.0032          DO 2 I=1,N
L.0033          FIT(I)=A+B*X(I)
L.0034          ERR(I)=(FIT(I)-Y(I))**2
L.0035          SUM=SUM+ERR(I)
L.0036  2       CONTINUE
L.0037          SUM=SUM/N
L.0038          WRITE(6,4)A,B,SUM
L.0039  4       FORMAT('T2,'INTERCEPT= ',F7.4,T20,'SLOPE= ',F6.4,T40,      ',F10.7)
L.0040          WRITE(6,5)(ERR(I),I=1,9)
L.0041  5       FORMAT(T2,12F6.4)
L.0042          XO=ALOG10(9.84)
L.0043          SEY=(ZZ-(YM**2)/N-B*(C-(XM*YM)/N))/(N-2)
L.0044          SX=Z-(XM**2)/N
L.0045          XTRA=1/N+((XO-F)**2)/SX
L.0046          TIMIL=SQRT(XTRA*SEY)
L.0047          WRITE(6,8)TIMIL
L.0048  8       FORMAT(T2,'LIMIT= ',F8.4)
L.0049  /DATA
L.0050    47.00 17.50 59.40 49.40 22.00 14.50  9.84 72.10 19.50
L.0051     3.10  7.90  2.40  3.00 12.28 15.31 14.61  1.20  7.42
```

```
   X-POINTS                Y-POINTS
 1.511999E+01            4.091000E+04
 1.045199E+02            2.843400E+04
 3.341999E+01            5.318500E+04
 3.045999E+01            5.827500E+04
 4.034999E+01            4.803900E+04
 5.720998E+02            2.912430E+05
 1.389999E+01            3.810000E+04
 1.791999E+02            1.480570E+05
 1.129999E+01            3.234900E+04

NO. OF POINTS =      9

OPTIONS FOUND:-  PTS  FIT  LOGX  LOGY

COND='PTS,FIT=LINE,LOGX,LOGY,'          LABEL=' '  LAB_POS=  8

XTITLE='((R**2).SIGMA(V**2))'     YTITLE='TOTAL CHARGE WEIGHT (KG)'

TITLE='GRAPH OF TOTAL ENERGY PRESENT IN A SIGNAL'

CONTROL_MESSAGE=' '

DESCRIPTION=' THIS GRAPH PLOTS THE ENERGY IN A SEISMIC SIGNAL, OBTAINED FROM THE SQUARE
            ' OF THE SUM OF THE GROUND PARTICLE VELOCITIES MULTIPLIED BY THE HYPOCENTRAL
            ' DISTANCE SQUARED, AGAINST THE TOTAL CHARGE WEIGHT OF A MINING BLAST
            '
            '
            '
            '
            '

XMIN= 9.999998E-01      XMAX= 2.999997E+00      XINC= 7.407407E-02      XLEN= 2.700000E+01;
YMIN= 4.000000E+00      YMAX= 6.000000E+00      YINC= 1.111111E-01      YLEN= 1.800000E+01;
  Y =  4.821385E-01 X +  3.961949E+00
  VARIANCE= 3.270351E-02
```

APPENDIX C3 Initialisation program for 'STANDARD LABEL' tape

```
L.0001 //FAFLABEL JOB 003,LABEL,MSGLEVEL=1,CLASS=B
L.0002 /*SETUP          TAPE=(RIETSL, VOLUME TO BE LABELED)
L.0003 /*JOBPARM R=073
L.0004 // EXEC INITT
L.0005 //SYSIN DD *
L.0006 //
```

APPENDIX C4 Program for transferring data from a 'NO LABEL' to a 'STANDARD LABEL' tape

SAT 3/3/80 (80-215)

```
L.0001 //FOBTRANS  JOB 003,TRANS,MSGLEVEL=1,CLASS=B
L.0002 /*SETUP        TAPE=(RIET01,NL & NO RING,RIETSL,YES)
L.0003 /*ROUTE PRINT HOLD
L.0004 /*JOBPARM R=073
L.0005 //   EXEC  FORTGCLG,REGION.GO=100K,TIME.GO=2
L.0006 //FORT.SYSIN DD *
L.0007         REAL*4 VAL(1024)
L.0008         REAL*8 IN(256)
L.0009         INTEGER*2 OUT(1024)
L.0010         EQUIVALENCE (IN,OUT)
L.0011         READ(5,100)NFILES
L.0012 100     FORMAT(I10)
L.0013         DO 1 J=1,NFILES
L.0014         N=0
L.0015 8       READ(13,2,END=3,ERR=4) IN
L.0016 2       FORMAT(64(4A8))
L.0017         N=N+1
L.0018 400     DO 5 I=1,1024
L.0019 5       VAL(I)=OUT(I)
L.0020         WRITE(6,20)J,N
L.0021 20      FORMAT(/,5X,'FILE NO =',I3,5X,'BLOCK NO =',I3)
L.0022         WRITE(14) VAL
L.0023         GO TO 8
L.0024 4       WRITE(6,7)J,N
L.0025 7       FORMAT(/20X,'ERROR IN FILE',I3,5X,'BLOCK NUMBER',I3)
L.0026         GO TO 8
L.0027 3       WRITE(6,22)J
L.0028 22      FORMAT(/,5X,'END FILE NO',I3)
L.0029         END FILE 14
L.0030 1       CONTINUE
L.0031         REWIND 13
L.0032         STOP
L.0033         END
L.0034 //LKED.SYSLIB  DD
L.0035 //         DD  DSNAME=SYS1.FORTLIB,DISP=SHR
L.0036 //GO.FT13F001 DD UNIT=T800,DCB=RECFM=U,BLKSIZE=2048,EROPT=SKP,DEN=2),
L.0037 // VOL=(,RETAIN,SER=RIET01),
L.0038 // DISP=(OLD,PASS),LABEL=(2,NL,,IN)
L.0039 //GO.FT14F001 DD UNIT=TAPE,VOL=SER=RIETSL,DCB=(RECFM=VBS,LRECL= 052,
L.0040 // BLKSIZE=2048),LABEL=(047,,,OUT),DSN=FILE047,DISP=(NEW,PASS)
L.0041 //GO.SYSIN DD *
L.0042           1
L.0043 //
```

APPENDIX C5

Plotting programme

To ensure that the digital data stored on the magnetic tape was an accurate representation of the original analog signal this program was used to plot the digital data.

Any number of files can be plotted at once, the number preferred in this investigation being 8. The data input which is required is as follows:

(i) The file number on the tape which is to be read (e.g. 097 is the first file read in this case).

(ii) The number of samples to be skipped in a particular block (*each* block contains 1024 samples).

(iii) The number of blocks to be skipped.

(iv) The total number of samples to be read.

Note (ii) - (iv) are all typed on the same line, e.g. corresponding to file 97 the input is:

bb30Obbbb3b1024

APPENDIX C5

Plotting programme

To ensure that the digital data stored on the magnetic tape was an accurate representation of the original analog signal this program was used to plot the digital data.

Any number of files can be plotted at once, the number preferred in this investigation being 8. The data input which is required is as follows:

(i) The file number on the tape which is to be read (e.g. 097 is the first file read in this case).

(ii) The number of samples to be skipped in a particular block (each block contains 1024 samples).

(iii) The number of blocks to be skipped.

(iv) The total number of samples to be read.

Note (ii) - (iv) are all typed on the same line, e.g. corresponding to file 97 the input is:

bb300bbbb3b1024

```
L.0001 //CH /71 #104#112#
L.0002 //R#GCOALS JOB 006,TRANS,MSGLEVEL=1,CLASS=B                    RGREEN
L.0003 /*SETUP      TAPE=(RIETSL SL & NC RING)
L.0004 /*ROUTE  PRINT RCLD
L.0005 /*JOBPARM F=07C
L.0006 //   EXEC    FORTGCLG,REGION.GO=180K,TIME.GO=5
L.0007 //FOR1.SYSIN DD *
L.0008       DIMENSION IBUF(2048)
L.0009       REAL*4 X(50500)
L.0010       REAL*4 CUT(1024)
L.0011       CALL ERRSET(212,256,256)
L.0012       CALL ERRSET(213,256,256)
L.0013       CALL PLOTS(IBUF,6000)
L.0014       CALL PLOT(0.0,2.0,-3)
L.0015       NFILES=8
L.0016       DO 1 JJ=1,NFILES
L.0017       N=0
L.0018       READ(5,115)K,NSKIP, NTOT
L.0019  115  FORMAT(3(I5))
L.0020       NSK=NSKIP+1
L.0021       DO 9 I=1,NSK
L.0022    9  READ(13,END=4,ERR=6) CUT
L.0023       GO TO 200
L.0024  4    IF(N.NE.0) GO TO 1
L.0025       WRITE(6,100)JJ
L.0026  100  FORMAT(50X,'FILE NO=',I5,5X,'EMPTY FILE')
L.0027       GO TO 1
L.0028  6    M=N+1
L.0029       WRITE(6,101)JJ,M
L.0030   101 FORMAT(//,50X,'FILE NO=',I5,5X,'ERROR BLOCK=',I5,/)
L.0031       GO TO 9
L.0032  200  N=N+1
L.0033       IF(N.GT.1) GO TO 600
L.0034       MM=0
L.0035       DO 700 I=K,1024
L.0036       MM=MM+1
L.0037       IF(MM.EQ.NTOT) GO TO 5
L.0038  700  X(MM)=CUT(I)
L.0039       GO TO 9
L.0040  600  DO 5 I=1,1024
L.0041       MM=MM+1
L.0042       IF(MM.GE.NTOT) GO TO 10
L.0043    5  X(MM)=CUT(I)
L.0044       GO TO 9
L.0045   10  DO 1000 I=1, 50
L.0046  1000 READ(13,END=1,ERR=1)CUT
L.0047   1   CALL GRAPH(X,MM,JJ)
L.0048       CALL PLOT(2.,0.,999)
L.0049       STOP
L.0050       END
L.0051       SUBROUTINE GRAPH(X,NPTS,JJ)
L.0052       DIMENSION X(1)
L.0053       CALL PLOT(2.5,0.0,-3)
L.0054       FILE = JJ
```

```
L.0055          BLKS = NPTS/1024
L.0056          CALL NUMBER(0.,-1.,0.,0.5,FILE,0.,-1)
L.0057          CALL PLCT(0.,0.,3)
L.0058          WRITE(6,20)NPTS
L.0059    20    FORMAT(//,30X,'NPTS =',I5)
L.0060          BIG=0.0
L.0061          DO 1 I=1,NPTS,3
L.0062    1     BIG=AMAX1(BIG,ABS(X(I)))
L.0063          XM = 2.*BIG
L.0064          YM = 25./FLOAT(NPTS)
L.0065          DO 2 J=1,NPTS
L.0066    2     CALL PLCT(X(J)*XM,FLOAT(J)*YM,2)
L.0067          RETURN
L.0068          END
L.0069 //LKED.SYSLIB  DD
L.0070 //         DD   DSN=SYS2.PLOTLIB,DISP=SHR
L.0071 //GO.FT13F001 DD UNIT=2400,VOL=SER=RIETSL,DCB=(RECFM=VR,LRECL=02052,
L.0072 // BLKSIZE=02048),LABEL=(097,,,IN),DSN=FILE097,DISP=(OLD,KEEP)
L.0073 //GO.FT13F002 DD UNIT=2400,VOL=SER=RIETSL,DCB=(RECFM=VR,LRECL=02052,
L.0074 // BLKSIZE=02048),LABEL=(103,,,IN),DSN=FILE103,DISP=(OLD,KEEP)
L.0075 //GO.FT13F003 DD UNIT=2400,VOL=SER=RIETSL,DCB=(RECFM=VR,LRECL=02052,
L.0076 // BLKSIZE=02048),LABEL=(107,,,IN),DSN=FILE107,DISP=(OLD,KEEP)
L.0077 //GO.FT13F004 DD UNIT=2400,VOL=SER=RIETSL,DCB=(RECFM=VR,LRECL=02052,
L.0078 // BLKSIZE=02048),LABEL=(112,,,IN),DSN=FILE112,DISP=(OLD,KEEP)
L.0079 //GO.FT13F005 DD UNIT=2400,VOL=SER=RIETSL,DCB=(RECFM=VR,LRECL=02052,
L.0080 // BLKSIZE=02048),LABEL=(114,,,IN),DSN=FILE114,DISP=(OLD,KEEP)
L.0081 //GO.FT13F006 DD UNIT=2400,VOL=SER=RIETSL,DCB=(RECFM=VR,LRECL=02052,
L.0082 // BLKSIZE=02048),LABEL=(121,,,IN),DSN=FILE121,DISP=(OLD,KEEP)
L.0083 //GO.FT13F007 DD UNIT=2400,VOL=SER=RIETSL,DCB=(RECFM=VR,LRECL=02052,
L.0084 // BLKSIZE=02048),LABEL=(122,,,IN),DSN=FILE122,DISP=(OLD,KEEP)
L.0085 //GO.FT13F008 DD UNIT=2400,VOL=SER=RIETSL,DCB=(RECFM=VR,LRECL=02052,
L.0086 // BLKSIZE=02048),LABEL=(123,,,IN),DSN=FILE123,DISP=(OLD,KEEP)
L.0087 //PLOTSAVG     DD UNIT=PLOTOUT,SPACE=(CYL,(3,3),RLSE),DISP=(,PASS)
L.0088 //GO.SYSIN DD *
L.0089      300     3 1024
L.0090      300     3 1024
L.0091      300     2 1024
L.0092      300     2 1024
L.0093      300     2 1024
L.0094        0     5 1024
L.0095        0     5 1024
L.0096        0     0 1024
L.0097 //
```

APPENDIX C6 Program for calculating accelerations numerically from velocity-time records

MON 28/1/80 (80-028)

```
L.0001
L.0002 //RWGAWGUS JOB 006,TRANS,MSGLEVEL=1,CLASS=B                    RGREEN
L.0003 /*SETUP        TAPE=(RIETSL SL 4 NO RING,COALED,YES)
L.0004 /*ROUTE  PRINT HOLD
L.0005 /*JOBPARM R=070
L.0006 //   EXEC  FORTGCLG,REGION.GO=150K,TIME.GO=5
L.0007 //FORT.SYSIN DD *
L.0008       REAL F(2000)
L.0009       REAL DX(2000)
L.0010       REAL*4 X(2048)
L.0011       REAL*4 OUT(1024)
L.0012       CALL ERRSET(212,256,256)
L.0013       CALL ERRSET(218,256,256)
L.0014       NFILES=1
L.0015       DO 3 JJ=1,NFILES
L.0016       N=0
L.0017       READ(5,115)K,NSKIP, NTOT
L.0018  115  FORMAT(3(I5))
L.0019       NSK=NSKIP+1
L.0020       DO 9 I=1,NSK
L.0021    9  READ(13,END=4,ERR=6) OUT
L.0022       GO TO 200
L.0023  4    IF(N.NE.0) GO TO 1
L.0024       WRITE(6,100)JJ
L.0025  100  FORMAT(50X,'FILE NO=',I5,5X,'EMPTY FILE')
L.0026       GO TO 1
L.0027    6  N=N+1
L.0028       WRITE(6,101)JJ,N
L.0029    101 FORMAT(//,50X,'FILE NO=',I5,5X,'ERROR BLOCK=',I5,/)
L.0030       GO TO 9
L.0031  200  N=N+1
L.0032       IF(N.GT.1) GO TO 600
L.0033       MM=0
L.0034       DO 700 I=K,1024
L.0035       MM=MM+1
L.0036       IF(MM.EQ.NTOT) GO TO 5
L.0037  700  X(MM)=OUT(I)
L.0038       GO TO 9
L.0039  600  DO 5 I=1,1024
L.0040       MM=MM+1
L.0041       IF(MM.GE.NTOT) GO TO 10
L.0042     5 X(MM)=OUT(I)
L.0043       GO TO 9
L.0044   10  DO 1000 I=1, 50
L.0045 1000  READ(13,END=1,ERR=1)OUT
L.0046  1    J=1
L.0047       WRITE(6,102)MM
L.0048  102  FORMAT(40X,'TOTAL MM=',I5)
L.0049       DC=0.0
L.0050       DO 13 I=1,1024
L.0051       DC=DC+X(I)
L.0052  13   CONTINUE
L.0053       DC=DC/1024.0
L.0054       DO 33 I=1,1024
```

```
L.0055          F(I)=X(I)-DC
L.0056 33       CONTINUE
L.0057 2        DO 12 I=1,1024
L.0058          FR=F(I+2*J)
L.0059          FL=F(I)
L.0060          DX(I)=(FR-FL)/(2.0*J)
L.0061 12       CONTINUE
L.0062 3        WRITE(14)(DX(I),I=1,1024)
L.0063          STOP
L.0064          END
L.0065 //LKED.SYSLIB  DD
L.0066 //             DD  DSN=SYS2.PLOTLIB,DISP=SHR
L.0067 //GO.FT13F001 DD UNIT=2400,VOL=SER=RIETSL,DCB=(RECFM=VA,LRECL=02052,
L.0068 // BLKSIZE=02048),LABEL=(85,,,IN),DSN=FILE085,DISP=(OLD,KEEP)
L.0069 //GO.FT14F001 DD UNIT=TAPE,VOL=SER=COALED,DCB=(RECFM=VBS,LRECL=02052,
L.0070 // BLKSIZE=2048),LABEL=(089,,,OUT),DSN=FILE089,DISP=(NEW,PASS)
L.0071 //GO.SYSIN DD *
L.0072   0     2 1024
L.0073 //
```

```
L.0001 //PAFSECON JOB 003,TRANS,MSGLEVEL=1,CLASS=B                    MARAN
L.0002 /*SETUP      TAPE=(COALED SL & NO RING,RIETSL YES)
L.0003 /*ROUTE   PRINT HOLD
L.0004 /*JOBPARM R=070
L.0005 //   EXEC  FORTGCLG,REGION.GO=150K,TIME.GO=5
L.0006 //FORT.SYSIN DD *
L.0007       REAL DX(2000)
L.0008       REAL*4 X(2048)
L.0009       REAL*4 Y(2048)
L.0010       REAL*4 OUT(1200)
L.0011       CALL ERRSET(212,256,256,256)
L.0012       CALL ERRSET(218,256,256,256)
L.0013       NFILES=2
L.0014       DO 1 JJ=1,NFILES
L.0015       N=0
L.0016       READ(5,115)NX,NSKIP, NTOT
L.0017  115  FORMAT(3(I5))
L.0018       NSK=NSKIP+1
L.0019       DO 9 I=1,NSK
L.0020   9   READ(13,END=4,ERR=6) OUT
L.0021       GO TO 200
L.0022   4   IF(N.NE.0) GO TO 1
L.0023       WRITE(6,100)JJ
L.0024 100   FORMAT(50X,'FILE NO=',I5,5X,'EMPTY FILE')
L.0025       GO TO 1
L.0026   6   M=N+1
L.0027       WRITE(6,101)JJ,M
L.0028   101 FORMAT(//,50X,'FILE NO=',I5,5X,'ERROR BLOCK=',I5,/)
L.0029       GO TO 9
L.0030 200   N=N+1
L.0031       IF(N.GT.1) GO TO 600
L.0032       MM=0
L.0033       DO 700 I=K,1024
L.0034       MM=MM+1
L.0035       IF(MM.EQ.NTOT) GO TO 5
L.0036       IF(JJ.EQ.1) X(MM)=OUT(I)
L.0037 700   IF(JJ.EQ.2) Y(MM)=OUT(I)
L.0038       GO TO 9
L.0039   600 DO 5 I=1,1024
L.0040       MM=MM+1
L.0041       IF(MM.GE.NTOT) GO TO 10
L.0042       IF(JJ.EQ.1) X(MM)=OUT(I)
L.0043   5   IF(JJ.EQ.2) Y(MM)=OUT(I)
L.0044       GO TO 9
L.0045   10  DO 1000 I=1, 50
L.0046  1000 READ(13,END=1,ERR=1)OUT
L.0047  1    KK=691
L.0048       JJ=547
L.0049       K=KK-1
L.0050       J=JJ-1
L.0051       P=X(K)
L.0052       Q=Y(J)
L.0053       WRITE(6,333)P,Q
L.0054  333  FORMAT(I2,'P= ',F7.1,' Q= ',F7.1)
```

```
L.0055 .        DO 12 I=1,1000
L.0056          K=K+I
L.0057          J=J+1
L.0058          DX(I)=(Y(J)-Q)-(X(K)-P)
L.0059 12       CONTINUE
L.0060          WRITE(14) (DX(I),I=1,1000)
L.0061          STOP
L.0062          END
L.0063 //LKED.SYSLIB   DD
L.0064 //         DD   DSN=SYS2.PLOTLIB,DISP=SHR
L.0065 //GO.FT13F001 DD UNIT=2400,VOL=SER=COALED,DCB=(RECFM=VR,LRECL=02052,
L.0066 // BLKSIZE=02048),LABEL=(90,,,IN),DSN=FILE090,DISP=(OLD,KEEP)
L.0067 //GO.FT13F002 DD UNIT=2400,VOL=SER=COALED,DCB=(RECFM=VR,LRECL=02052,
L.0068 // BLKSIZE=02048),LABEL=(94,,,IN),DSN=FILE094,DISP=(OLD,KEEP)
L.0069 //GO.FT14F001 DD UNIT=2400,VOL=SER=RIETSL,DCB=(RECFM=VBS,LRECL=02052,
L.0070 // BLKSIZE=02048),LABEL=(140,,,OUT),DSN=FILE140,DISP=(NEW,PASS)
L.0071 //GO.SYSIN DD *
L.0072      0     0 1024
L.0073      0     0 1024
L.0074 //
```

APPENDIX C8 Program for calculation of cross-correlation between two data files

NGN 28/1/80 (80-028)

```
L.0001 //HANDECEM JOB 006,TRANS,MSGLEVEL=1,CLASS=B                    FRED
L.0002 /*SETUP      TAPE=(COALED SL & NO RING)
L.0003 /*ROUTE  PRINT HOLD
L.0004 /*JOBPARM R=070
L.0005 //   EXEC   FORTGCLG,REGION.GO=150K,TIME.GO=5
L.0006 //FORT.SYSIN DD *
L.0007       REAL DX(2000)
L.0008       REAL*4 X(2048)
L.0009       REAL*4 Y(2048)
L.0010       REAL*4 OUT(1200)
L.0011       CALL ERRSET(212,256,256)
L.0012       CALL ERRSET(218,256,256)
L.0013       NFILES=2
L.0014       DO 1 JJ=1,NFILES
L.0015       N=0
L.0016       READ(5,115)K,NSKIP, NTOT
L.0017  115  FORMAT(3(15))
L.0018       NSK=NSKIP+1
L.0019       DO 9 I=1,NSK
L.0020   9   READ(13,END=4,ERR=6) OUT
L.0021       GO TO 200
L.0022 4     IF(N.NE.0) GO TO 1
L.0023       WRITE(6,100)JJ
L.0024 100   FORMAT(50X,'FILE NO=',I5,5X,'EMPTY FILE')
L.0025       GO TO 1
L.0026   6   M=N+1
L.0027       WRITE(6,101)JJ,M
L.0028  101. FORMAT(//,50X,'FILE NO=',I5,5X,'ERROR BLOCK=',I5,/)
L.0029       GO TO 9
L.0030 200   N=N+1
L.0031       IF(N.GT.1) GO TO 600
L.0032       MM=0
L.0033       DO 700 I=K,1024
L.0034       MM=MM+1
L.0035       IF(MM.EQ.NTOT) GO TO 5
L.0036       IF(JJ.EQ.1) X(MM)=OUT(I)
L.0037 700   IF(JJ.EQ.2) Y(MM)=OUT(I)
L.0038       GO TO 9
L.0039   600 DO 5 I=1,1024
L.0040       MM=MM+1
L.0041       IF(MM.GE.NTOT) GO TO 10
L.0042       IF(JJ.EQ.1) X(MM)=OUT(I)
L.0043 5     IF(JJ.EQ.2) Y(MM)=OUT(I)
L.0044       GO TO 9
L.0045   10  DO 1000 I=1, 50
L.0046  1000 READ(13,END=1,ERR=1)OUT
L.0047 1     KK=691
L.0048       JJ=547
L.0049       SS=0.0
L.0050       TT=0.0
L.0051       VV=0.0
L.0052       LL=1
L.0053       K=KK-1
L.0054       J=JJ-1
```

```
L.0055          P=X(K)
L.0056          Q=Y(J)
L.0057          DO 12 I=1,1000
L.0058          K=K+1
L.0059          J=J+1
L.0060          SS=SS+(X(K)-P)**2
L.0061          TT=TT+(Y(J)-Q)**2
L.0062          VV=VV+(X(K)-P)*(Y(J)-Q)
L.0063 12       CONTINUE
L.0064          CORR=VV/SQRT(SS*TT)
L.0065          WRITE(6,134)CORR
L.0066 134      FORMAT('0','NORMALISED CROSS CORRELATION = ',F8.3)
L.0067          STOP
L.0068          END
L.0069 //LKED.SYSLIB  DD
L.0070 //             DD  DSN=SYS2.PLOTLIB,DISP=SHR
L.0071 //GO.FT13F001 DD UNIT=2400,VOL=SER=COALED,DCB=(RECFM=VR,LRECL=02052,
L.0072 // BLKSIZE=02048),LABEL=(90,,,IN),DSN=FILE090,DISP=(OLD,KEEP)
L.0073 //GO.FT13F002 DD UNIT=2400,VOL=SER=COALED,DCB=(RECFM=VR,LRECL=02052,
L.0074 // BLKSIZE=02048),LABEL=(94,,,IN),DSN=FILE094,DISP=(OLD,KEEP)
L.0075 //GO.SYSIN DD *
L.0076      0     0 1024
L.0077      0     0 1024
L.0078 //
```

APPENDIX C9

Spectral analysis program

This program makes use of a subroutine HARM, which is a package program on the IBM360, and is capable of doing three-dimensional Fourier Transforms. Only one-dimensional transforms were performed in this particular program.

The first specification that is required is the sampling rate (SPS) at which the analog data was sampled. The program processes 256 samples for each event and the time window T is therefore given by 256/SPS. The response of the recording system is then read. This was experimentally determined by Spottiswoode and McGarr (13), and is shown below in Figure C9.1

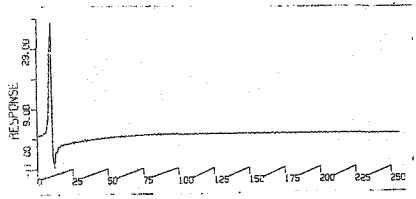

FIGURE C9.1 Experimentally determined system response

A low-pass filtering facility is provided. The order of the polynomial specifying the filter determines the sharpness of the cut-off at the low-pass frequency. Any frequency may be specified, or, as in our investigation, no filtering may be necessary. This was because the recording equip-

ment was located far from an A.C. power source, and so no distorting noise was introduced into the signals.

The seismic data is then read, either from a STANDARD LABEL tape (as described before) or a WITS data file. This data is then checked to see if a DC offset is present or not. If it is present the DC offset is removed from the data. The data is windowed with a "cosine bell" to prevent ringing, as described in Chapter 5. Deconvolution of the seismic data with the system response is then performed. This is to obtain the actual raw seismic data, before it is recorded by the recording equipment.

Various functions are then calculated and plotted. These are: (i) The Fourier Transform of the filtered, windowed and deconvolved raw data which represents the relative magnitudes of the frequency content of the signal. (ii) The velocity-time relationship after inverse transforming. This is usually very similar to the original raw data except the higher frequencies are somewhat attenuated. (iii) The displacement-time relation which is simply calculated from a numerical backward difference formula. (iv) The energy present in the seismic signal. This is calculated from a summation of the square of the velocity. This value is used extensively in Chapter 5. (v) The power spectrum of the velocity-time relation. This is effectively the square of the rectified Fourier Transform and emphasizes any predominant frequencies. This function served as the basis for checking whether there was a possibility of resonance occurring in the hanging-wall. (vi) Displacement spectrum vs. frequency which is plotted on log-log axes. This function has been used to predict source parameters for earthquakes (14 and 15).

```
L.0001 //RWGCRAB JOB 006,BPI,MSGLEVEL=1,CLASS=B
L.0002 /*SETUP      TAPE=(RIETSL SL & NO RING)
L.0003 /*ROUTE  PRINT HOLD
L.0004 //   EXEC FORTXCLG,REGION.GO=100K,TIME.GO=5
L.0005 //FORT.SYSIN DD *
L.0006        DIMENSION F(260),RESP(260),SPEC(130),IS(64),S(64),TAPE(9),EN(258)
L.0007       1,BIP(260),POWS(130),FRLOG(130),PAT(126),IBUF(1000),FF(260)
L.0008        COMPLEX CF(129),CRESP(129),B(128)
L.0009        EQUIVALENCE (CF(1),F(3)),(CRESP(1),RESP(3)),(BIP(1),B(1))
L.0010        COMMON TIME(258)
L.0011 C   THIS PROGRAMME IS WRITTEN FOR A DATA WINDOW OF 256 SAMPLES
L.0012 C   SPS = NO. OF SAMPLES PER SECOND (DIG. RATE) FOR THE DATA.
L.0013 C  THE PERIOD OF THE SAMPLE ANALYSED SHOULD GIVE 256 SAMPLES (2**8)
L.0014 C  E.G. FOR SPS =640   THEN T = 0.4 SECS.
L.0015        SPS=209
L.0016        T=256/SPS
L.0017        DO 40 I=1,256
L.0018 40     TIME(I)=I
L.0019        TIME(257)=0.
L.0020        XINC=12.0
L.0021        TIME(258)=256/XINC
L.0022        PI =3.1416
L.0023        TCON=4*PI/((256/SPS)**2)
L.0024 C
L.0025 C     TIME SCALE OF PLOTS : 1MM=2.56 SAMPLES=0.004SEC (I.E. 10 CM AXIS)
L.0026 C
L.0027        CALL PLOTS(IBUF,4000)
L.0028        READ(5,10)(RESP(I),I=1,256)
L.0029 10     FORMAT(16F5.2)
L.0030        READ(5,1155)(TAPE(I),I=1,9)
L.0031 1155   FORMAT(9F5.3)
L.0032        XOT=0.0
L.0033        IRS=-1
L.0034        CALL QRSH(IRS,NFILES,XINC,XOT)
L.0035        SAS=256
L.0036        CALL QWRITE(RESP,' RESPONSE    ',' D.U./MICRON     ')
L.0037 C
L.0038 C
L.0039 C     RESP: OUTPUT IN D.U. OF SYSTEM WITH AN IMPULSE INPUT OF 1 MICRON,
L.0040 C     IN 1920 MICRONS/SEC FOR 1/1920 SEC,
L.0041 C     SAMPLED AT 1920 SAMPLES/SEC, GAINS 1 & 50.
L.0042 C
L.0043 C
L.0044        CALL RHARI(RESP,7,IS,S,IFERR,1)
L.0045 C
L.0046 C     RESP : D.F.T. OF RESP, NPTS = 256, T(RESP) =1.231SEC,
L.0047 C     CRESP : COMPLEX EQUIVALENT OF RESP.
L.0048 C
L.0049        DO 41 I=1,128
L.0050 41     CRESP(I)=CRESP(I)/1.625
L.0051        WRITE(6,25)RESP
L.0052 25     FORMAT(16F8.4)
L.0053 C
L.0054 C     CRESP = CRESP/1.625 : RESPONSE IN FREQUENCY DOMAIN IS D.F.T.
```

```
L.0055 C     OF IMPULSE RESPONSE DIVIDED BY A FACTOR OF 2/T, T(RESP)=1.231SEC.
L.0056 C     CRESP IN D.L./MICRON/SEC.
L.0057 C
L.0058 C      NOR = ORDER OF THE POLYNOMIAL FOR FILTERING.
L.0059 C      WL : CUT OF FREQUENCY.
L.0060 C       IFIL> 0 APPLY LOW PASS FILTER.
L.0061 C     NFILES = TOTAL NO OF FILES(= EVENTS).
L.0062 C
L.0063         JFR=123
L.0064         READ(5,120) NFILES,IFIL,NOR,WL
L.0065 120     FORMAT(I5,I1,I4,F5.0)
L.0066         IF(IFIL) 16,13,17
L.0067 17      CALL BLFIL(8,NOR,WL,JFR,PAT)
L.0068         IRS=0
L.0069         CALL ORSH(IRS,NFILES,XINC,XOT)
L.0070         CALL RRITE(8,' FILT RESP ',' LOW PASS 40HZ')
L.0071         CALL ORSH(IRS,NFILES,XINC,XOT)
L.0072         CALL RRITE(PAT,' % ATTEN.  ','    PER CENTAGE ')
L.0073 14      IRS=1
L.0074         DO 1 NEV =1,NFILES
L.0075         WRITE(6,19) NEV
L.0076 19      FORMAT('1',T50,'FILE NUMBER ',I4,/,T50,16('*'))
L.0077         CALL ORSH(IRS,NFILES,XINC,XOT)
L.0078         CALL SYMBOL(0.0,5.0,0.6,'EVENT NO.',90.0,9)
L.0079         VEN=FLOAT(NEV)
L.0080         CALL NUMBER(0.0,11.0,0.6,VEN,90.0,-1)
L.0081         XOT=2.0
L.0082         IRS=-1
L.0083         CALL PLOT(XOT,0.,-3)
L.0084         READ(5,121) GAIN,KSKIP,NSKIP,NTOT
L.0085 121     FORMAT(F5.2,I5,I2,I5)
L.0086
L.0087
L.0088         IF (NTOT.EQ.0) NTOT=256
L.0089         CALL READT (F,NEV,KSKIP,NSKIP,NTOT)
L.0090 C   READ(5,125) (F(K),K=1,NTOT)
L.0091 C 125FORMAT(16F5.2)
L.0092         WRITE(6,1153)NEV
L.0093 1153    FORMAT(12,'INPUT FROM FILE NO. ',F5.1)
L.0094         WRITE(6,1151)(F(I),I=1,NTJT)
L.0095 1151    FORMAT(16F5.0)
L.0096 C
L.0097 C     F : RAW SEISMOGRAM IN D.U., SAMPLED AT 'SPS' SAMPLES/SEC
L.0098 C   GAIN = FACTOR TO NORMALIZE RAW DATA TO GAINS 1:REC. 50:REP.
L.0099 C   REC GAINS W.R.T. GAIN 1 ARE AS FOLLOWS:  2=*1.45 3=*4.13 4=*18.18
L.0100 C   5=*55.0 6=*17 .7 7=*455  REP GAINS ARE ABSOLUTE.(E.G. 100 = *100)
L.0101 C         E.G. IF REC=1 & REP=100 THEN GAIN =0.5
L.0102 C
L.0103         DC=0.
L.0104         DO 2 I=1,256
L.0105 2       DC=DC+F(I)
L.0106         DC=DC/256.
L.0107         WRITE(6,20)GAIN,DC
L.0108 20      FORMAT(' GAIN=',F8.4,', DC REMOVED',F8.0)
L.0109         DO 3 I=1,256
L.0110 3       F(I)=(F(I)-DC)*GAIN
L.0111         DO 4 I=1,9
L.0112         F(I)=F(I)*TAPE(I)
L.0113         II=257-I
```

```
..0114 4      F(II)=F(II)*TAPE(I)
..0115 C
..0116 C     F : SEISMOGRAM IN D.U., GAINS 1 & 50, WINDOWED WITH COSINE BELL.
..0117 C
L.0118        CALL ORSH(IRS,NFILES,XINC,XOT)
..0119        CALL RRITE(F,' RAW DATA    ',' D.U.,GAINS 1&50')
..0120        CALL RHAR1(F,7,IS,S,IFERR,2)
..0121 C
L.0122 C     F : D.F.T. OF SEISMOGRAM, GAINS 1 & 50, NPTS = 256, T = 256/SPS SEC.
L.0123 C     CF : COMPLEX EQUIVALENT OF F.
..0124 C
L.0125        IRS=0
L.0126        XOT=0.0
L.0127        CALL ORSH(IRS,NFILES,XINC,XOT)
L.0128        CALL PRITE(F,' TRANSFORM  ',' FREQ. DOMAIN    ')
L.0129 C     DECONVOLUTION OF DATA BY SYSTEM RESPONSE  CRESP.
L.0130        DO 5 I=1,128
L.0131        CF(I)=CF(I)*CRCSP(I)
..0132        IF(IFIL.GT. 0) CF(I)=CF(I)*B(I)
L.0133 5      SPEC(I)=ALOG10(CABS(CF(I))/(1*TCON))
..0134        WRITE(6,2021)IFIL
L.0135 2021   FORMAT(12,'IFIL=',I3)
L.0136        IF(IFIL.EQ.0) GO TO 8
L.0137        CALL ORSH(IRS,NFILES,XINC,XOT)
L.0138        CALL PRITE(F,' FILT. TRANS',' FREQ. DOMAIN  ')
L.0139 C    FF  IS FILTERED RAW DATA.
L.0140        DO 49 K=1,256
L.0141 49     FF(K)=F(K)
L.0142        CALL RHAR1 (FF,7,IS,S,IFERR,-2)
L.0143        CALL ORSH(IRS,NFILES,XINC,XOT)
L.0144        CALL RRITE(FF,' FILT RAW D ',' TIME DOMAIN    ')
L.0145 C
L.0146 C     CF : D.F.T. OF GROUND VELOCITY IN MICRONS/SEC, NPTS=256,T = 256/SPS SEC.
L.0147 C     F : REAL EQUIVALENT OF CF.
L.0148 C     SPEC : AMPLITUDE SPECTRAL DENSITY IN MICRON-SEC.
L.0149 C     TCON = 4*PI/(T**2) = 4*PI*(SPS/256)**2
..0150 C
..0151 C    SCALING OF AMPLITUDE SPECTRAL PLOT.
L.0152 C    REDUCE 1ST HARMONIC BY 'RAT' IF AMP. OF 1ST IS >DC BY 2.0
L.0153 8      SPEC(129)=AMAX1(SPEC(2),SPEC(3),SPEC(4))
L.0154        DO 1142 I=1,129
L.0155        POWS(I)=(CABS(CF(I)))**2
L.0156 1142   CONTINUE
L.0157        RAT=10.**(SPEC(1)-SPEC(129))
L.0158        IF(RAT-2.)51,51,50
L.0159 50     F(3)=F(3)/RAT
L.0160        F(4)=F(4)/RAT
L.0161 51     SPEC(130)=0.2
L.0162        SS=SPEC(129)
L.0163        ISS=IFIX(SS)
L.0164        SS=FLOAT(ISS)
L.0165        SPEC(129)=SS
L.0166        F(1)=0.
L.0167        CALL RHAR1(F,7,IS,S,IFERR,-2)
L.0168 C
L.0169 C     F : GROUND VELOCITY IN MICRONS/SEC,SAMPLED AT 'SPS' SAMPLES PER SEC.
L.0170 C    DC & FUNDEMENTAL OVER 256/SPS SECS REMOVED.
L.0171 C
L.0172        IRS=1
```

```
L.0173          CALL ORSH(IRS,NFILES,XINC,XOT)
L.0174          CALL PRITE(F,' VELOCITY    ',' MICRONS/SEC.   ')
L.0175          IRS=0
L.0176          F(1)=0.
L.0177          EN(1)=0.
L.0178          DO 6 I=2,256
L.0179          EN(I)=EN(I-1)+(F(I)**2)/SPS
L.0180 6        F(I)=F(I-1)+F(I)/SPS
L.0181          WRITE(6,111)EN(256)
L.0182 111      FORMAT(12,'TOTAL ENERGY = ',F12.4)
L.0183 C
L.0184 C        F : GROUND DISPLACEMENT IN MICRONS, AT 'SPS' SAMPLES/SEC..
L.0185 C        EN : INTEGRAL OF VEL**2 OVER TIME (IN MICRONS**2/SEC),
L.0186 C             AT 'SPS' SAMPLES PER SECOND.
L.0187          CALL ORSH(IRS,NFILES,XINC,XOT)
L.0188 C
L.0189          CALL PRITE(F,' DISP        ',' MICRONS        ')
L.0190          CALL ORSH(IRS,NFILES,XINC,XOT)
L.0191          CALL PRITE(EN,' ENERGY      ',' MICRONS**2/SEC.')
L.0192          SAS=128
L.0193          CALL ORSH(IRS,NFILES,XINC,XOT)
L.0194          CALL PRITE(POWS,'POWER SPEC  ','FREQ. DOMAIN    ')
L.0195          IRS=1
L.0196          XOT=18
L.0197          CALL ORSH(IRS,NFILES,XINC,XOT)
L.0198          CALL PSPEC(SPEC,XOT)
L.0199          IRS=-1
L.0200 1        XOT=0.0
L.0201 999      CALL PLOT(0.0,0.0,999)
L.0202          STOP
L.0203          END
L.0204          SUBROUTINE PRITE(F,A,B)
L.0205          DIMENSION F(258),G(258),A(3),B(4)
L.0206          COMMON TIME(258)
L.0207          CALL SCALE(F,5.,256,1,10.)
L.0208          CALL AXIS(0.,0.,A,12,5.,90.,F(257),F(258),10.)
L.0209          CALL LINE(TIME,F,256,1,0,0)
L.0210 C  PLOT OF TIME OR FREQUENCY AXIS.
L.0211 C  PLOTS A TICK EVERY 25 UNITS
L.0212          SPS=(1/TIME(257))*25
L.0213          TIC=0.0
L.0214          CALL PLOT(0.0,0.0,3)
L.0215          DO 2 J=1,225,25
L.0216          CALL PLOT(TIC,-0.0,2)
L.0217          CALL PLOT(TIC,-0.2,2)
L.0218          VAL=FLOAT(J-1)
L.0219          CALL NUMBER(TIC,-0.5,0.2,VAL,0.,-1)
L.0220 2        TIC=TIC+SPS
L.0221          NN=IFIX(ALOG10(F(258)+1.0E10))-10
L.0222          FAC=10.**NN
L.0223          DO 1 I=1,256
L.0224 1        G(I)=F(I)/FAC
L.0225          WRITE(6,20)A,G
L.0226 20       FORMAT(/,3A4,/,(16F8.2))
L.0227          WRITE(6,21)NN,A
L.0228 21       FORMAT(' *10.**',I2,4A4)
L.0229          RETURN
L.0230          END
L.0231          SUBROUTINE ORSH (IRSET,NOF,XINC,XOTHR)
```

```
L.0232 C   URSH  SHIFTS ORIGIN OF PLOTTER TO A NEW POSITION AT XO & YO CMS
L.0233 C         FROM PREVIOUS ORIGIN.
L.0234 C   X/YIP/XIP ARE THE INCREASE OF THE ORIGIN POSITION FROM THE LEFT
L.0235 C         BOTTOM CORNER OF THE PLOTTER/PAPER.
L.0236 C   XMAX/YMAX : MAX. DISTANCES ALONG THE PLOTTER X & Y AXIS.
L.0237 C   IRSET  < 0 :START A NEW SET OF PLOTS AT PREVIOUS ORIGIN.
L.0238 C          = 0 :CONTINUE ABOVE PREVIOUS PLOT.
L.0239 C          > 0 :RETURN TO BOTTOM OF PAPER FOR NEXT PLOT.
L.0240 C   XOTHR :INCREASE IN X ORIGIN IF RESET EXTERNALLY.
L.0241 C   NOF : CURRENT FILE NUMBER.  XINC : INCREMENT ALONG X AXIS,DEFINES ITS
L.0242 C                                        A PLOT LENGTH.
L.0243         XO=0.0
L.0244         X=X+XOTHR
L.0245         XIP =XINC+1.5
L.0246         YMAX=24.0
L.0247         XMAX=300
L.0248         IF(IRSET) 10,11,12
L.0249 10          YIP=0.0
L.0250         YO=0.0
L.0251         GO TO 1
L.0252 12      YO=-YIP
L.0253         XO=XIP
L.0254         YIP=0.0
L.0255         GO TO 1
L.0256 11      YO=6.0
L.0257         YIP=YO+YIP
L.0258         IF(YIP.LT.YMAX) GO TO 1
L.0259         YIP=YIP-YO
L.0260         YO=-YIP
L.0261         YIP=0.0
L.0262         XO=XIP
L.0263         X=X+XO
L.0264 1       IF(X.LT.XMAX) GO TO 2
L.0265         WRITE(6,66) XMAX,NOF
L.0266 66      FORMAT(5X,'****X MAX. X-DISTANCE OF ',F5.0,'CMS EXCEEDED ON ',
L.0267     *'PLOTTER',/,T10,'PROG. TERMINATED DURING FILE',I4)
L.0268         RETURN 995
L.0269 2       CALL PLOT(XO,YO,-3)
L.0270         YO=ABS(YO)
L.0271         RETURN
L.0272         END
L.0273         SUBROUTINE READT(X,JJ,K,NSKIP,NTOT)
L.0274 C   THIS SUBROUTINE READS A FILE FROM A TAPE.
L.0275 C   THE FILES ARE READ IN THE ORDER OF THE //GO.FT00F000 STATMENTS.
L.0276         REAL*4 X(50500)
L.0277         REAL*4 CUT(1024)
L.0278         CALL ERRSET(212,256,256)
L.0279         CALL ERRSET(210,256,256)
L.0280 C             JJ= FILE NUMBER  I.E. //FT13F00JJ
L.0281 C              K= NO. OF SAMPLES TO BE SKIPPED IN THE FIRST BLOCK TO BE READ.
L.0282 C         NSKIP= NO. OF BLOCKS TO BE SKIPPED FROM THE BEGINNING OF THE FILE.
L.0283 C           NTOT= TOTAL NO. OF SAMPLES TO BE READ.
L.0284 C                   ( 1 BLOCK = 1024 SAMPLES)
L.0285         N=0
L.0286 C   READS BLOCKS THAT ARE TO BE SKIPPED.
L.0287         NSK=NSKIP+1
L.0288         DO 9 I=1,NSK
L.0289 9       READ(13,END=4,ERR=6) CUT
L.0290         GO TO 200
```

```
L.0291  4       IF(N.NE.0) GO TO 1
L.0292          WRITE(6,100)JJ
L.0293  100     FORMAT(20X,'FILE NO=',I5,5X,'EMPTY FILE')
L.0294          GO TO 1
L.0295  8       M=M+1
L.0296          WRITE(6,101)JJ,M
L.0297    101   FORMAT(//,20X,'FILE NO=',I5,5X,'ERROR BLOCK=',I5,/)
L.0298          GO TO 9
L.0299  200     N=N+1
L.0300          IF(N.GT.1) GO TO 600
L.0301          MM=0
L.0302          DO 700 I=K,1024
L.0303          MM=MM+1
L.0304          IF(MM.EQ.NTOT) GO TO 5
L.0305  700     X(MM)=OUT(I)
L.0306          GO TO 9
L.0307  600     DO 5 I=1,1024
L.0308          MM=MM+1
L.0309          IF(MM.GE.NTOT) GO TO 10
L.0310        5 X(MM)=OUT(I)
L.0311          GO TO 9
L.0312  C       READ REMAINING BLOCKS OF CURRENT FILE WHICH HAVE NOT BEEN USED
L.0313    10    DO 1000 I=1, 50
L.0314  1000    READ(13,END=1,ERR=1)OUT
L.0315  1       RETURN
L.0316          END
L.0317          SUBROUTINE BLFIL(B,NOR,WL,JFR,PAT)
L.0318          DIMENSION A(20),PAT(400),N(20),BR(200),BI(200),FD9(200)
L.0319          COMPLEX B(200)
L.0320  C     THIS SUBROUTINE GENERATES A BUTTERWORTH LOW PASS FILTER OF ORDER NOR
L.0321  C     WITH A CUT OF FREQUENCY OF WL. THE FILTER IS CALCULATED OVER A
L.0322  C     FREQUENCY WINDOW OF JFR. B(J) IS THE COMPLEX INVERSE BUTTERWORTH
L.0323  C     POLYNOMIAL RESPONSE FUNCTION.
L.0324  C               CALCULATION OF THE POLYNOMIAL COEFFICIENTS.
L.0325          A(1)=1.0
L.0326          GAM=3.1416/(2*NOR)
L.0327          NOR=NOR+1
L.0328          DO 10 J=2,NOR
L.0329          MU=J-1
L.0330  10      A(J)=A(J-1)*(COS((MU-1)*GAM)/SIN(MU*GAM))
L.0331  C               SET ADDITIONAL VALUES FOR NOR NOT EQUAL TO A POWER OF 4.
L.0332          DO 20 J=1,4
L.0333  20      A(NOR+J)=0.0
L.0334  C               CALCULATION OF THE POLYNOMIAL
L.0335          P0=1
L.0336          DO 30 I=1,JFR
L.0337          P=FLOAT(I)/WL
L.0338            DO 30 KI=2,4,NOR
L.0339            KR=KI+1
L.0340          BR(I)=P0-P*A(KR)+P*(KR+2)
L.0341          BI(I)=P*A(KI)-P*A(KI+2)
L.0342          B(I)=CMPLX(BR(I),BI(I))
L.0343          R(I)=1/B(I)
L.0344  C               CALCULATION OF THE % ATTENUATION AND FREQUENCY FALL OFF.
L.0345          PAT(I)=1/(1+P**(2*NOR-1))*100
L.0346  30      PAT(I)=100-PAT(I)
L.0347  50      NR=NOR-1
L.0348            WRITE(6,100) NR,WL
L.0349  100     FORMAT(//,T10,'LOW PASS BUTTERWORTH FILTER APPLIED.',5X,
```

```
L.0350        *'ORDER= ',I2,' CUT OF FREQUENCY = ',F5.2)
L.0351         DO 105 J=2,NOR
L.0352  105   N(J)=J-1
L.0353         WRITE(6,110)((A(J),N(J)),J=2,NOR)
L.0354  110   FORMAT(15,'BUTTERWORTH POLYNOMIAL IS :',/,5X,'1+',F6.2,
L.0355       *'*S**',I2,/,5X,'+',F6.2,'*S**',I2))
L.0356         WRITE (6,120)
L.0357  120    FORMAT('15,'PER CENT ATTENUATION IN 1HZ. STEPS :')
L.0358         WRITE(6,130) (PAT(K),K=1,JPR)
L.0359  130    FORMAT(1X,16F5.0)
L.0360         RETURN
L.0361         END
L.0362         SUBROUTINE PSPEC(SPEC,XDT)
L.0363         DIMENSION SPEC(130),XLOG(130)
L.0364  C     PSPEC PLOTS THE SPECTRUM OF 1 TO 128HZ ON A LOG LOG AXIS OF SCM/DECADE.
L.0365  C        I.E. XLOG(130)=0.2 LOG UNITS PER CM.
L.0366         CALL PLOT(0.0,15.0,-3)
L.0367         DO 1 I=1,128
L.0368  1      XLOG(I)=ALOG10(FLOAT(I))
L.0369         XLOG(129)=0.0
L.0370  C   A SETS THE START OF THE VERT LOG AXIS SCALE AT 3+3/5  DECADES FROM THE ORIG.
L.0371         A=3.5118*(10**(SPEC(129)-2.0))
L.0372         B=SPEC(130)
L.0373         XLOG(130)=0.2
L.0374         CALL LGAXS(0.,-18.,' LOG AMP(DISPL) SPECTRUM.',25,28.0,90.,
L.0375        *A,B)
L.0376         CALL LGAXS(15.,-18.,' ',-1,28.0,90.,A,B)
L.0377         A=1.0
L.0378         B=XLOG(130)
L.0379         CALL LGAXS(0.,10.,' ',1,15.,0.,A,B)
L.0380         CALL LGAXS(0.,-18.,'LOG FREQUENCY',-13,15.,0.,A,B)
L.0381         CALL LINE(XLOG,SPEC,128,1,-1,1)
L.0382         WRITE(6,22)SPEC
L.0383  22     FORMAT('0LOG AMPLITUDE SPECTRAL DENSITY (MICRON-SEC.)',/,
L.0384        *(16F8.2))
L.0385         CALL PLOT(XDT,-15.,-3)
L.0386         RETURN
L.0387         END
L.0388  //LKED.SYSLIB DD
L.0389  //                DD  DSN=SYS2.PLOTLIB,DISP=SHR
L.0390  //LKED.SYSLIN DD
L.0391  //                DD *,DCB=BLKSIZE=80
L.0392    INCLUDE       DD1(HWBRHAR1)
L.0393  //GO.DD1          DD  DSN=ACM.HXN0006.LOAD,DISP=SHR
L.0394  //GO.FT13F001 DD UNIT=TAPE,VOL=SER=RIETSL,DCB=(RECFM=VB,LRECL=02052,
L.0395  // BLKSIZE=02048),LABEL=(006,,,IN),DSN=FILE006,DISP=(OLD,KEEP)
L.0396  //GO.FT13F002 DD UNIT=TAPE,VOL=SER=RIETSL,DCB=(RECFM=VB,LRECL=02052,
L.0397  // BLKSIZE=02048),LABEL=(016,,,IN),DSN=FILE016,DISP=(OLD,KEEP)
L.0398  //GO.FT13F003 DD UNIT=TAPE,VOL=SER=RIETSL,DCB=(RECFM=VB,LRECL=02052,
L.0399  // BLKSIZE=02048),LABEL=(049,,,IN),DSN=FILE049,DISP=(OLD,KEEP)
L.0400  //GO.PLOTA01   DD  UNIT=PLOTOUT,SPACE=(CYL,(3,3),RLSE),DISP=(,PASS)
L.0401  //GO.SYSIN DD *
L.0402     10   20   37   44  102  111  330  730 3055 3772 -617-1040 -525 -543 -355 -353
L.0403   -280 -316 -277 -284 -265 -255 -242 -239 -212 -239 -207 -213 -207 -185 -199 -169
L.0404   -184 -136 -173 -143 -147 -134 -130 -129 -120 -108 -109 -107 -112  -85  -98  -81
L.0405    -87  -72  -86  -66  -69  -67  -47  -49  -47  -42  -38  -36  -37  -30  -35
L.0406    -31  -26  -16  -27  -28   -9   -7  -19  -12  -12   -1    4   -2    2   -9    9
L.0407      6   -2   23   -5  -13   43  -12   26    2   15   25   19    6   20    6   34
L.040d     15    9   21   36   12   25   11   12   26   20   22   21   25   33    1   44
```

```
..0409     16    23    33    20    27    20    27    15    20    35    19    30    20    20    23    16
..0410     22    40    25    10    26    21    35     7    26    14    25    27    18    21    31    11
..0411     26    19    18    35    23    21     3    32    34     2    37    12    32     8    18    13
..0412     31     6    23    10     3    27    34   -11    34    16     8    16    22    32    10    13
..0413      5    21     8    15     5    25    -7    19    10    21     1    12     3    19     0    23
..0414      7    23     5    13    11    -3    25     1    10   -14    23    10     8     1    13     4
..0415     -4    25     5    10    -1     0    11     5    11     1    11    -6    -4    20     5     9
..0416      3     2    -7    21   -11     8    19    -6    15    -2    -1     3    -3    18    -6    15
..0417    -12     4     5    -3     8    13    -1    -9     5   -10     5    -2     3    -1     6     9
..0418 .024 .095 .206 .345 .500 .655 .794 .905 .976
..0419     10     8    40.
..0420  0.25   256  7    0
..0421  1.20   550  0    0
..0422  3.25    20  4    0
..0423 //
```

REFERENCES

1. Thoenen, J.R. and Windes, S.L., Seismic effects of quarry blasting, Bulletin 442, United States Bureau of Mines, 1942.

2. Crandell, F.J., Ground vibrations due to blasting and its effect upon structures, Journal of the Boston Society of Civil Engineers, vol. 36, No. 2.

3. Langefors, H, Kihlström, B. and Westerberg, H., Ground vibrations in blasting, Water Power, February, 1958.

4. Rupert, G.B. and Clark, C.B., Criteria for the proximity of surface blasting to underground coal mines, Proceedings of the 18th Symposium of Rock Mechanics, Keystone, CRlorado, June 22-24, 1977.

5. Edwards, A.T. and Northwood, T.D., Experimental studies of the effects of blasting on structures, The Engineer, vol. 210, 1960

6. Green, R.W., Investigations of claims of blasting induced damage, Bernard Price Institute, University of Witwatersrand, Johannesburg, South Africa.

7. Oriard, L.L., Blasting effects and their control in open-pit mining, Geotechnical Practice for Stability in Open-Pit Mining, A.I.M.E., 1972.

8. Keil, L.D. and Burgess, A.S., Blast vibration monitoring of rock excavations, Canadian Geotechnical Journal, vol. 14, 1977, pp. 603-619.

9. Ambraseys, N.R. and Hendron, A.J., Dynamic behaviour of rock masses, Rock Mechanics in Engineering Practice, John Wiley and Sons, London, 1968.

10. Green, R.W., A data acquisition and processing system with applications to seismological problems in Southern Africa, Ph.D. thesis, University of the Witwatersrand, 1979.

11. Langefors, H. and Kihlstrom, B., Rock Blasting, John Wiley and Sons Inc., New York, 1963, pp. 262-264.

12. Salamon, M.D.G. and Oravecz, K.I., Rock Mechanics in Coal Mining, Chamber of Mines of South Africa, 1976.

13. Spottiswoode, S. [illegible] and McGarr, A., Source parameters of tremors in a deep level [illegible] mine, B.S.S.A. vol. 65, No. 1, 1975, pp. 93-112.

14. Nichols, H.R., [illegible]nson, C.F. and Duvall, W.I., Blasting vibrations and their effects on structures, Bulletin 656, United States Department of the Interior, Bureau of Mines, 1956.

15. Dowding, C.H. and Rozen, A., Damage to Rock Tunnels from Earthquake Shaking, Journal of the Geotechnical Engineering Division, February, 1978.

16. Aki, K., Generation and propagation of G waves from the Niiguata earthquake of June 16, 1964, Bulletin of the Earthquake Research Institute, Tokyo University, vol. 44, 1966, pp. 73-88.

17. Patterson, J.T. Review of the problem of blasting damage, Professional Safety, vol. 22, No. 1, January, 1977, pp. 30-36.

18. Bracewell, R., The Fourier Transform and its applications, McGraw-Hill, 1965.

19. Brune, J., Tectonic stress and the spectra of seismic shear waves from earthquakes, Journal of Geophysical Research, vol. 76, No. 20, 1970, p. 5002.

20. Dowding, C.H., Response of Buildings to Ground Vibrations Resulting from Construction Blasting, Ph.D. Thesis, University of Illinois, Urbana, Illinois.

21. Green, R.W., A portable multi-channel seismic recorder and a data processing system, Bulletin of the Seismological Society of America, vol. 63, No. 2, pp. 423-431.

22. Telford, W.M., Geldart, L.P., Sheriff, R.E. and Keys, D.A., Applied Geophysics, Cambridge University Press, Cambridge, 1976, Chapter 4, pp. 370-385.